

UNCLASSIFIED

AD NUMBER
AD886550
NEW LIMITATION CHANGE
TO Approved for public release, distribution unlimited
FROM Distribution authorized to U.S. Gov't. agencies and their contractors; Critical Technology; JUN 1971. Other requests shall be referred to Air Force Rocket Propulsion Laboratory, Attn: RPPR/STINFO, Edwards AFB, CA 93523.
AUTHORITY
AFRPL ltr, 20 Dec 1971

THIS PAGE IS UNCLASSIFIED

AFRPL-TR-71-80

2

B

AD 886550

AD No. \_\_\_\_\_  
DRC FILE COPY

# AIR-AUGMENTED COMBUSTION OF BORON AND BORON-METAL ALLOYS

Henry T.-S. Hsia  
United Technology Center

FINAL REPORT AFRPL-TR-71-80

June 1971

CONTRACT NO. F04611-70-C-0065

COLOR ILLUSTRATIONS REPRODUCED  
IN BLACK AND WHITE

CE

This document is subject to special export controls and each transmittal to foreign governments or foreign nationals may be made only with prior approval of AFRL (FPR/S) INFC., Edwards, California 93523.

United States Air Force  
Air Force Systems Command  
Air Force Rocket Propulsion Laboratory  
Edwards, California 93523

UTC 2385-FR

107

ERRATA

AFRPL-TR-71-80

AIR-AUGMENTED COMBUSTION OF BORON AND BORON-METAL COMPOUNDS

Air Force Rocket Propulsion Laboratory

Page

- 3 Footnote\* - change "page 92." to "page 94."
- 5 Paragraph 2, line 11 - change to " $P_j = P \ln \frac{1}{1-X}$  where X is the mold fraction of the oxidant in the gas and P is the static pressure.  $\alpha$  is the stoichiometric fuel-oxidant coefficient (e.g., 4/3 for the reaction of boron or aluminum with oxygen)."
- 9 Subsection b., line 4 - change reference number "(14)" to "(16)"
- 30 Table VI, third column from the right - change column heading from "C\* Effective" to "C\* Efficiency"
- 52 New paragraph 1, line 5 - change "tract" to "trace"
- 68 Lines 1 and 2 - change "pages II-1 and II-2" to "pages 69 and 70" and change "pages II-3 through II-23." to "pages 71 through 91."
- 92 Paragraph 1, line 1 - change "Reference II" to "reference 11"
- 92 Paragraph 1, second F listing - change "F" to "G"

When U. S. Government drawings, specifications, or other data are used for any purpose other than a definitely related Government procurement operation, the Government thereby incurs no responsibility nor any obligation whatsoever, and the fact that the Government may have formulated, furnished, or in any way supplied the said drawings, specifications, or other data, is not to be regarded by implication or otherwise, or in any manner licensing the holder or any other person or corporation, or conveying any rights or permission to manufacture, use, or sell any patented invention that may in any way be related thereto.

2

DOCUMENT CONTROL DATA - R & D

(Security classification of title, body of abstract and indexing annotation must be entered when the overall report is classified)

1. ORIGINATING ACTIVITY (Corporate author) United Technology Center		2a. REPORT SECURITY CLASSIFICATION Unclassified	
		2b. GROUP	
3. REPORT TITLE Air-Augmented Combustion of Boron and Boron-Metal Alloys			
4. DESCRIPTIVE NOTES (Type of report and inclusive dates) Final Report			
5. AUTHOR(S) (First name, middle initial, last name) Henry T.-S. Hsia			
6. REPORT DATE 9 August 1971		7a. TOTAL NO. OF PAGES 93	7b. NO. OF REFS 21
8a. CONTRACT OR GRANT NO. F04611-70-C-0065		9a. ORIGINATOR'S REPORT NUMBER(S) UTC 2385-FR	
b. PROJECT NO. UTC 2385-FR		9b. OTHER REPORT NO(S) (Any other numbers that may be assigned this report) AFRPL-TR-71-80	
c.			
d.			
10. DISTRIBUTION STATEMENT This document is subject to special export controls and each transmittal to foreign governments or foreign nationals may be made only with prior approval to AFRPL (RPPR/STINFO), Edwards, California 93523.			
11. SUPPLEMENTARY NOTES Details of illustrations in this document may be better studied on microfiche		12. SPONSORING MILITARY ACTIVITY United States Air Force Air Force Systems Command Air Force Rocket Propulsion Laboratory Edwards, California 93523	
13. ABSTRACT High speed cinematography was used to study the combustion characteristics of powdered boron, and of compounds of boron and magnesium, lithium, or aluminum, all of which were LiF-doped or undoped. An optical burner apparatus was used operating on CO-O <sub>2</sub> -air at 5 to 40 psia and at several temperatures. Ignition delay and burning times were derived from the film tracks of burning particles. The boron-metal compounds gave ignition delay times in the range of 0-8 msec and burning times of 2-15 msec, both considerably shorter than the corresponding times for elemental boron. X-ray diffraction analyses of the residues collected in the exhaust from MgB <sub>12</sub> and LiB <sub>2</sub> combustion indicated a high degree of oxidation. Wet chemical analysis of the MgB <sub>12</sub> residue confirms the maximum combustion efficiency attainable. The favorable results obtained clearly indicate that the boron-metal compounds are much better fuels than elemental boron in air-augmented rocket systems flying at conditions under which satisfactory afterburning of boron-loaded propellants has not been accomplished. Further study aiming toward the use of some of the promising borides in air-augmented propulsion is discussed.			

14. KEY WORDS	LINK A		LINK B		LINK C	
	ROLE	WT	ROLE	WT	ROLE	WT
Air-Augmentation						
Boride						
Boron						
Combustion						

# **AIR-AUGMENTED COMBUSTION OF BORON AND BORON-METAL ALLOYS**

Henry T.-S. Hsia

Details of illustrations in  
this document may be better  
studied on microfiche

This document is subject to special export controls and each transmittal to foreign governments or foreign nationals may be made only with prior approval of AFRPL (RPPR/STINFO), Edwards, California 93523.

UTC 2385-FR

FOREWORD

This report covers research performed during the period 15 May 1970 through 15 June 1971 and is submitted by the author 9 August 1971. This report contains no classified information extracted from other classified documents.

BPSN: 623148  
PROJECT NUMBER: 3148  
PROGRAM ELEMENT NUMBER: 6.2.3.02F  
CONTRACT NUMBER: F04611-70-C-0065  
CONTRACTOR NAME AND ADDRESS: United Technology Center  
Division of United Aircraft Corporation  
P. O. Box 358  
Sunnyvale, CA 94088

CONTRACTOR REPORT NUMBER: UTC 2385-FR  
PROJECT OFFICER: Alan W. McPeak, Captain, USAF/LKCP  
LABORATORY HAVING  
PRIME INTEREST: Air Force Rocket Propulsion Laboratory  
Edwards AFB, CA 93523

This technical report has been reviewed and is approved.

Alan W. McPeak, Captain, USAF  
Project Engineer

## ABSTRACT

High speed cinematography was used to study the combustion characteristics of powdered boron, and of compounds of boron and magnesium, lithium, or aluminum, all of which were LiF-doped or undoped. An optical burner apparatus was used operating on CO-O<sub>2</sub>-air at 5 to 40 psia and at several temperatures. Ignition delay and burning times were derived from the film tracks of burning particles. The boron-metal compounds gave ignition delay times in the range of 0-8 msec and burning times of 2-15 msec, both considerably shorter than the corresponding times for elemental boron. X-ray diffraction analyses of the residues collected in the exhaust from MgB<sub>12</sub> and LiB<sub>2</sub> combustion indicated a high degree of oxidation. Wet chemical analysis of the MgB<sub>12</sub> residue confirms the maximum combustion efficiency attainable. The favorable results obtained clearly indicate that the boron-metal compounds are much better fuels than elemental boron in air-augmented rocket systems flying at conditions under which satisfactory afterburning of boron-loaded propellants has not been accomplished. Further study aiming toward the use of some of the promising borides in air-augmented propulsion is discussed.

## CONTENTS

Section		Page
I	INTRODUCTION AND SUMMARY	1
II	TECHNICAL DISCUSSION	3
	1. Background	3
	2. Metal Borides	6
	a. Aluminum Borides	7
	b. Magnesium Borides	9
	c. Lithium Borides	9
	d. Estimated Heat Release of Borides	9
	e. Analysis of Test Samples	9
	3. Experiments	10
	a. Test Apparatus	10
	b. Gas Supply System	23
	c. Control Console and Sequencer	23
	d. Photography	26
	e. Data Recording	27
	f. Particle Size Separation	27
	g. Safety Equipment	27
	4. Calibration of Burner Test Conditions	27
	5. Experimental Results and Discussion	31
	a. Combustion Characteristics	31
	b. Residue Collection and Analysis	48
III	CONCLUSIONS AND RECOMMENDATIONS	55
	APPENDIX I: Theoretical Equilibrium Calculation for CO-O <sub>2</sub> -Air Combustion	57
	APPENDIX II: X-Ray Diffraction Data	68
	APPENDIX III: Preparation Methods and Cost of Boron-Metal Compounds	92
	REFERENCES	94

## ILLUSTRATIONS

Figure		Page
1	Scanning Electron Micrographs of Boron (-325 Mesh) and Aluminum Boride ( $\text{AlB}_2$ -200 Mesh, $\text{AlB}_{12}$ -325 Mesh) Powders	12
2	Scanning Electron Micrographs of Magnesium Boride Powders ( $\text{MgB}_2$ -200 Mesh, $\text{MgB}_6$ and $\text{MgB}_{12}$ -325 Mesh)	13
3	Scanning Electron Micrographs of Lithium Boride Powders (325 Mesh)	14
4	Schematic Diagram of the Test Setup	15
5	Test Setup	16
6	Optical Burner	17
7	Particle Feed Mechanism	20
8	Typical Residue from Combustion of $\text{MgB}_2$ Collected on Tungsten Rod	22
9	Ejector	24
10	Schematic Diagram of Sequencer	25
11	Typical Particle Traces	28
12	Typical Pressure and Temperature Traces	32
13	Burning of $\text{MgB}_2$ , $\text{LiB}_2$ , $\text{AlB}_2$ and Boron Particles	39
14	Burning of a Shower of Particles	40
15	Ignition Delay and Burning Time for 37 to $44\mu$ $\text{MgB}_2$	41
16	Ignition Delay and Burning Time for 37 to $44\mu$ $\text{LiB}_2$	42
17	Ignition Delay and Burning Time for 37 to $44\mu$ $\text{AlB}_2$	43
18	Ignition Delay and Burning Time for 37 to $44\mu$ $\text{MgB}_{12}$ at $1,650^\circ\text{K}$	44
19	Ignition Delay and Burning Time for 37 to $44\mu$ $\text{LiB}_{12}$ at $1,650^\circ\text{K}$	45
20	Ignition Delay and Burning Time for 37 to $44\mu$ $\text{AlB}_{12}$ at $1,650^\circ\text{K}$	46
21	Ignition Delay for 37 to $44\mu$ Boron	47
22	Ignition Delay and Burning Time for $\text{AlB}_2$ at $1,650^\circ\text{K}$	49
23	Ignition Delay and Burning Time for $\text{MgB}_2$ at $1,650^\circ\text{K}$	50
24	Ignition Delay for Boron at $1,650^\circ\text{K}$	51
25	Typical Scanning Electron Micrographs of Combustion Residues	53

## TABLES

Table		Page
I	Properties of Fuels	4
II	Physical Properties of Aluminum Borides	7
III	Phase Composition of Aluminum Borides	8
IV	Estimated Heat Release of Borides Relative to Boron	10
V	Analysis of Borides	11
VI	Theoretical and Measured Test Conditions	30
VII	X-Ray Diffraction of Combustion Residues	33
VIII	X-Ray Diffraction of Residue from Combustion of 1-1/2% LiF Doped Particles	36

## SECTION I

### INTRODUCTION AND SUMMARY

With the current development of air-augmented rocket and Scramjet systems much interest has arisen in the use of solid fuel particles as high-energy additives to the liquid or solid primary propellants. Boron has outstanding potential as an additive to propellants because of its high volumetric heat of combustion with oxygen. However, this potential can only be realized if efficient combustion of the boron with oxygen in air is attained in the ramburner over the desired wide range of flight altitude and Mach numbers. Earlier work has shown a direct relationship between ramburner pressure and boron combustion efficiency: low ramburner pressure leads to poor performance. Previous work sponsored by the Air Force has suggested that the use of catalytic dopants, for example a coating of LiF deposited on the boron particle surface, may facilitate combustion by lowering the particle ignition temperature even at low pressures. Another approach is to replace elemental boron with a boron compound or alloy such as  $AlB_x$ ,  $MgB_x$  or  $LiB_x$ . The objective of this program was to evaluate the merits of using such compounds<sup>x</sup> of boron and dopants. The program involved three closely related phases:

- A. Phase I: A literature survey for available information from both U. S. and foreign sources on compounds or alloys of boron. Selected physical properties and compositions of each compound, alloy, or mixture were determined as needed.
- B. Phase II: Combustion testing of the compounds and discrete mixtures selected in Phase I. The combustion testing was conducted in the optical burner apparatus constructed at UTC under Contract AFO4(611)-11544. Photography and chemical analysis of the residues were the primary data gathering methods.
- C. Phase III: This phase consisted of the data reduction, presentation and recommendations derived as a result of the work accomplished under Phases I and II.

This report summarizes the work accomplished in this program. In Phase I the available literature on aluminum, magnesium, and lithium borides, which is mostly of foreign origin, was reviewed; synopses of the pertinent information are given herein. Eight borides which have been obtained or prepared for the program were analyzed for purity on the basis of chemical, spectrographic, or X-ray diffraction analyses. In Phase II, the burner apparatus was modified and calibrated for operation with a  $CO_2$ -air system at 5, 10, 15, 25 and 40 psia and at various temperatures. Particles of boron,  $MgB_2$ ,  $MgB_{12}$ ,  $LiB_2$ ,  $LiB_{12}$ ,  $AlB_2$  and  $AlB_{12}$  with particle sizes from 37 to 74 $\mu$  were burned at these conditions. Two runs were made on each test material doped with 1.5% LiF.

Particle tracking by high speed cinematography and analysis of collected residues were successfully carried out after initial technical difficulties had been overcome. The data obtained were analyzed in Phase III. The ignition delay of the borides was found to lie in the range of 0-8 msec and their burning time between

2 and 15 msec. In general, these times decreased with increasing pressure and temperature, and with decreasing particle size.

The elemental boron particles had similar ignition delay times but their combustion was so slow that they were still burning when they left the 12-in. chamber which had a residence time of 14-24 msec, or they would even cease to burn before they had traversed the chamber. At each temperature burning of the borides appeared to be more complete at lower chamber pressures, probably due to the fact that low pressures favor vapor phase burning.

The result of X-ray diffraction analysis of the residue from the combustion of  $MgB_2$  and  $MgB_{12}$  at 1400°K or higher temperatures indicated a strong pattern of the magnesium borate  $Mg_2B_2O_5$ , and a weak pattern indicating a trace of the higher borides  $MgB_4$ ,  $MgB_6$  or  $MgB_{12}$ , but in most cases no trace of their component metals magnesium and boron. When  $LiB_2$  was burned at 1400 and 1650°K, X-ray diffraction analysis of the residue gave a strong pattern of lithium borate,  $Li_2O \cdot 2B_2O_3$ , or  $Li_2O \cdot 3B_2O_3$  and no trace of unburned borides or their component metals lithium and boron. On the other hand a residue from  $LiB_{12}$  combustion at 1650°K gave a strong pattern of unburned materials indicating poor combustion. In the case of  $AlB_2$  and  $AlB_{12}$ , aluminum was found in the residues alongside the aluminum borates  $9Al_2O_3 \cdot 2B_2O_3$  and  $2Al_2O_3 \cdot B_2O_3$ , and aluminum oxide,  $\alpha Al_2O_3$ , and boron oxide,  $B_2O_3$ . Unburned boron was found in the residues from almost all the test burning elemental boron. Wet chemical analyses were performed on the residues from  $MgB_2$  and  $MgB_{12}$  combustion at 15 psia and 1650°K. Based on the percentages of the constituents in the residues, the combustion efficiencies were determined as 62% for  $MgB_2$  and 100% for  $MgB_{12}$ .

Two runs were made on each of the seven test materials doped with 1.5% LiF. In nearly all cases the addition of LiF shortened the ignition delay, to practically zero. However the effect on burning time was so irregular that no clear conclusion can be drawn. Comparing the X-ray diffraction patterns of residues from the combustion of doped and undoped particles, it can be concluded that doping yielded some improvement in the degree of oxidation of  $MgB_{12}$ ,  $AlB_2$ ,  $AlB_{12}$ ,  $LiB_2$ ,  $LiB_{12}$  and boron, but gave no clear cut effect with  $MgB_2$ .

The favorable results obtained in this program lead to a practical solution to the problem of low pressure combustion of boron through the boron-metal compound technique and may overcome the difficulty in the design of a practical and efficient air-augmented rocket system flying at conditions under which afterburning of boron-loaded propellants has not heretofore been satisfactorily accomplished.

## SECTION II.

### TECHNICAL DISCUSSION

Several of the low atomic weight metals are excellent potential rocket fuels. Heats of combustion data (Table I) indicate that when heat evolved per unit weight of metal oxide is taken as a measure of metal fuel value, boron, aluminum, lithium, and magnesium are better fuels than carbon. In a volume-limited vehicle system, boron appears most attractive because of its high heat of combustion per unit volume. However, in practice boron in powder form has been found to be more difficult to burn than other metal powders. This can be attributed<sup>(1)\*</sup> to the fact that the boiling point of boron oxide lies below that of boron itself. Thus, combustion must take place on the surface of the metal particle. On the other hand, the boiling points of the oxides of aluminum, lithium, and magnesium lie above that of each respective metal, so that the metal burns in the vapor phase. Thus it has been shown both theoretically and experimentally that boron differs considerably from other light metals in its combustion properties.

#### 1. BACKGROUND

Ignition of metal fuel particles can take place only when they have been heated to their ignition temperature. Initially, heat is supplied primarily by convection, and the heating time is proportional to the square of the particle diameter. As the particle temperature increases, heating by surface reactions becomes important; the heating rate accelerates and becomes proportional to the particle diameter. Most of the total time to ignition is spent in the slow convective heating regime, and this ignition delay time is usually roughly proportional to the particle diameter squared.

The particle temperature history is given by the solution of the following equation<sup>(2)</sup>

$$\frac{d T_p}{dt} = \frac{6}{\rho_p C_p d} \left[ \frac{k_g \text{Nu}}{d} (T_g - T_p) - \sigma \epsilon T_p^4 \right]$$

where  $k_g$  denotes the thermal conductivity of the gas, Nu the Nusselt number,  $\rho_p$  the particle density,  $C_p$  the particle heat capacity,  $T_p$  the particle temperature,  $T_g$  the gas temperature,  $d$  the diameter,  $\sigma$  the Stefan-Boltzmann constant, and  $\epsilon$  the emissivity of the particle.

The equation shows that a high value of Nu and a low value of  $\rho_p C_p$  lead to rapid heating of the particle; this is true for lithium, magnesium, and aluminum. Aluminum has an ignition temperature similar to that of boron, and

---

\*Parenthetical superscript numbers denote references appearing on page 92.

TABLE I

## PROPERTIES OF FUELS

Fuel	$\rho_{p3}$ g/cm <sup>3</sup>	M	$C_p$ cal/°C g	$\frac{\rho_p}{M}$	$\rho_{pC}$	Heat of Combustion Unit Weight of Oxide kcal/g	Heat of Combustion Unit Weight of Fuel kcal/g	Heat of Combustion Unit Volume of Fuel <sub>3</sub> kcal/cm <sup>3</sup>
Boron	2.37	10.82	0.307	0.231	0.767	3.02	14.0	33.2
Aluminum	2.70	26.97	0.214	0.100	0.578	3.93	7.4	20.0
Magnesium	1.74	24.32	0.242	0.0716	0.421	3.56	5.900	10.30
Lithium	0.53	6.94	0.79	0.0763	0.419	4.43	9.540	5.05
Carbon	2.25	12.01	0.165	0.1875	0.372	2.14	7.830	17.63

those of magnesium and lithium are considerably lower. Thus, the ignition delay of these three metals will be shorter than that of boron. Compounds or alloys of these metals with boron will also have a different heatup profile and lower ignition delay time than pure boron.

Previous studies have indicated that three different controlling mechanisms are involved in determining the combustion time of metal particles. Boron apparently burns by the diffusion of the oxidizing species to the particle surface, followed by surface reaction and diffusion of the gaseous combustion products away from the surface.<sup>(3,4)</sup> This sequence occurs because the vapor pressure of boron oxide exceeds that of boron at the combustion temperature. The combustion rate in this case is limited by the rate of diffusion of the oxidizer through the combustion products. A theory developed by Spalding<sup>(5)</sup> indicates that the burning time is proportional to the square of the initial particle diameter, is independent of pressure, and depends only slightly on temperature.

Belyaev<sup>(6)</sup> has recently made a successful correlation of aluminum particle burning rates in fuel-rich gases, assuming that water and carbon dioxide are equally effective oxidants. If there are more than one oxidizing species,  $j$ , in the gas, Macek and Semple<sup>(2)</sup> suggested a generalized expression to calculate the burning time,  $t$ , of a metal particle with original diameter  $d$ , as

$$\frac{1}{t} = \sum_j \frac{1}{t} = \frac{8\delta}{(\rho_p/M)d^2} \sum_j \frac{\beta_j P_j}{\gamma_j}$$

where  $\rho_p/M$  denotes the molar density of the metal particle given in Table I, and  $\delta$  the ratio of flame to particle diameter ( $\delta > 1$  for vapor phase combustion, e.g., 2.7 for aluminum;  $\delta = 1$  for surface burning, e.g., boron).  $\beta = D/RT_g$  where  $D$  is the diffusion coefficient and  $R$  the gas constant,  $T_g$  the gas temperature.  $P_j = P \ln \frac{1}{1-X_j}$  where  $X$  is the mole fraction of the oxidant in the gas,  $P$  the static pressure, and  $\gamma$  the stoichiometric fuel-oxidant coefficient (e.g., 4/3 for the reaction of boron or aluminum with oxygen).

When the diffusion contribution of carbon dioxide is included, the calculated burning times in dry gases agree with the experiment to within 10 to 20%. Typical burning times for boron were found to be 12 to 15 msec for 35 $\mu$  particles, and 20 to 25 msec for 44 $\mu$  particles. The burning time decreased slightly with increasing gas temperature.

A shock tube study was conducted by Uda<sup>(7)</sup> to determine the ignition limit of clouds of boron particles in air. The boron samples, consisting of 30 - 50 $\mu$  agglomerated particles ignited at a reflected shock temperature of about 1,900°K at 1 atm pressure. The ignition temperature decreased steadily with increasing pressure, to about 1400°K at 20 atm. Ignition of the 0.015 $\mu$  particles appeared to be insensitive to pressure, and the ignition temperature stayed constant at 1150°K. For a constant reflected shock pressure, the ignition temperature decreased with decreasing particle size. The ignition delay time of the 0.015 $\mu$  particles decreased as the reflected shock temperature increased. It was less than 1 msec at 1140°K and decreased to less than 0.1 msec above 1400°K.

The studies of boron combustion thus indicate that ignition and burning are sensitive to pressure and temperature conditions, and to particle size, type of oxidizing environment, and particle concentration. As indicated by equations (1) and (2), the properties of metals such as lithium, magnesium, and aluminum, if used in conjunction with boron, will contribute to shorter ignition delay and burning times. The shorter burning time is due mainly to the fact that these metal particles burn by a vapor phase mechanism. It seems to be logical to consider compounds or mixtures of boron and these other metals as candidate fuels.

In evaluating boron-rich solid propellants for air-augmented systems, Sims, Lee, and Gonzales (8) replaced boron with boron compounds, including  $ZrB_2$ ,  $B_4C$ ,  $TiB_2$ ,  $AlB_2$ , and  $MgB_2$ . Some promising data were obtained, but the exploratory investigation was too limited to provide systematic results.

In another approach experimental results were obtained which indicate that the ignition temperature of powdered boron in oxygen can be markedly decreased by the addition of doping impurities (9) to the metal. LiF is one of the promising dopants, which probably increases the diffusion of boron ions through the oxide surface layer, or increases oxygen diffusion through the oxide film. The ignition temperature of boron doped with 1% LiF was reduced by 160°C.

In a recent air-augmentation study, Rosenberg, et al. (10) investigated the effect of boron in a fuel-rich primary combustion and the efficiency of the secondary combustion for both solid and liquid primaries under simulated air-augmentation flight regimes. The test variables they investigated were secondary  $L^*$ , boron particle size and loading, temperature and pressure of the secondary air, air to primary flow ratio, and primary mixture ratio in the liquid system. They demonstrated that the boron combustion efficiency was dependent not only upon the residence time of the solid boron in the secondary chamber but also on the secondary chamber pressure; adequate boron combustion at low pressures could not be achieved by simply increasing the  $L^*$  of the secondary chamber. Other methods had to be found to increase the combustion rate of the boron in order to effect an increase in the performance of the system within reasonable  $L^*$  limits. Doping of boron with LiF provided one successful means of increasing the boron combustion rate.

## 2. METAL BORIDES

As discussed in the preceding sub-section, the physical and thermochemical properties of the candidate borides or alloys of boron with other metals will control their heat-up, ignition and burning characteristics when they are used as particulate fuel additives in a secondary combustion system, and thus will determine how their performance will compare with that of boron alone. For instance, they may provide an increase of overall fuel density with little loss in energy released. In general, all the metal borides have very high melting points and are known as refractory materials. (11) Since metal borides have not been considered previously as fuel additives, their thermochemical properties are not readily available. The following subsections summarize accessible data, mostly taken from foreign publications.

a. Aluminum Borides

There are five reported and authenticated phases in the aluminum boron system<sup>(12)</sup>:  $AlB_2$ ,  $AlB_{10}$ ,  $\alpha-AlB_{12}$ ,  $\beta-AlB_{12}$ ,  $\gamma-AlB_{12}$ . No information has been found on  $AlB_6$ . The three forms of  $AlB_{12}$  and  $AlB_{10}$  are hard materials with structures similar to boron or boron carbide, where  $AlB_2$  is a soft graphite-like material of hexagonal structure. Some of the physical properties of aluminum borides are shown in Table II.

TABLE II  
PHYSICAL PROPERTIES OF ALUMINUM BORIDES

<u>Boride</u>	<u>Crystal Structure</u>	<u>Theoretical Density g/cm<sup>3</sup></u>	<u>Melting Point °F</u>
$AlB_2$	Hexagonal	3.16	3,010±90
$AlB_{10}$	Orthorhombic	2.54	4,390±90
$\alpha-AlB_{12}$	Tetragonal	2.58	3,925±90
$\beta-AlB_{12}$	Orthorhombic	2.60	4,015±90
$\gamma-AlB_{12}$	Orthorhombic	2.56	-

Serebryanskii and Epel'baum<sup>(13)</sup> reported that the boron-containing specimens were prepared from pure elemental aluminum and boron in a tubular furnace. They give the phase composition in relation to specimen composition and synthesis temperature as shown in Table III.

Formation and decomposition processes of aluminum borides were investigated by Atoda et al.<sup>(14)</sup> using Differential Thermal Analysis, X-ray and chemical analysis techniques on samples prepared in an electric furnace.  $AlB_2$  begins to form at 600°C and decomposes into the  $\alpha-AlB_{12}$  phase above 920°C. The latter is stable up to at least 1900°C; it decomposes above 1900°C, separating elemental Al.

The energies of combustion of  $AlB_2$  and  $\alpha-AlB_{12}$  were measured by Domalski and Armstrong<sup>(15)</sup> in a bomb calorimeter using fluorine as the oxidant. From the data obtained in these experiments the heats of formation of  $AlB_2$  and  $\gamma-AlB_{12}$  were calculated as  $-16\pm 3$  and  $-48\pm 10$  kcal/mol, respectively. The lack of precision in these values is due to uncertainties in the impurity corrections and in the heats of formation of the combustion products.

TABLE III  
 PHASE COMPOSITION OF ALUMINUM BORIDES

Original composition		Synthesis temperature, °C									
% B	% Al	650°	700°	800°	900°	950°	1000°	1100°	1200°	1300°	1400°
28.9	71.1		AlB <sub>2</sub> , Al			AlB <sub>2</sub> Al					
44.9	55.1										
55.0	45.0										
61.9	38.1										
70.9	29.1										
76.5	23.5	AlB <sub>2</sub> +Al		AlB <sub>2</sub>		α-AlB <sub>12</sub>					
80.3	19.7										
82.5	17.5										

α-AlB<sub>12</sub>+Al

α-AlB<sub>12</sub>

#### b. Magnesium Borides

The magnesium-boron system displays a wide range of mutual solubility:  $MgB_2$  will dissolve in magnesium; on the other hand, if  $MgB_2$  is heated above  $300^\circ C$ , it will lose magnesium progressively to form  $MgB_4$ ,  $MgB_6$ , and  $MgB_{12}$ .<sup>(11)</sup> The magnesium borides<sup>(14)</sup> react with free oxygen,  $MgB_2$  at  $580^\circ C$  and  $MgB_4$  at  $400^\circ C$ , but the reactions are not complete at  $1100^\circ C$ .  $MgB_2$  reacts with water and with HCl at  $15^\circ C$  to produce 97% hydrogen and 3% boranes;  $MgB_4$  reacts only with boiling HCl while the other borides do not react at all.

The heat of formation of  $MgB_{12}$  was estimated as  $-34.4$  kcal/mol,<sup>(17)</sup> compared to  $-21.98$  kcal/mol for  $MgB_2$  as listed in JANAF Thermochemical Data.

#### c. Lithium Borides

Information on lithium borides is scarce. Markovskii and Kondrashev<sup>(18)</sup> reported that by electrolysis of lithium borate a product was obtained containing 82.9% B and 9.4% Li, probably a mixture of elemental boron and  $LiB_6$ . No other lithium borides are mentioned in the open literature.

#### d. Estimated Heat Release of Borides

In the absence of information on the heats of formation of some of the borides considered in this program, the heat release from the reaction of the borides with oxygen was calculated on the basis of heat release data on each of the two component elements. The results are compared to pure boron in Table IV.

From the viewpoint of volumetric heat release, the lithium borides appear to be the best fuel additives among the metal borides, followed by the aluminum and the magnesium borides.

#### e. Analysis of Test Samples

All the nine (9) compounds specified in the program, i.e.  $AlB_2$ ,  $AlB_6$ ,  $AlB_{12}$ ,  $MgB_2$ ,  $MgB_6$ ,  $MgB_{12}$ ,  $LiB_2$ ,  $LiB_6$  and  $LiB_{12}$ , were obtained in the form of chemical compounds, except  $AlB_6$ . No information could be found in the literature on  $AlB_6$  and it probably does not exist as a compound. The others are either available commercially or were specially synthesized for this program. The purity of each boride was determined from chemical, spectrographic, or X-ray diffraction analyses as summarized in Table V.

The  $MgB_6$  obtained showed a medium pattern of  $MgB_2$  and a weak pattern of  $MgB_{12}$ ; the  $LiB_6$  showed a strong pattern of  $LiB_{12}$  and a weak pattern of  $LiB_2$ . It is likely that  $MgB_6$  and  $LiB_6$  are unstable and temperature dependent; although formed in the synthesis process at high temperature, they may be transformed into other borides during the cooling period.

TABLE IV

## ESTIMATED HEAT RELEASE OF BORIDES RELATIVE TO BORON

	B	AlB <sub>2</sub>	AlB <sub>6</sub>	AlB <sub>12</sub>	MgB <sub>2</sub>	MgB <sub>6</sub>	MgB <sub>12</sub>	LiB <sub>2</sub>	LiB <sub>6</sub>	LiB <sub>12</sub>
Heat release per unit weight of fuel relative to boron	1.0	0.798	0.895	0.942	0.598	0.780	0.871	0.730	0.895	0.944
Volumetric heat release relative to boron	1.0	0.740	0.860	0.918	0.697	0.840	0.911	0.918	0.969	0.982

Scanning electron beam micrographs were taken of all the borides at 300, 1000 and 3000 magnification. Micrographs of an elemental boron powder were also taken for reference. In the following micrographs the borides appear as agglomerates of amorphous particles of various sizes (Figures 1, 2 and 3).

## 3. EXPERIMENTS

The major components of the test facility were the optical burner apparatus; a gas supply system; an optical system for high speed photography; a device for exhaust residue sampling; a control console and sequencer for remote control of ignition, flow valves, camera and particle sampling, plus electronic recording equipment monitoring pressures and temperatures. The general arrangement of the test setup is shown in Figures 4 and 5.

## a. Test Apparatus

The major piece of test equipment used in this program was previously constructed at UTC under contract AF04(611)-11544.<sup>(19)</sup> Several modifications were made to meet the requirements of the current contract; the major ones were (1) use of a CO/O<sub>2</sub> flame instead of a H<sub>2</sub>/O<sub>2</sub> flame, to eliminate the effect of the presence of water vapor on the combustion; (2) installation of an ejector system attached to the burner exhaust duct for maintaining low chamber pressure conditions, (3) installation of a thermocouple to monitor the flame temperature and (4) extending the running period to facilitate collection of adequate amounts of exhaust residue. A large part of the experimental effort in the first six months of the program was devoted to carrying out these modifications and to calibrating of the burner.

## (i) Optical Burner

The optical burner, shown in Figure 6, consisted of a combustion chamber of 1-in. I.D. fitted with a transparent Vycor window and operating with carbon monoxide and oxygen. The fuel/oxygen injector had a central port, through which the oxygen was admitted, surrounded by six manifolded fuel jets. The fuel inlets ended in a series of jets canted 45° to the axis of the burner. These jet impinged on the oxygen jets which were canted outward at 45°. A 1/16-in. O.D.,

TABLE V  
ANALYSIS OF BORIDES

Borides	Wet Chemical Analysis	Spectrographic Analysis	X-Ray Analysis
AlB <sub>2</sub> (55.2/44.4) (a)	Al 55.2% B 43.9% C 0.18% H 0.002% N 0.18% O 0.61%		AlB <sub>2</sub> Medium weak pattern AlB <sub>12</sub> Trace Al <sub>2</sub> O <sub>3</sub> Trace Al Medium pattern
AlB <sub>12</sub> (17.1/82.9)	Al 18-20% B 78-81% Fe 0.05% Si 0.2% C 0.8% Mg 0.5% ZR 0.1%		AlB <sub>12</sub> α-phase good pattern Al <sub>2</sub> O <sub>3</sub> 5 weak lines of α-phase
MgB <sub>2</sub> (52.9/47.1)	Mg 52.6%	Si 0.01-0.1% Mn 0.03-0.3% Cu 0.003-0.3% Fe 0.03-0.3% Pb 0.003-0.03% Al 0.01-0.1%	MgB <sub>2</sub> Strong pattern MgB <sub>4</sub> Trace MgO Trace
MgB <sub>6</sub> (27.3/72.7)	Mg 26.97%	Si 0.01-0.1% Mn 0.03-0.3% Cu 0.003-0.3% Fe 0.03-0.3% Pb 0.003-0.03% Al 0.01-0.1%	MgB <sub>2</sub> Medium pattern (b) MgB <sub>12</sub> Weak pattern MgO Trace
MgB <sub>12</sub> (15.8/84.2)	Mg 15.25%	Si 0.01-0.1% Mn 0.03-0.3% Cu 0.003-0.3% Fe 0.03-0.3% Pb 0.003-0.03% Al 0.01-0.1%	MgB <sub>12</sub> Strong pattern MgB <sub>2</sub> Trace
LiB <sub>2</sub> (24.3/75.7)	Li 24.1%	Si 0.01-0.1% Mn 0.03-0.3% Cu 0.003-0.3% Fe 0.03-0.3% Pb 0.003-0.03% Al 0.01-0.1%	Perfect pattern
LiB <sub>6</sub> (9.8/90.2)	Li 9.79%	Si 0.01-0.1% Mn 0.03-0.3% Cu 0.003-0.3% Fe 0.03-0.3% Pb 0.003-0.03% Al 0.01-0.1%	LiB <sub>12</sub> Strong pattern (c) LiB <sub>2</sub> Weak pattern
LiB <sub>12</sub> (5.1/94.9)	Li 5.2%	Si 0.01-0.1% Mn 0.03-0.3% Cu 0.003-0.3% Fe 0.03-0.3% Pb 0.003-0.03% Al 0.01-0.1%	Perfect pattern

Note: (a) Number in parenthesis is the weight ratios, metal to boron  
 (b) No MgB<sub>6</sub> detected although chemistry was perfect  
 (c) No LiB<sub>6</sub> detected although chemistry was perfect

NOT REPRODUCIBLE

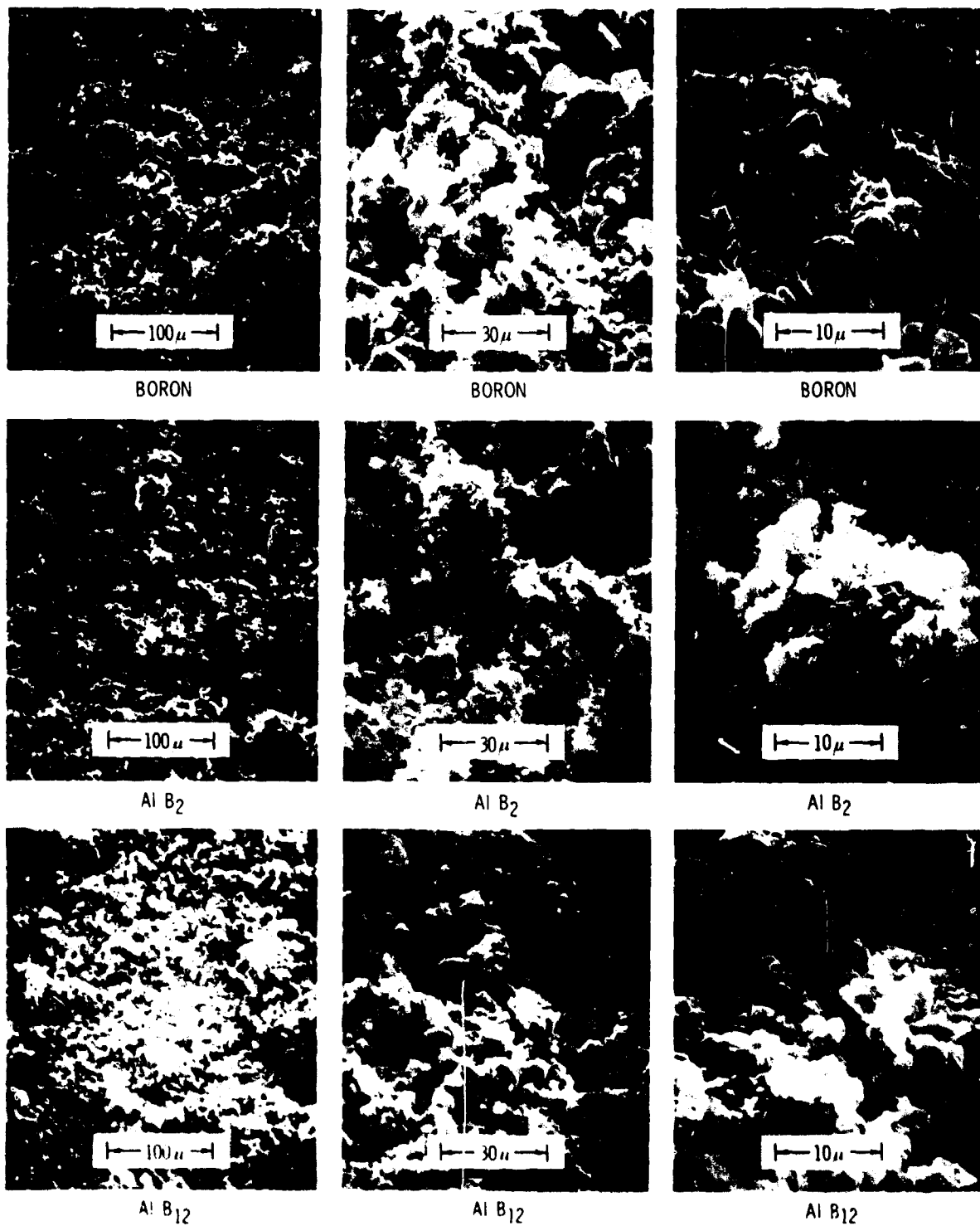
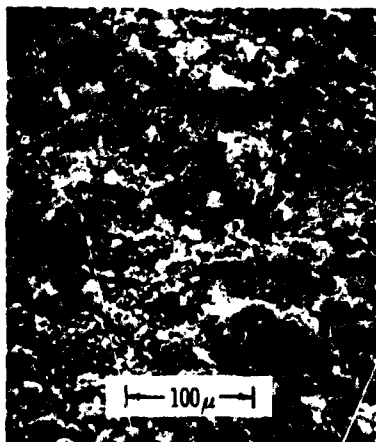


Figure 1. Scanning Electron Micrographs of Boron (325 mesh) and Aluminum Boride (AlB<sub>2</sub>-200 mesh, AlB<sub>12</sub>-325 mesh) Powders

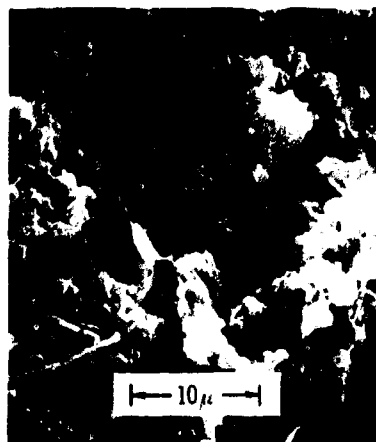
NOT REPRODUCIBLE



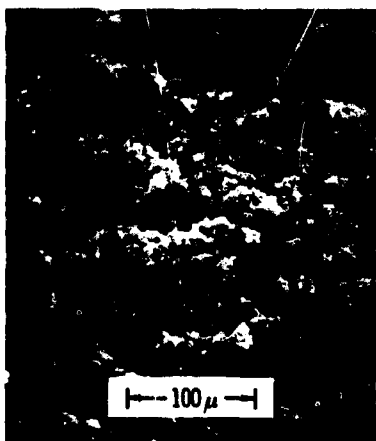
Mg B<sub>2</sub>



Mg B<sub>2</sub>



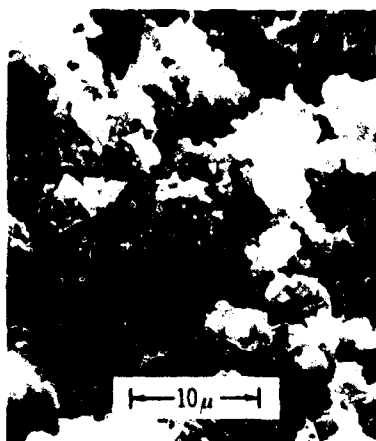
Mg B<sub>2</sub>



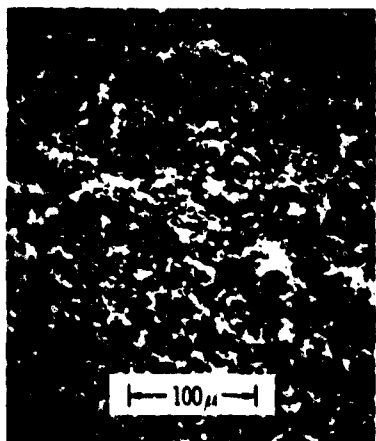
Mg B<sub>6</sub>



Mg B<sub>6</sub>



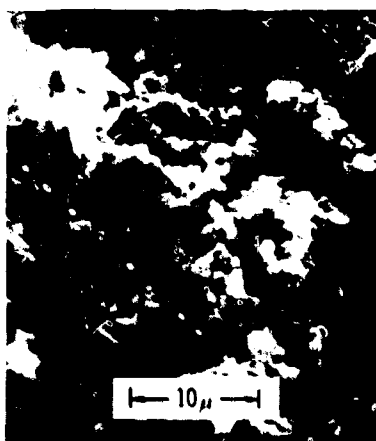
Mg B<sub>6</sub>



Mg B<sub>12</sub>



Mg B<sub>12</sub>



Mg B<sub>12</sub>

Figure 2. Scanning Electron Micrographs of Magnesium Boride Powders (MgB<sub>2</sub>-200 mesh, MgB<sub>6</sub> and MgB<sub>12</sub> -325 mesh)

NOT REPRODUCIBLE

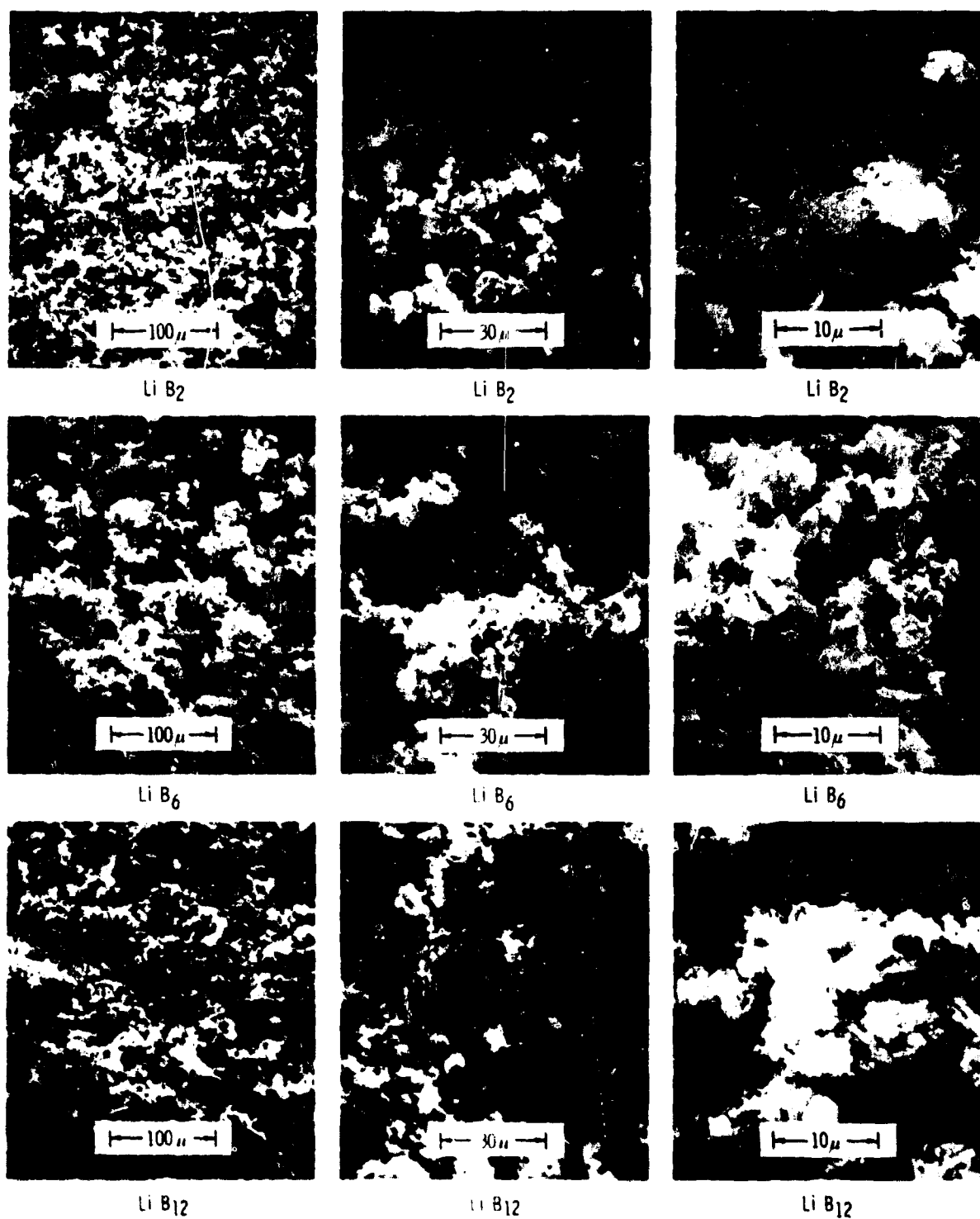


Figure 3. Scanning Electron Micrographs of Lithium Boride Powders (325 mesh)

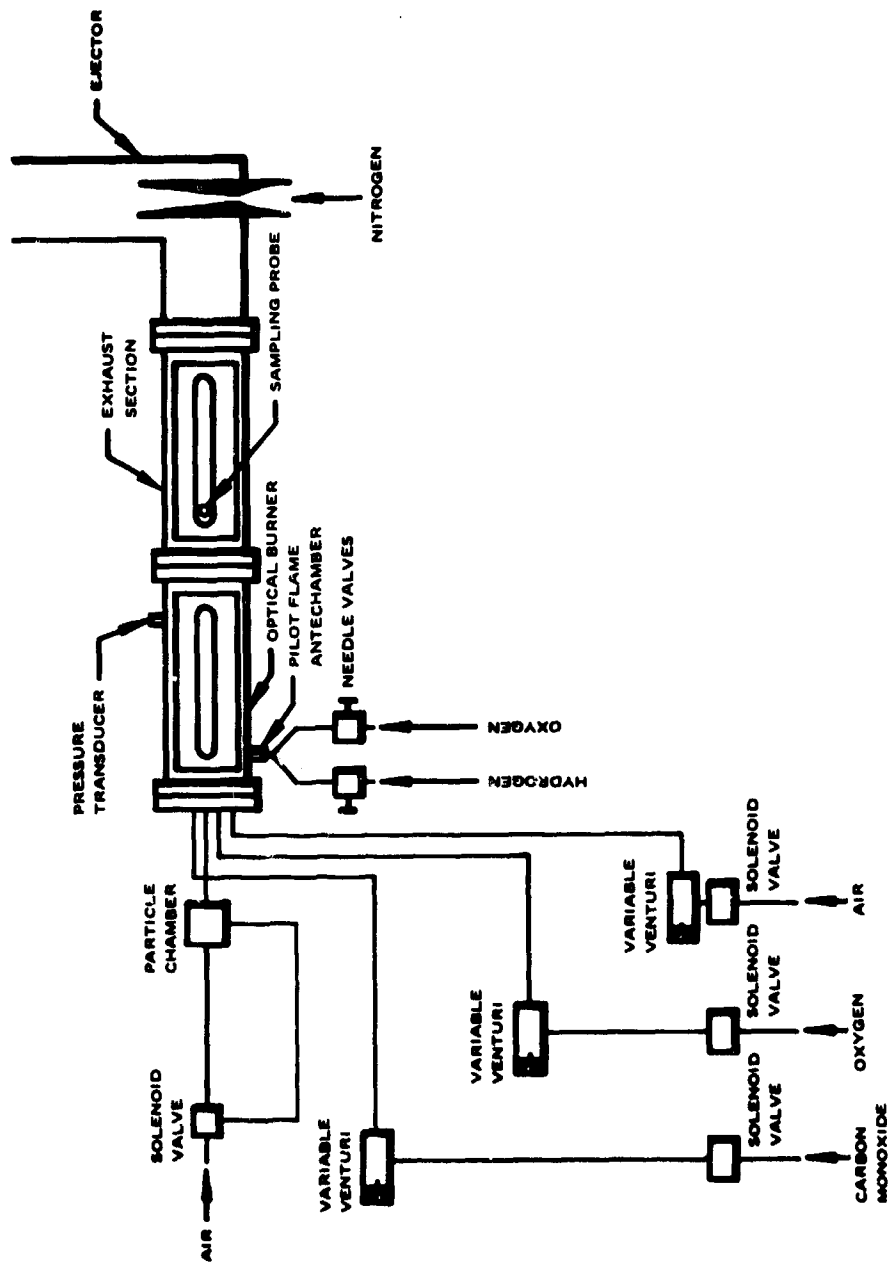


Figure 4. Schematic Diagram of the Test Setup

NOT REPRODUCIBLE

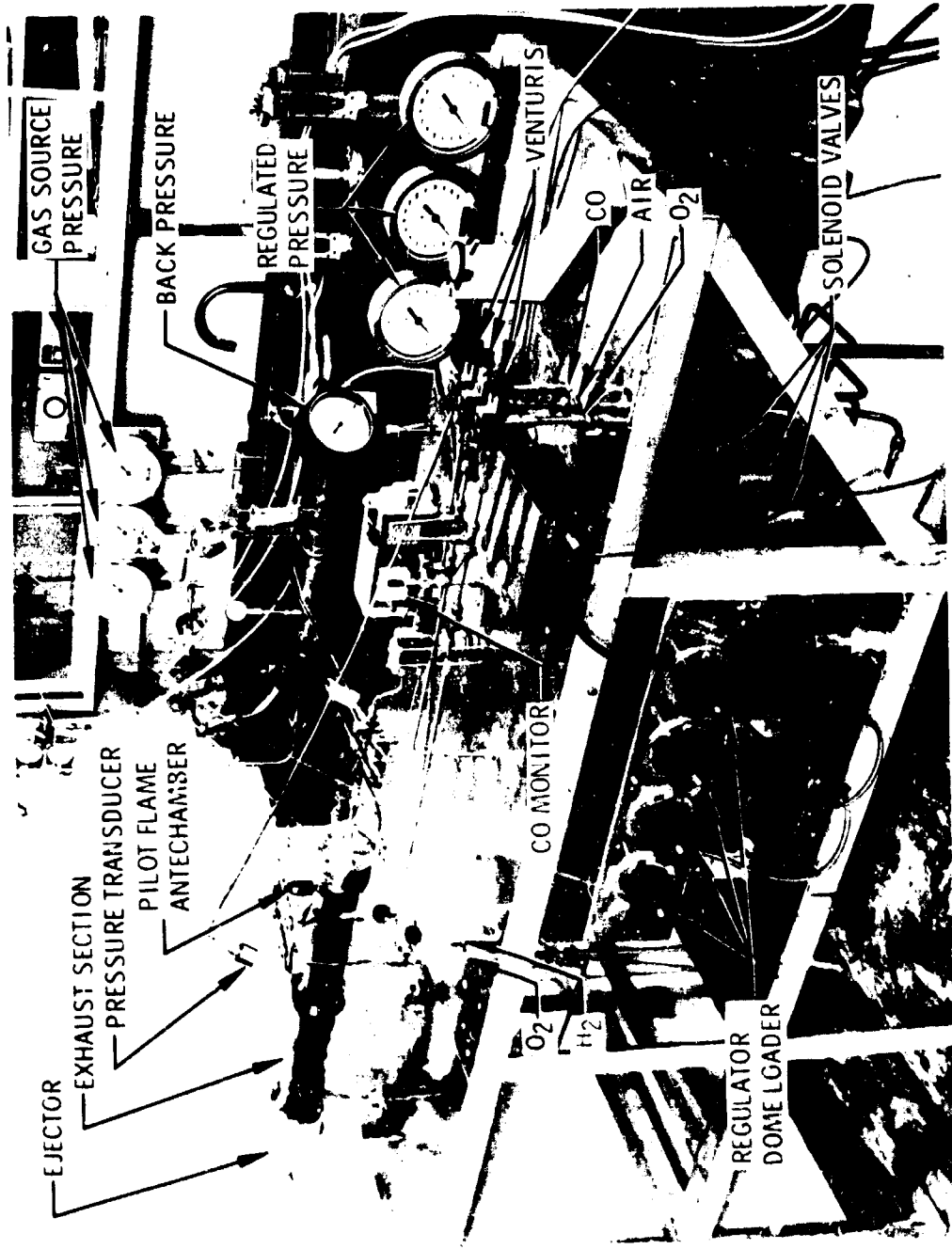
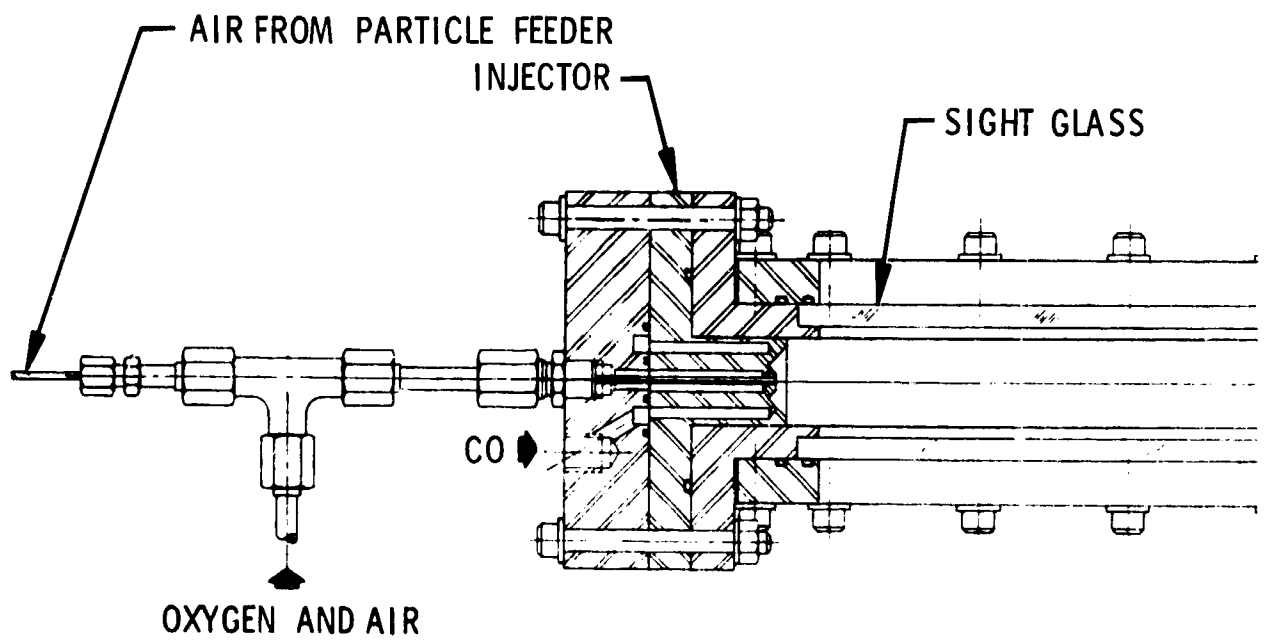
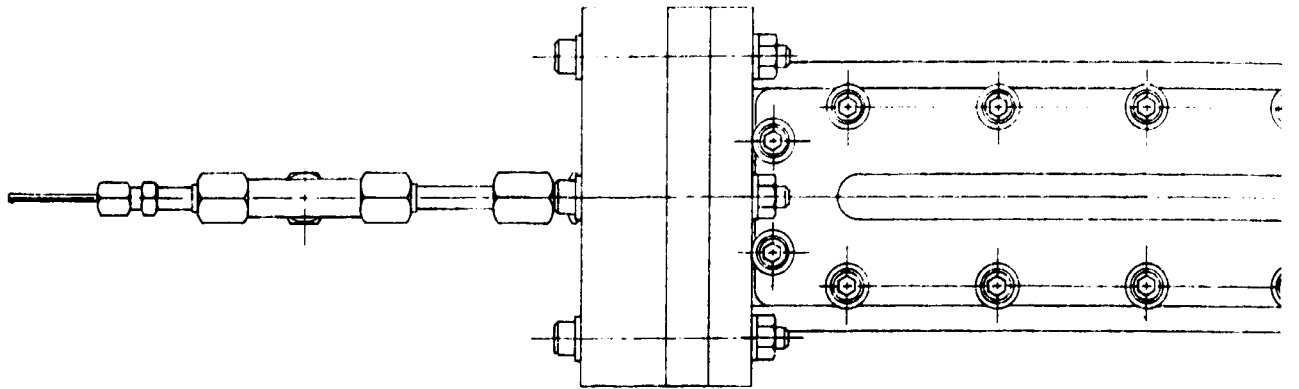


Figure 5. Test Setup

A



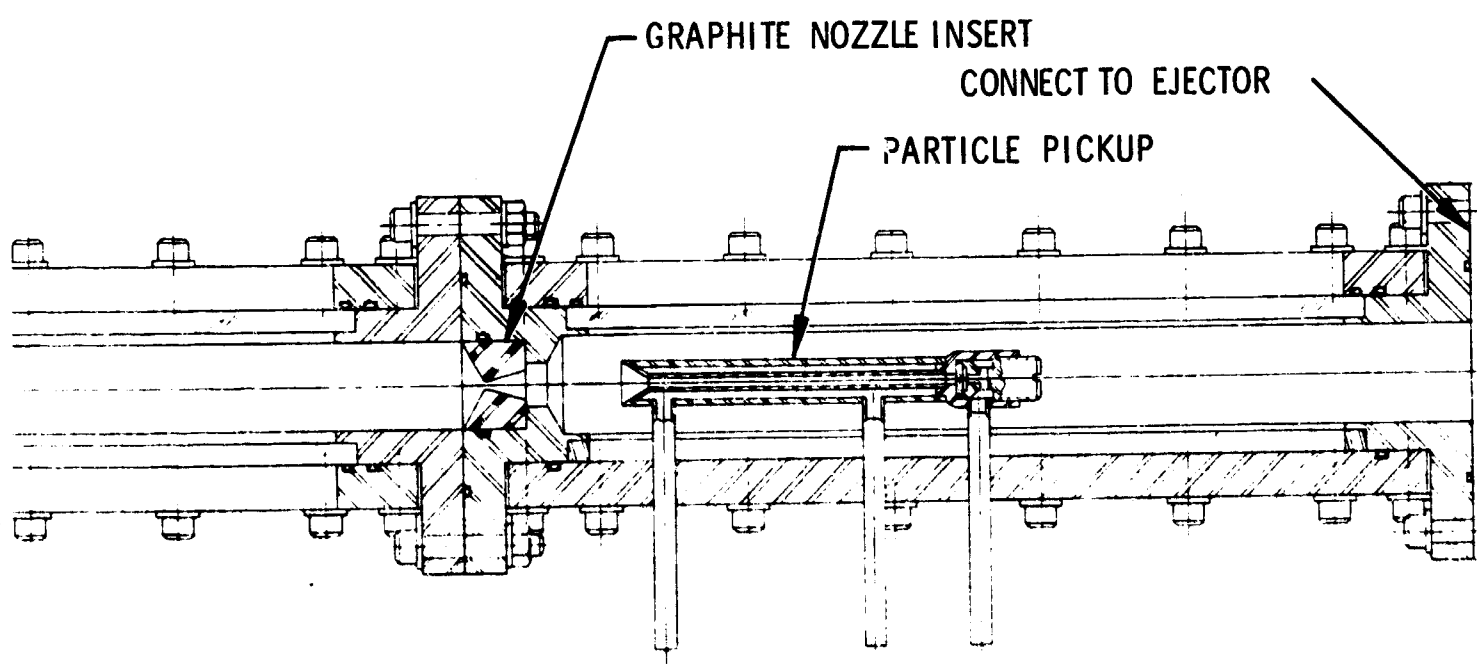
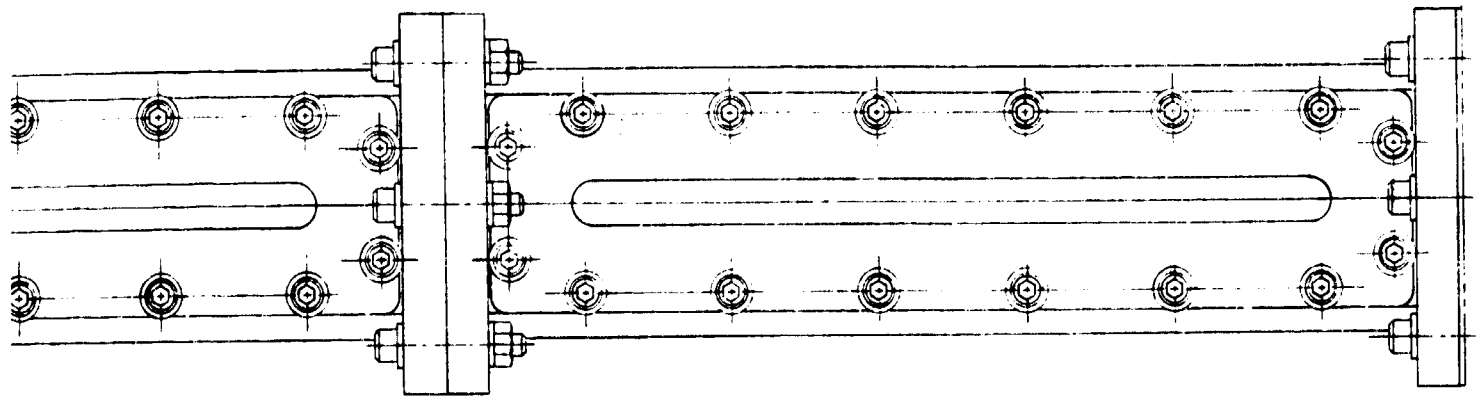


Figure 6. Optical Burner

0.020-in. I.D. stainless steel capillary tube was fitted coaxially inside the oxygen inlet port and served for the injection of solid fuel. Air was used as the carrier for the solid particles and at the same time served as a diluent to lower the temperature of the burnt gases. Four combustion chambers, with lengths of 3, 6, 9 and 12 in., were available. Taps for monitoring pressures and temperature were installed near the exhaust end of the chamber.

An exhaust duct was mounted downstream of a replaceable nozzle section. This duct could be fitted with two windows or a sampling probe. Five different sizes of graphite inserts were fabricated for use in the replaceable nozzle section to yield 5, 10, 15, 25 and 40 psia burner pressure at a specific flow rate setting. Difficulty was experienced in maintaining the desired temperature level, or sometimes even sustaining combustion, when large throat inserts were used. Using a 12-in. long chamber instead of the 6-in. chamber, thus increasing the  $L^*$  by a factor two and facilitating combustion, did not fully resolve the problem. However, a trial-and-error adjustment of  $\text{CO}$ ,  $\text{O}_2$  and air flow rates made it possible to obtain the desired pressure and temperature level for each specific size of nozzle throat insert.

## (2) Ignition System

Ignition was initiated by a pilot flame in an antechamber attached to the main burner which was itself ignited by a spark plug. Originally, the pilot flame operated on small amounts of  $\text{CO}$  and  $\text{O}_2$  regulated by needle valves. Problems were encountered in obtaining a stable pilot  $\text{CO}$  flame since ignition was very sensitive to the gas flow rates and the flame often went out when the spark was turned off. High gas flow rates or long spark durations resulted in rough starts, burnout of the spark plug, and window breakage. On the other hand, low pilot flow rates or short spark durations failed to give good combustion and caused carbon to deposit on the window in the main burner. The problem was resolved by switching to a  $\text{H}_2/\text{O}_2$  pilot flame and by installing fixed orifices in lieu of the needle valves to insure a stoichiometric flow rate ratio in the pilot gas supply. Satisfactory ignition of the main burner gas was achieved with a pilot flame turned on for the first second only, in total run times up to 10 seconds. Any effect of the presence of water vapor on the combustion of the materials under investigation should be negligible under these circumstances.

## (3) Particle Feed System

The particle feed system is shown in Figure 7. The diluent air supply to the main burner also provided the air supply to the particle injector. The latter was taken off through a tee placed downstream of the main air venturi so that no correction to the chamber condition was necessary for the air injected through the particle feeder. A check valve in the main air line downstream of the tee provided a small pressure drop which was independent of the absolute pressure of the system. This pressure drop assured a positive flow of air through the particle feeder throughout a firing.

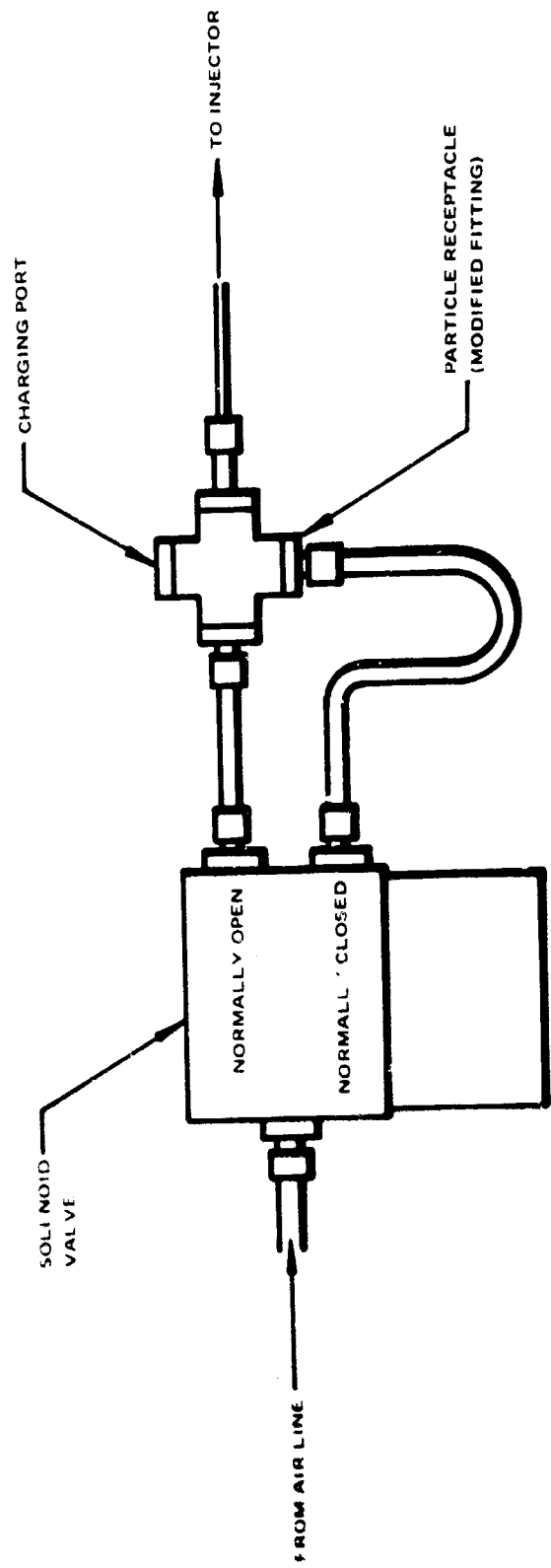


Figure 7. Particle Feed Mechanism

In operation, air began to flow through the particle injector as soon as the main combustion gas valves opened. The solenoid valve on the injector was not activated, and the air flowed through the normally open port without disturbing the particle container. After six seconds of firing, when flow rates and pressures had stabilized, the injector solenoid valve was activated; the air flow was diverted through a stainless steel fine mesh screen which supported the particle charge, and the latter was fed into the combustion chamber.

To feed the particle charge evenly into the chamber, the solenoid was energized via an electric switching device which turned on and off at 6-7 cycles/sec. The fine mesh screen experienced burnout when loaded with a large quantity of  $\text{LiB}_2$  during residue collection runs, probably caused by reaction taking place between the  $\text{LiB}_2$  and the air. The screen was therefore replaced by a stainless steel ball which covered the bottom port of the particle container and kept the particle charge in place, and floated in the container when air was introduced through the bottom port.

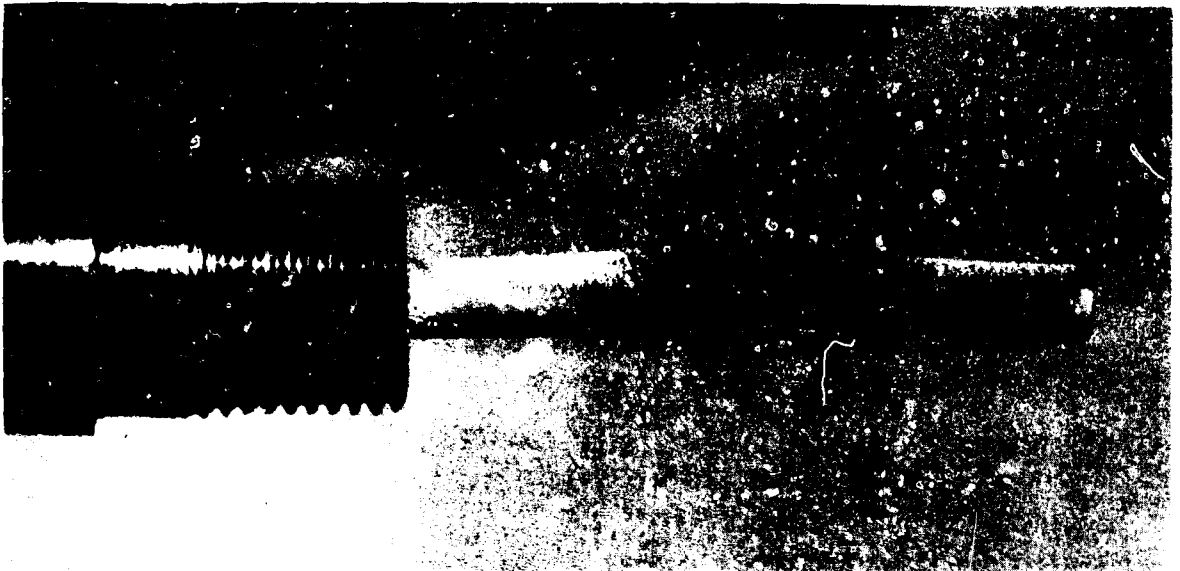
#### (4) Sampling Probe

The sampling probe available from the program carried out under a previous contract was a miniature water-cooled condenser designed for insertion into the exhaust gases immediately downstream of the nozzle (Figure 6). In the previous program, difficulties were experienced in obtaining samples; the sampling probe burned out twice, once because of inadequate cooling water and once because of a faulty weld. These difficulties repeated themselves during the present program and it was found to be impractical to make the probe operative. Instead, a commercial water-cooled gas sampling probe (United Sensor and Control Corporation GC-24-24-050) was obtained and used.  $1.2\mu$  porous filter paper installed and supported by a fine mesh screen particle trap was used in the outlet duct of the sampling probe for combustion residue collection. However, the amount of residue collected during a test run was too small for X-ray diffraction analysis. Alternatives were therefore sought, and a much simpler technique resulted which made it possible to collect adequate amounts of the burned or unburned particles issuing from the burner. This consisted of a 1/8-in. diameter tungsten rod inserted across the gas-particle stream. The residues deposited on the rod and showed color variations reflecting the radially varying exhaust gas-particle composition (Figure 8). The residues scraped from the rod also had the advantage of representing an average exhaust sample of the entire flow field, while a stationary probe could collect a sample at one radial position only. The tungsten rod technique was used throughout the residue collection test runs. It should, however, be realized that the particles scraped from the rod do not represent a properly weighted average sample of the particles in the exhaust flow, because the diameter of the rod was constant while the annular cross-section of the flow is a function of the radial position. Thus the sample from the rod gave too much weight to the core flow where the heavier particles would tend to concentrate.

NOT REPRODUCIBLE



(a) Facing The Exhaust Stream



(b) Side View of (a)

Figure 8. Typical Residue from Combustion of  $MgB_2$  Collected on Tungsten Rod

## (5) Ejector System

An ejector system was designed, fabricated and installed to provide the exhaust vacuum required for the low pressure runs. The ejector system replaced a closed vacuum tank originally installed, which presented a potential hazard due to the possibility of the formation of an explosive mixture in the tank. As shown in Figure 9, the ejector used nitrogen from a high pressure reservoir to drive the exhaust gas through the concentric channel. The back pressure reached the desired 2 psia as required to permit running the combustion chamber at 5 psia.

### b. Gas Supply System

All CO, O<sub>2</sub> and air used were supplied by commercial bottled gases (air and O<sub>2</sub> by Liquid Carbonic Corp., CO commercial grade by Matheson Company). Three sets of regulators, valves and control venturis were provided for control of the flow of CO, O<sub>2</sub> and air. A fourth system, originally designed to be compatible with fluorine, served as a spare. Remotely operated regulators reduced the supply pressure to the desired working pressure. The gases were metered through variable venturis calibrated with nitrogen against standard orifices.

### c. Control Console and Sequencer

A schematic diagram of the control console containing the sequencer for operating the optical burner system is shown in Figure 10. This sequencer provided for programmed operation of the burner control components. Six individual channels were available; one channel was hard-wired in, the other five could be programmed by utilizing a patchboard to set up the desired sequence. Five of the outputs provided 28-vdc power, the sixth supplied a contact closure for remote starting of recorders. A manual switch for purging the burner with inert gas was also provided.

To provide the most versatility, the sequencer made use of a relay-controlled switch, switch driver, and patch panel. This allowed the operator to set up a sequence in which power would switch any function on and off repeatedly, and to vary the time for each condition.

The stepper switch was relay-operated and consisted of 10 banks of contacts; each bank contained 10 active positions and a home position. One bank of contacts was used to supply timing resistors for the driver, and one bank was used for supplying power to a series of lights which indicated the position of the switch. Five banks were wired to the patch panel for programming, one bank was hard-wired in for the ignition function, and the remaining two banks were spares.

The stepper switch driver was a solid-state device used to switch power on and off the stepper switch solenoid. The time that the switch was in any one position could be varied by connecting an ex-

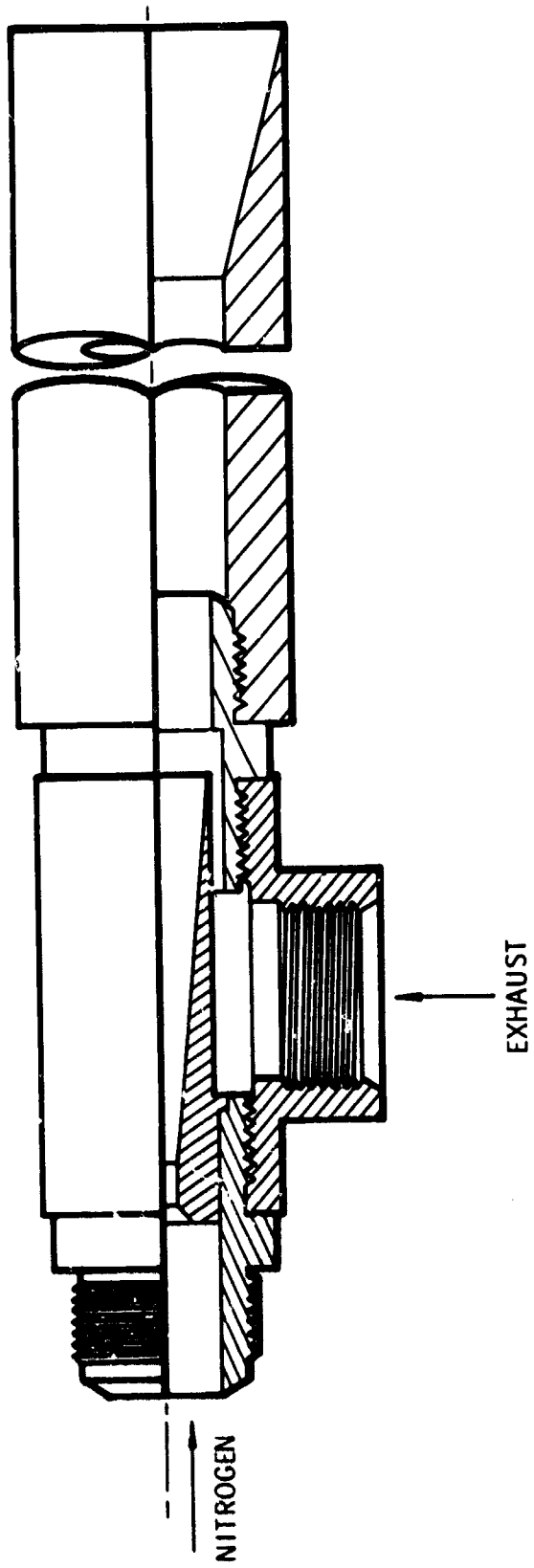
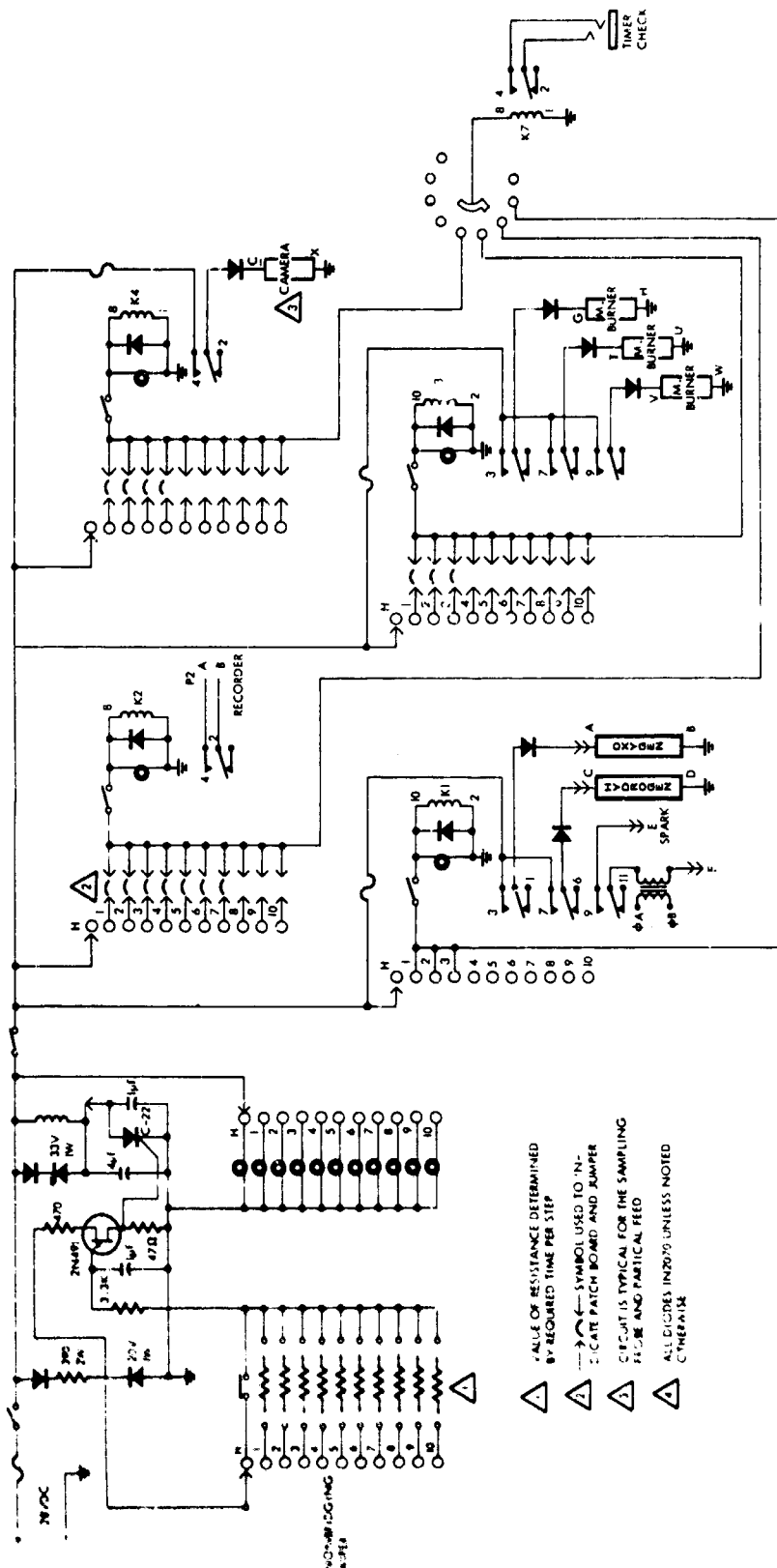


Figure 9. Ejector



- △ VALUE OF RESISTANCE DETERMINED BY REQUIRED TIME PER STEP
- △ SYMBOL USED TO INDICATE PATCH BOARD AND JUMPER
- △ CIRCUIT IS TYPICAL FOR THE SAMPLING FLAME AND PARTIAL FEE
- △ ALL VALUES IN 2070 UNLESS NOTED OTHERWISE

Figure 10. Schematic Diagram of Sequencer

ternal resistor across the test jacks supplied for this purpose. One pair of jacks was supplied for each step position of the switch. The time for each step could be varied from approximately 70 msec to 5 sec. A variable resistance device was incorporated in the control console for quick and more precise adjustment of the sequence.

Provisions were included in the sequence to enable the operator to check the time duration of any step of the switch or the time duration of the entire sequence. A phone jack was provided on the side of the console; by plugging a standard timer into this jack and selecting the desired channel on the timer check rotary switch, the time for that particular event could be checked.

The patch panel consisted of 10 rows of 10 contacts. Two rows of contacts were utilized for each control function. One row of contacts was wired together and connected to the output function control switch. The other row was connected to the contacts of the stepper switch. The wiper of the stepper was wired to +27 vdc; as the stepper was advanced the contacts picked up the 28 v and applied it to the patch board. If a patch wire was plugged into the board this voltage was jumped onto the common bus and applied to the load. This was typical for each channel.

The function control switches were supplied power from the patch board. If a particular channel was patched in and the control switch turned on, an indicator light next to the switch lighted when that channel was activated, indicating that power was present and that a relay was energized. The contacts of the stepper switch had a low-power switching capacity; therefore, an additional relay was used to supply power to the load. Loads requiring up to 5 amp at 28 vdc could be powered from this sequencer. The recorder channel was an exception to the above; instead of switching 28 vdc to the output, it supplied a contact closure which was used to turn a recorder on and off remotely.

The emergency shutdown switch was the main power shut-off switch. In order to have power available to the output, this switch had to be in the "on" position. If for any reason it became necessary to cut off power to the load during the sequence, the red switch guard was pushed down which cut off all output power. The sequencer would continue to step through the remaining steps until it hit the home position where it would stop; however, no power would be supplied to the load during this time.

d. Photography

Two cameras were originally used in this study, a Hycam\* K-1001 and an Automax† pulse camera. The use of the pulse camera at different settings only occasionally produced usable particle traces. On the other hand, excellent results were obtained with the Hycam camera at frame speeds of 2000 per second and f/2.8 lens aperture. To distinguish burning particles from merely glowing particles, color film was used instead of the black and white film (Linagraph) tried

\* Red Lake Laboratories, Santa Clara, California

† Triad Corporation, Los Angeles, California

in the beginning. Kodak Ektachrome type EF has an ASA rating of 160. By special processing an equivalent rating of ASA 640 was obtained. The high speed of the camera was used to limit the motion of the particles in each frame and thereby permit measurement of the velocity by comparing the location in subsequent frames. Typical particle traces are shown in successive frames in Figure 11. As can be seen, the ignition delay and burning times could be determined from the locations which a particle started and finished its burning process.

e. Data Recording

A platinum-platinum/10% rhodium thermocouple (Tempton, Inc.) was used to measure the flame temperature just upstream of the exhaust nozzle during calibration. The burner pressure was monitored by a CEC (Consolidated Engineering Corporation) pressure transducer model 4-327-001, connected to a pressure tap located at 90° to the thermocouple connection. Both temperature and pressure measurement were recorded by a CEC recorder type 5-124.

f. Particle Size Separation

All the particles procured were separated by particle size, using No. 200, 250, 270, 325 and 400 mesh brass sieves in a Roto-Tab shaker. MgB<sub>2</sub>, AlB<sub>2</sub> and B powders, originally-200 mesh (less than 74μ), were separated into four size lots between 37, 44, 53, 63 and 74μ. The other powders originally -325 mesh (less than 44μ), were sieved into one size lot between 37 and 44μ. In most of the test runs, 37-44μ particles were used.

g. Safety Equipment

Since carbon monoxide is classified as a chemical asphyxiant, the burner cell exhaust was ducted through the outside wall of the building. During test operation, a CO monitor (UNICO Model 888) in the room was activated to insure no CO had escaped.

#### 4. CALIBRATION OF BURNER TEST CONDITIONS

The test conditions were originally intended to be 5, 10, 15, 25 and 40 psia at 2000 and 1700°K, using a nozzle with 0.336-in. throat diameter. Pictures taken in early runs showed that nearly all particles were still burning when they left the 12-in. chamber, making it impossible to determine the total burning time. To increase the particle residence time in the chamber, the nozzle diameter was changed to 0.200 in. It was also early decided to drop the temperature settings to 1650 and 1400°K in view of the success in getting ignition of MgB<sub>2</sub> at these lower temperatures. Difficulty was encountered in obtaining a precise 5 psia setting at these two temperature levels without further adjustment of the throat size. As a compromise a setting of 5 psia at 1250°K was accepted. The measured pressures and temperatures at nine conditions used are listed in Table VI, along with the flow rates of CO, O<sub>2</sub> and

NOT REPRODUCIBLE

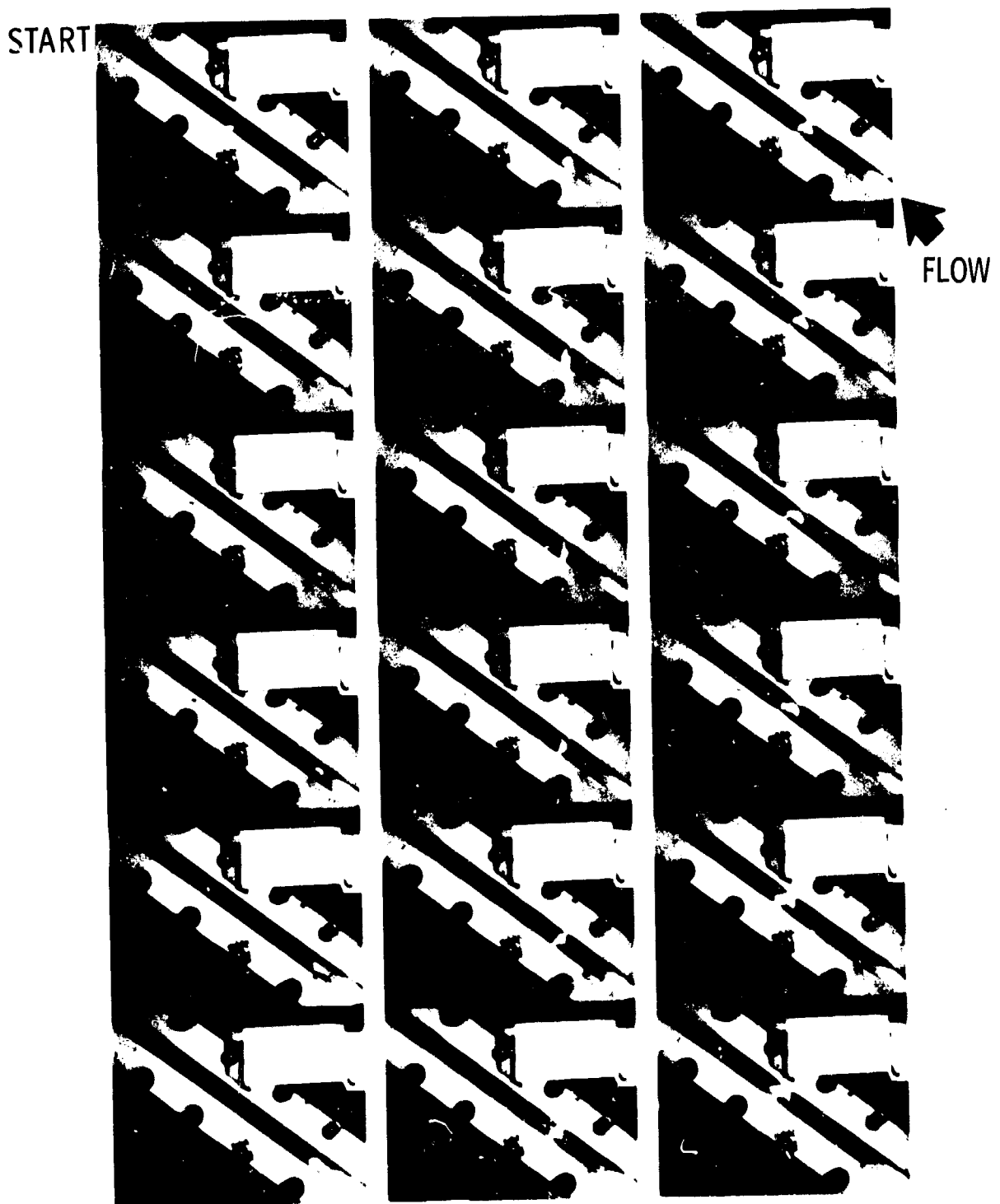


Figure 11. Typical Particle Traces (Run No. 4-12-71-7,  
44 to 53 $\mu$  MgB<sub>2</sub> burned at 1650°K, 14.5 psia)  
(Sheet 1 of 2)

NOT REPRODUCIBLE

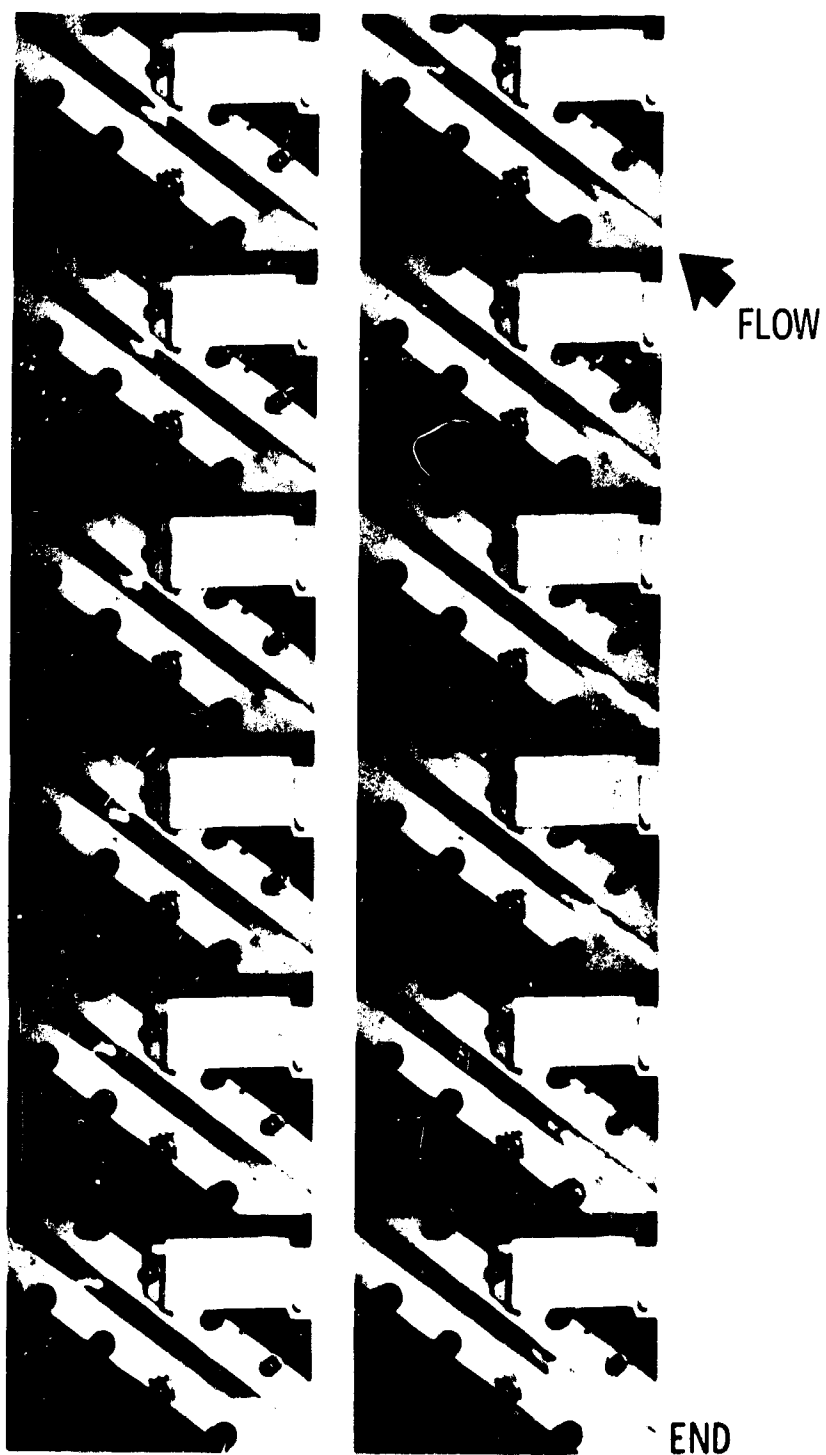


Figure 11. Typical Particle Traces (Run No. 4-12-71-7,  
44 to 53 $\mu$  MgB<sub>2</sub> burned at 1650°K, 14.5 psia)  
(Sheet 2 of 2)

TABLE VI

THEORETICAL AND MEASURED TEST CONDITIONS

Cal-Station Number	Flow Rate, lb/sec		Air CO <sub>2</sub> Ratio	D <sub>t</sub> in.	A <sub>t</sub> in. <sup>2</sup>	Theoretical				Measured			Residence Time, sec		
	O <sub>2</sub>	Air				T <sub>c</sub> , °K	C <sub>t</sub> , fps	Γ <sub>c</sub> , psia	M	T <sub>c</sub> , °K	P <sub>c</sub> , psia	V <sub>c</sub> , in./sec		C <sub>t</sub> <sup>*</sup> Effective	
UTC 1515-21	0.00262	0.004625	0.0081	1.118	0.2	0.0314	2576	4069	61.77	34.06	1650	41.5	0.662	658	14.4
-22	0.0019	0.003315	0.00427	0.818	0.2	0.0314	2696	4172	39.14	34.46	1675	26.8	0.685	631	15.1
-23	0.0017	0.003	0.00557	0.119	0.2	0.0314	2963	4348	22.61	35.39	1650	14.8	0.655	608	15.6
-24	0.00107	0.001867	0.000239	0.081	0.2	0.0314	2926	4329	13.60	35.29	1625	9.5	0.698	548	17.3
-25	0.002135	0.003695	0.01418	2.432	0.2	0.0314	1893	3489	69.06	32.15	1430	44	0.638	740	12.8
-26	0.001675	0.002325	0.00456	0.991	0.2	0.0314	2612	4108	37.22	34.15	1400	25	0.672	550	17.3
-27	0.001186	0.002075	0.002305	0.707	0.2	0.0314	2709	4191	23.08	34.51	1400	15.2	0.658	557	17.1
-28	0.00083	0.001515	0.000902	0.384	0.2	0.0314	2802	4260	13.71	34.81	1410	9.4	0.687	515	18.4
-29	0.000502	0.000875	0.000318	0.231	0.2	0.0314	2798	4261	7.144	34.86	1250	5.5	0.77	406	23.4

air. A typical pressure and temperature trace is shown in Figure 12.

Calculations were carried out to evaluate the theoretical equilibrium conditions for the CO-O<sub>2</sub>-air combustion system at pressures corresponding to a given set of mass flow rates and given throat area. The results are listed in Table VI.

The characteristic velocity c\* was computed from the relationship between pressure, flow rate and throat area. Comparing the experimental values with the theoretical ideal characteristic velocity, c\* efficiencies were derived which are also listed in Table VI.

The mean gas velocity, V<sub>c</sub>, in the burner cell was calculated from the flow rate, the measured temperature T<sub>c</sub> and pressure P<sub>c</sub>, and the theoretical molecular weight M<sub>c</sub> by using the relationship

$$V_c = \frac{\dot{w} R_o T_c}{A_c M_c P_c}$$

where R<sub>o</sub> is the universal gas constant and A<sub>c</sub> the cross-sectional area of the chamber. This velocity was later spot-checked against the particle velocity measurement obtained by high-speed photography, assuming no particle lag. Good agreement was found.

The thermal properties of the gas system and the composition of the combustion products were also printed out in the thermochemical computer program study. These data are attached as Appendix I.

## 5. EXPERIMENTAL RESULTS AND DISCUSSION

The objective of the experimental study was to determine ignition delay times and burn times by photographic tracking of doped and undoped boron and boron-metal compounds, and to determine the combustion efficiencies by X-ray diffraction or wet chemical analyses. The parameters studied were the particle chemical composition, the particle size, the combustion pressure and temperature, and the effects of dopants. Since particle tracking requires that only a small quantity of particles be used in order that individual particle traces can be studied, and residue collection required heavier particle loading to obtain adequate samples for analysis in the available run time, these two types of tests had to be run separately. In the majority of cases the test conditions in the two kinds of tests were identical; these conditions are listed in Tables VII and VIII, the pressures representing actual measured values. In runs with particles the thermocouple was removed to avoid obstruction of the flow. The temperatures listed are those measured previously in the calibration process; these were spot-checked occasionally to confirm a variance of the temperature reading of less than 2%.

### a. Combustion Characteristics

Nearly 100 combinations of test conditions were used. All 37-44μ particles were burned at 1650°K and 10, 15, 25 and 40 psia, and at 1250°K and 5 psia.

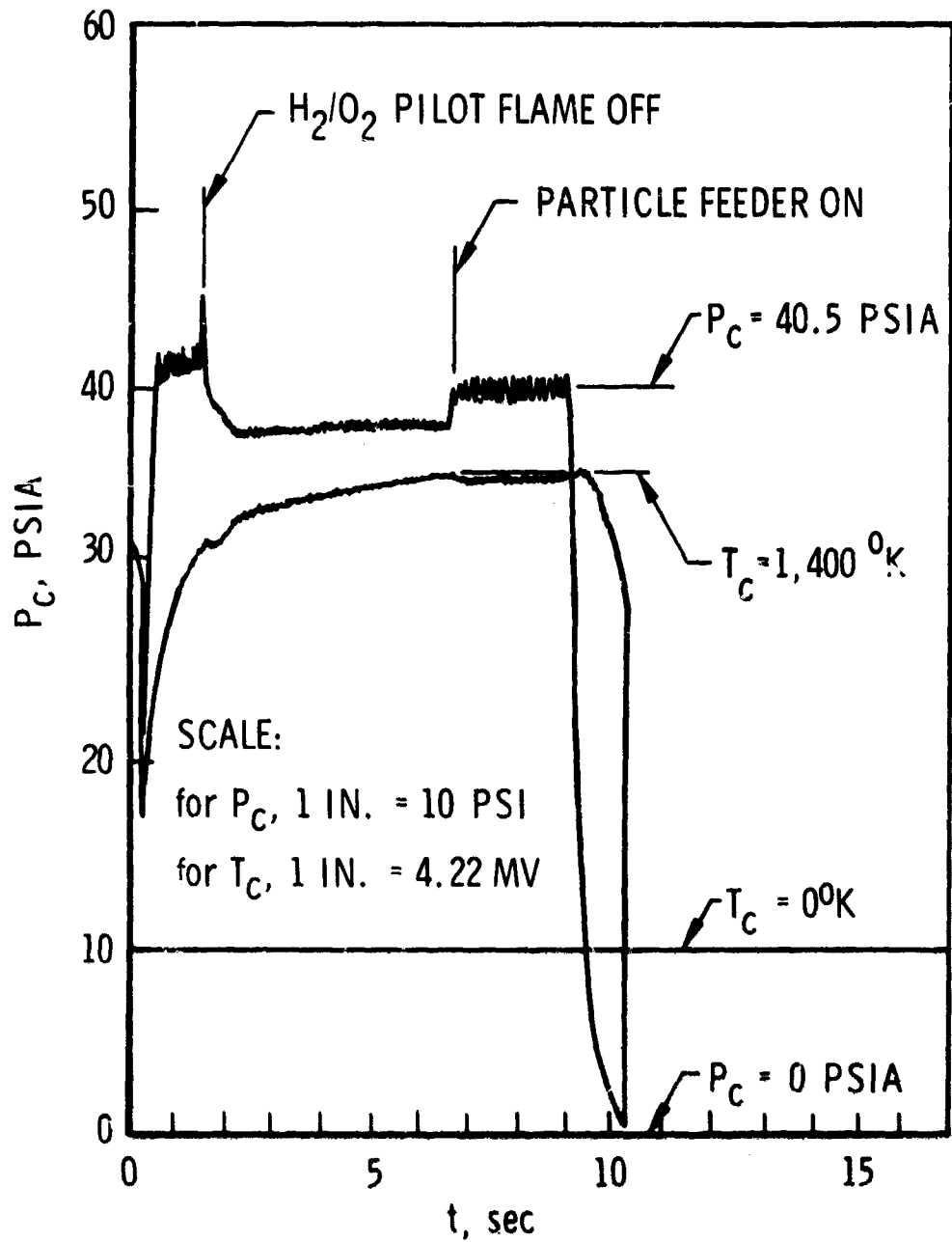


Figure 12. Typical Pressure and Temperature Traces

TABLE VII

X-RAY DIFFRACTION OF COMBUSTION RESIDUES

Residue Collection Run No.	Particles	Corresponding Particle Tracking			X-Ray Diffraction Pattern		
		P <sub>c</sub> pairs	Run No.	P <sub>c</sub> pairs	Major	Minor	Trace
4-28-71-3	MgB <sub>2</sub>	37.0	3-10-71-1	37.5	1430	MgB <sub>4</sub>	MgO
4-28-71-4	37-44μ	25.5	3-10-71-2	24.5	1400	MgB <sub>4</sub>	MgO
4-28-71-5		15.5	3-10-71-3	14.0	1400	MgB <sub>4</sub> , MgB <sub>6</sub>	Mg <sub>2</sub> B <sub>2</sub> O <sub>5</sub>
4-28-71-6		9.0	3-10-71-4	8.5	1410	MgB <sub>4</sub>	Mg <sub>2</sub> B <sub>2</sub> O <sub>5</sub>
4-28-71-1		5.0	3-10-71-5	5.8	1250	MgO	MgB <sub>6</sub>
4-28-71-7		43.0	3-8-71-1	42.0	1935	MgB <sub>4</sub> , MgB <sub>6</sub>	MgO
4-27-71-1		42.5	4-13-71-1	39.7	1650	MgB <sub>4</sub>	hexagonal B <sub>2</sub> O <sub>3</sub>
4-27-71-2		28.0	4-13-71-2	26.3	1675	MgB <sub>4</sub>	hexagonal B <sub>2</sub> O <sub>3</sub>
4-27-71-3	MgB <sub>2</sub>	15.5	4-13-71-3	14.0	1650	MgB <sub>4</sub>	hexagonal B <sub>2</sub> O <sub>3</sub>
4-28-71-2	37-44μ	10.0	4-13-71-4	8.3	1625	MgO	hexagonal B <sub>2</sub> O <sub>3</sub>
5-3-71-5	Boron	42.0	3-10-71-10	35.0	1430	B <sub>2</sub> O <sub>3</sub>	α B
5-3-71-6	37-44μ	26.5	3-10-71-9	25.0	1400	hexagonal B <sub>2</sub> O <sub>3</sub>	β B
5-3-71-7		16.0	3-10-71-8	14.0	1400	hexagonal B <sub>2</sub> O <sub>3</sub>	α B, β B
5-3-71-8		10.0	3-10-71-7	8.5	1410	hexagonal B <sub>2</sub> O <sub>3</sub>	α B
5-3-71-9		6.8	3-10-71-6	5.8	1250	hexagonal B <sub>2</sub> O <sub>3</sub> , α B	β B
5-3-71-10		41.0	-	-	1935	hexagonal B <sub>2</sub> O <sub>3</sub>	---
5-3-71-1		39.0	4-1-71-3	42.5	1650	hexagonal B <sub>2</sub> O <sub>3</sub>	β B
5-3-71-2		27.5	3-31-71-5	26.0	1675	hexagonal B <sub>2</sub> O <sub>3</sub>	hexagonal B <sub>2</sub> O <sub>3</sub>
5-3-71-3	Boron	15.2	3-31-71-6	15.0	1650	α B	hexagonal B <sub>2</sub> O <sub>3</sub>
5-3-71-4	37-44μ	11.5	4-1-71-2	9.0	1625	α B	hexagonal B <sub>2</sub> O <sub>3</sub>
5-4-71-5	AlB <sub>2</sub>	39.0	3-10-71-5	35.0	1430	Al	9Al <sub>2</sub> O <sub>3</sub> ·2B <sub>2</sub> O <sub>3</sub>
5-4-71-4	37-44μ	25.0	3-10-71-4	25.0	1400	2Al <sub>2</sub> O <sub>3</sub> ·B <sub>2</sub> O <sub>3</sub> , Al	B <sub>2</sub> O <sub>3</sub>
5-4-71-3		15.5	3-10-71-3	15.8	1400	Al	AlB <sub>2</sub> , 9Al <sub>2</sub> O <sub>3</sub> ·2B <sub>2</sub> O <sub>3</sub>
5-4-71-2		10.5	3-10-71-2	10.0	1410	Al	9Al <sub>2</sub> O <sub>3</sub> ·2B <sub>2</sub> O <sub>3</sub>
5-4-71-1		6.0	3-10-71-1	5.0	1250	Al	9Al <sub>2</sub> O <sub>3</sub> ·2B <sub>2</sub> O <sub>3</sub>
5-4-71-9		42.0	4-13-71-5	41.0	1650	2Al <sub>2</sub> O <sub>3</sub> ·B <sub>2</sub> O <sub>3</sub>	9Al <sub>2</sub> O <sub>3</sub> ·2B <sub>2</sub> O <sub>3</sub>
5-4-71-8		26.0	4-13-71-6	27.0	1675	2Al <sub>2</sub> O <sub>3</sub> ·B <sub>2</sub> O <sub>3</sub>	9Al <sub>2</sub> O <sub>3</sub> ·2B <sub>2</sub> O <sub>3</sub>
5-4-71-7	AlB <sub>2</sub>	14.5	4-13-71-7	14.3	1650	9Al <sub>2</sub> O <sub>3</sub> ·2B <sub>2</sub> O <sub>3</sub>	B <sub>2</sub> O <sub>3</sub>
5-4-71-6	37-44μ	10.0	4-13-71-8	8.0	1625	Al	B <sub>2</sub> O <sub>3</sub>



TABLE VII

X-RAY DIFFRACTION OF COMBUSTION RESIDUES (Concluded)

Residue Collection Run No.	Particles	Corresponding Particle Tracking		X-Ray Diffraction Pattern				
		P <sub>c</sub> psia	Run No.	P <sub>c</sub> psia	T <sub>c</sub> °K	Major	Minor	Trace
5-19-71-5	Boron	47.0	4-2-71-12	42.0	1650			
5-19-71-4	63-74μ	29.0	4-2-71-13	27.5	1675			
5-19-71-3	Boron	16.0	4-2-71-14	15.5	1650		hexagonal B <sub>2</sub> O <sub>3</sub>	
5-19-71-2	Boron	10.5	4-2-71-16	9.0	1625		hexagonal B <sub>2</sub> O <sub>3</sub>	α B, β B
5-19-71-1	63-74μ	5.0	4-2-71-15	5.0	1250		hexagonal B <sub>2</sub> O <sub>3</sub>	β B
	Boron		4-12-71-1	41.5	1650			
	44-53μ		4-12-71-2	27.0	1675			
	Boron		4-12-71-3	15.0	1650			
	44-53μ		4-12-71-4	9.0	1625			
5-20-71-5	MgB <sub>2</sub>	44.0	4-2-71-2	41.0	1650			
5-20-71-4	63-74μ	30.0	4-2-71-3	26.5	1675			
5-20-71-3	MgB <sub>2</sub>	15.0	4-2-71-4	14.0	1650			
5-20-71-2	MgB <sub>2</sub>	10.0	4-2-71-6	10.0	1625			
5-20-71-1	63-74μ	4.0	4-2-71-5	5.0	1250			
	MgB <sub>2</sub>		4-12-71-5	42.0	1650			
	44-53μ		4-12-71-6	27.5	1675			
	MgB <sub>2</sub>		4-12-71-7	15.4	1650			
	44-53μ		4-12-71-8	9.6	1625			
	AlB <sub>2</sub>		4-2-71-7	42.0	1650			
	63-74μ		4-2-71-8	27.0	1675			
	AlB <sub>2</sub>		4-2-71-9	14.5	1650			
	63-74μ		4-2-71-11	9.0	1625			
	AlB <sub>2</sub>		4-2-71-10	5.0	1250			
	AlB <sub>2</sub>		4-12-71-9	42.7	1650			
	44-53μ		4-12-71-10	28.0	1675			
	AlB <sub>2</sub>		4-12-71-11	15.4	1650			
	44-53μ		4-12-71-12	8.7	1625			

TABLE VIII

X-RAY DIFFRACTION OF RESIDUE  
FROM COMBUSTION OF 1½% LiF DOPED PARTICLES

Residue Collection Run No.	Particles	P <sub>c</sub>		Run No.	P <sub>c</sub>		T <sub>c</sub> °K	X-Ray Diffraction Pattern		
		Fsi	psia		psi	psi		Major	Minor	Trace
5-24-71-D1	Boron 37-44μ	44.0	40.0	4-20-71-1	B <sub>2</sub> O <sub>3</sub>	hexagonal B <sub>2</sub> O <sub>3</sub>	1650	---	---	---
5-24-71-D2	Boron 37-44μ	5.0	5.5	4-20-71-2	(Tungsten) <sup>a</sup>	B <sub>2</sub> O <sub>3</sub> , hexagonal B <sub>2</sub> O <sub>3</sub>	1250	---	---	---
5-24-71-D4	MgB <sub>2</sub> 37-44μ	42.0	42.0	4-20-71-3	Mg <sub>2</sub> B <sub>2</sub> O <sub>5</sub>	---	1650	---	αB, βB	---
5-24-71-D3	MgB <sub>2</sub> 37-44μ	5.0	5.0	4-20-71-4	MgO	MgB <sub>4</sub> , MgB <sub>2</sub>	1250	MgB <sub>4</sub> , MgB <sub>2</sub>	Mg <sub>2</sub> B <sub>2</sub> O <sub>5</sub>	---
5-24-71-	MgB <sub>2</sub> 37-44μ	42.3	42.0	4-20-71-5	Mg <sub>2</sub> B <sub>2</sub> O <sub>5</sub>	B <sub>2</sub> O <sub>3</sub>	1650	B <sub>2</sub> O <sub>3</sub>	---	---
5-24-71-D5	MgB <sub>2</sub> 37-44μ	4.5	5.0	4-20-71-6	B <sub>2</sub> O <sub>3</sub>	MgB <sub>12</sub>	1250	MgB <sub>12</sub>	Mg <sub>2</sub> B <sub>2</sub> O <sub>5</sub>	---
5-24-71-D14	LiB <sub>2</sub> 37-44μ	42.0	42.0	4-20-71-7	Li <sub>2</sub> O·2B <sub>2</sub> O <sub>3</sub>	---	1650	---	hexagonal B <sub>2</sub> O <sub>3</sub> , Li <sub>6</sub> B <sub>4</sub> O <sub>9</sub>	---
5-24-71-D13	LiB <sub>2</sub> 37-44μ	4.5	5.0	4-20-71-8	Li <sub>2</sub> O·2B <sub>2</sub> O <sub>3</sub>	---	1250	---	Li <sub>6</sub> B <sub>4</sub> O <sub>9</sub>	---
5-24-71-D12	LiB <sub>2</sub> 37-44μ	42.5	43.0	4-20-71-9	Li <sub>2</sub> O·4B <sub>2</sub> O <sub>3</sub>	LiB <sub>12</sub>	1650	LiB <sub>12</sub>	---	---
5-24-71-D11	LiB <sub>2</sub> 37-44μ	5.0	5.0	4-20-71-10	Li <sub>2</sub> O·4B <sub>2</sub> O <sub>3</sub>	LiB <sub>2</sub>	1250	LiB <sub>2</sub>	---	---
5-24-71-D8	AlB <sub>2</sub> 37-44μ	42.0	43.5	4-20-71-11	9Al <sub>2</sub> O <sub>3</sub> ·2B <sub>2</sub> O <sub>3</sub>	αAl <sub>2</sub> O <sub>3</sub>	1650	αAl <sub>2</sub> O <sub>3</sub>	B <sub>2</sub> O <sub>3</sub> , 2Al <sub>2</sub> O <sub>3</sub> ·B <sub>2</sub> O <sub>3</sub> , Al	---
5-24-71-D7	AlB <sub>2</sub> 37-44μ	6.0	5.0	4-20-71-12	Al	αAl <sub>2</sub> O <sub>3</sub>	1250	αAl <sub>2</sub> O <sub>3</sub>	B <sub>2</sub> O <sub>3</sub> , AlB <sub>12</sub>	---
5-24-71-D10	AlB <sub>2</sub> 37-44μ	42.0	44.5	4-20-71-13	hexagonal B <sub>2</sub> O <sub>3</sub> 9Al <sub>2</sub> O <sub>3</sub> ·2B <sub>2</sub> O <sub>3</sub>	αAl <sub>2</sub> O <sub>3</sub>	1650	αAl <sub>2</sub> O <sub>3</sub>	---	---
5-24-71-D9	AlB <sub>2</sub> 37-44μ	5.0	5.0	4-20-71-14	hexagonal B <sub>2</sub> O <sub>3</sub>	AlB <sub>12</sub> , 9Al <sub>2</sub> O <sub>3</sub> ·2B <sub>2</sub> O <sub>3</sub>	1250	AlB <sub>12</sub> , 9Al <sub>2</sub> O <sub>3</sub> ·2B <sub>2</sub> O <sub>3</sub>	---	---

<sup>a</sup>Tungsten scrapped from probe surface due to extremely small amounts of residue collected on the probe

With  $\text{MgB}_2$ ,  $\text{LiB}_2$ ,  $\text{AlB}_2$  and B additional tests were made at  $1400^\circ\text{K}$  and 10, 15, 25 and  $40 \text{ psia}$ .<sup>2</sup> In the study of the effects of particle size, additional tests were conducted with the  $44\text{-}53\mu$  and  $63\text{-}74\mu$  size lots of  $\text{MgB}_2$ ,  $\text{AlB}_2$  and B.

Particles were fed to the burner cell intermittently at 6-7 cycles/sec without much control over the number and spacing of the particles. Thus in the film of each run there are portions during which few particles were injected, and portions during which clouds of particles passed by. When a single particle or a sparse particle cloud was injected individual particle traces were clearly distinguishable on the film frames (Figure 11). When the particle concentration increased, ignition occurred closer to the injector, and at large concentration burning was established practically at the injector end of the cell. The density of radiation emanating from a burning cloud of particles was so great that individual particle traces can no longer be identified (Figures 13 and 14). This very early ignition is a consequence of the small average distance between particles which reduces the dissipation of the heat generated by oxidation.

As a result there is a wide range of scatter both in the ignition delay and the burning times of particles in the same test. Therefore average values were taken for each set of experimental conditions. The results are plotted as a function of chamber pressure in Figures 15 through 21, using temperature as a parameter. The ignition delay and burning time for the borides fall in the range of 0-8 msec and 2-15 msec respectively. In general, these times decrease with increasing pressure and temperature, except for  $\text{MgB}_2$ ; the burning time data on this compound are so scattered that no trend can be identified. The elemental boron particles showed a similar ignition delay but their combustion was so slow that in general they were still burning when they left the 12-in. chamber, which had a residence time of 14-24 msec. Alternatively combustion of some boron particles would cease well within the chamber, long before all the boron could possibly have been consumed. It was reported<sup>(2)</sup> that the combustion of boron particles occurs in two successive stages. After the initial heatup, the boron particle becomes luminous, glows for a short period of time, dies out, and reignites to burn completely in a second stage which is much brighter and longer than the first stage. In the current experiment most of the boron particles were probably burning in the first stage only.

The flame of the  $\text{CO-O}_2$ -air mixture had a deep blue color which changed to bright green when magnesium boride, aluminum boride or boron particles were released into it; the lithium boride seeded flame has a pink hue (See Figure 13). At  $1650^\circ\text{K}$ , the degree of flame brightness fell in the following sequence:  $\text{MgB}_2$ ,  $\text{MgB}_{12}$ , B,  $\text{AlB}_{12}$ ,  $\text{AlB}_2$ ,  $\text{LiB}_{12}$  and  $\text{LiB}_2$ . The particle traces of magnesium and lithium borides were often very hazy especially so at low pressures, indicating vapor phase burning. In respect to sharpness of the particle traces at  $1650^\circ\text{K}$  the particles fell in the following descending order: B,  $\text{AlB}_2$ ,  $\text{AlB}_{12}$ ,  $\text{MgB}_{12}$ ,  $\text{MgB}_2$ ,  $\text{LiB}_{12}$  and  $\text{LiB}_2$ . At 5 psia and  $1250^\circ\text{K}$ ,  $\text{LiB}_2$  showed some hazy traces; only dim burning clouds were observed when other particles were used. The degree of flame brightness under this condition fell in the order  $\text{LiB}_{12}$ ,  $\text{LiB}_2$ , B,



Figure 13. Typical Burning of  $MgB_2$ ,  $LiB_2$ ,  $AlB_2$ , and Boron Particles

Details of illustrations in  
this document may be better  
studied on microfiche

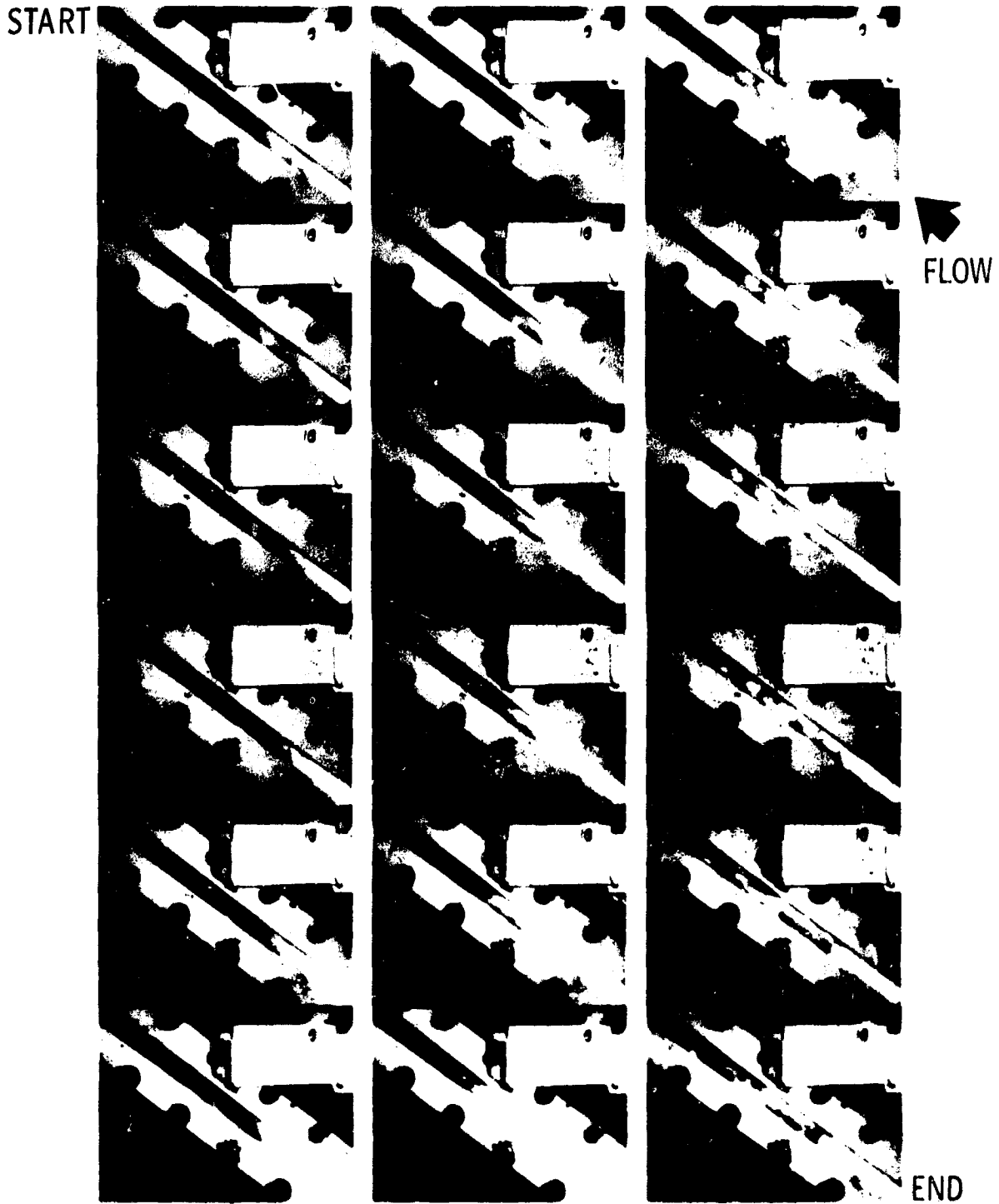


Figure 14. Burning of a Shower of Particles (Run No. 4-13-71-10, 37 to 44 $\mu$  LiB<sub>7</sub>, burned at 1675<sup>o</sup>K, 27 psia)

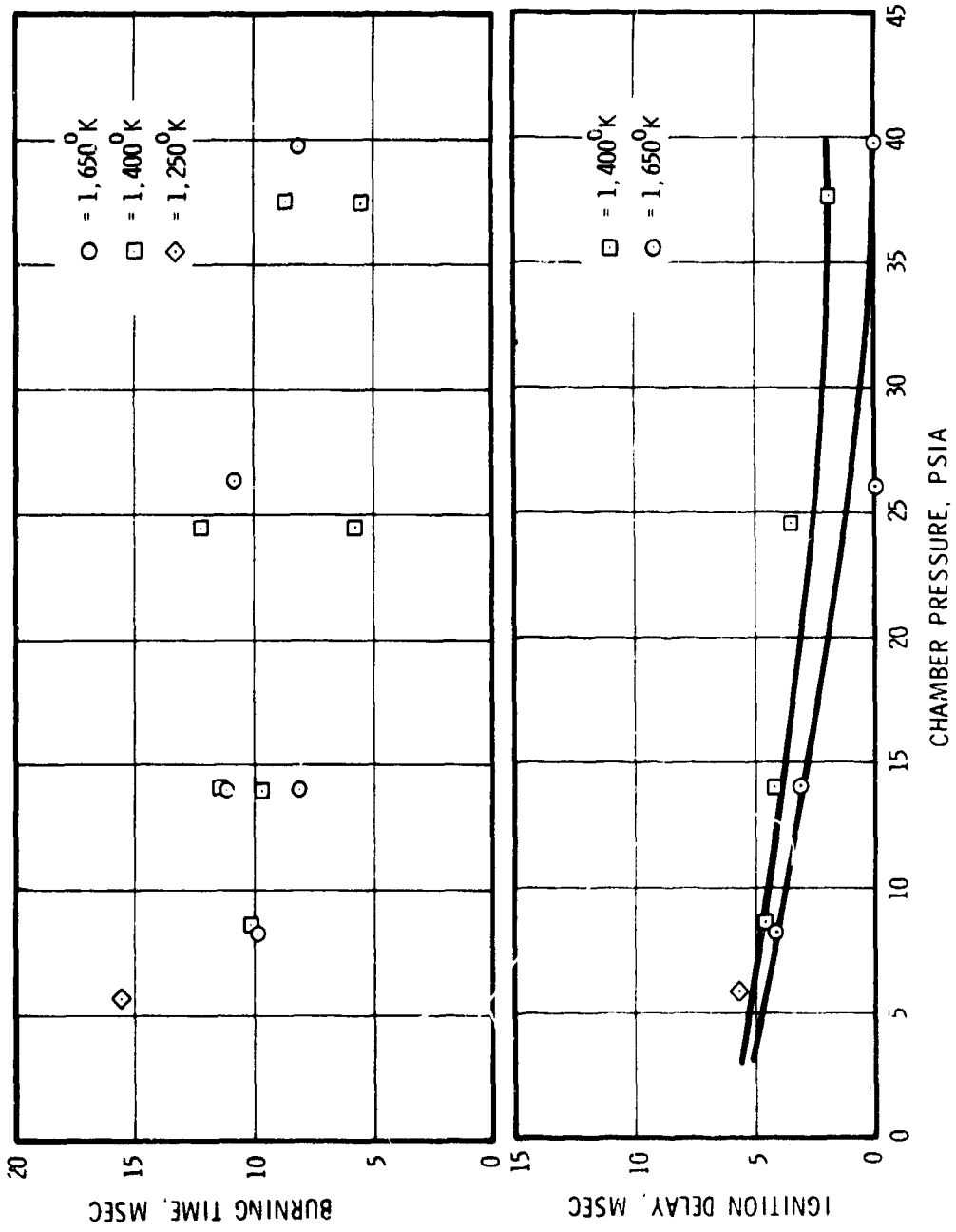


Figure 15. Ignition Delay and Burning Time for 37 to 44μ MgB<sub>2</sub>

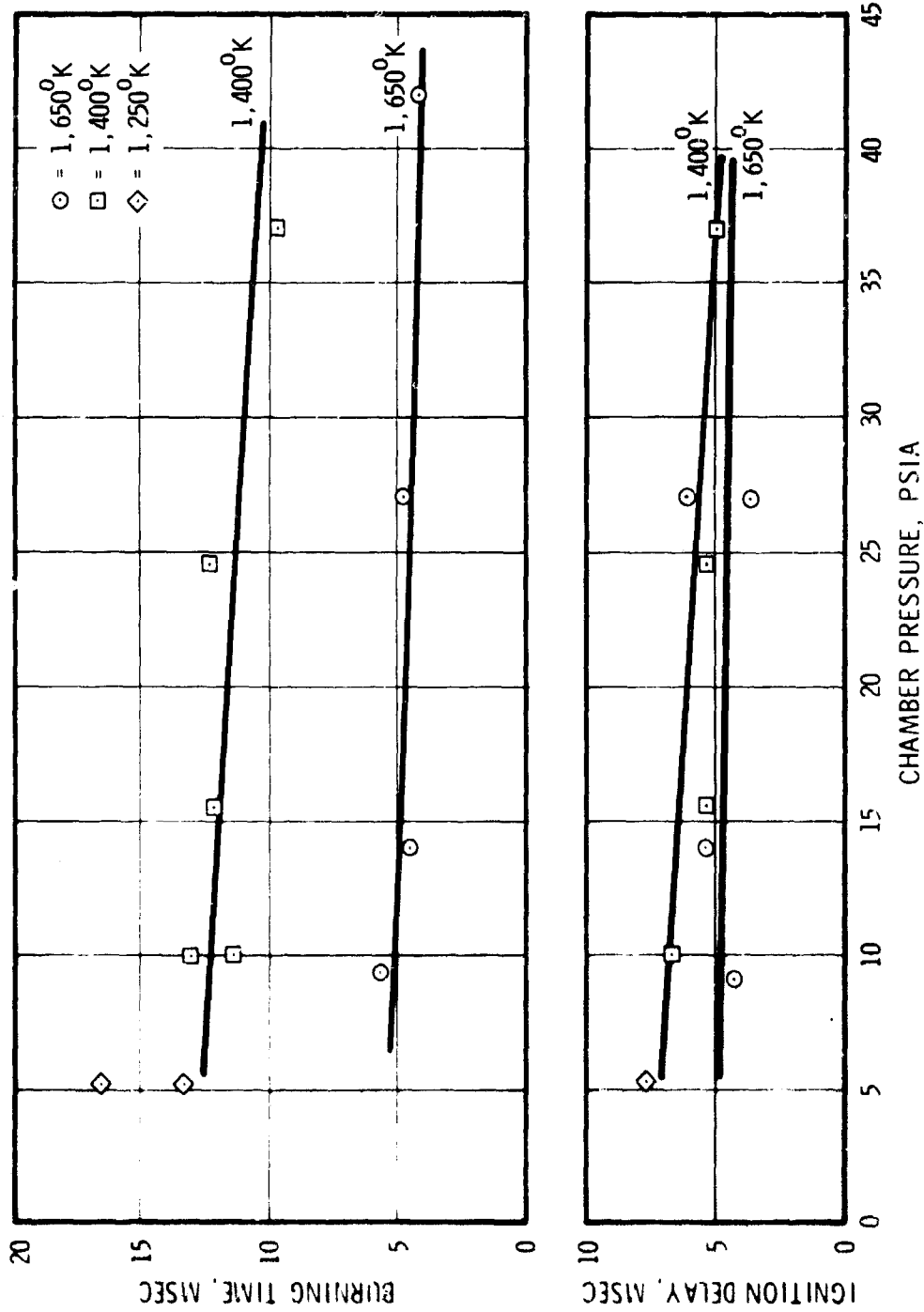


Figure 16. Ignition Delay and Burning Time for 44μ Li-B<sub>2</sub>

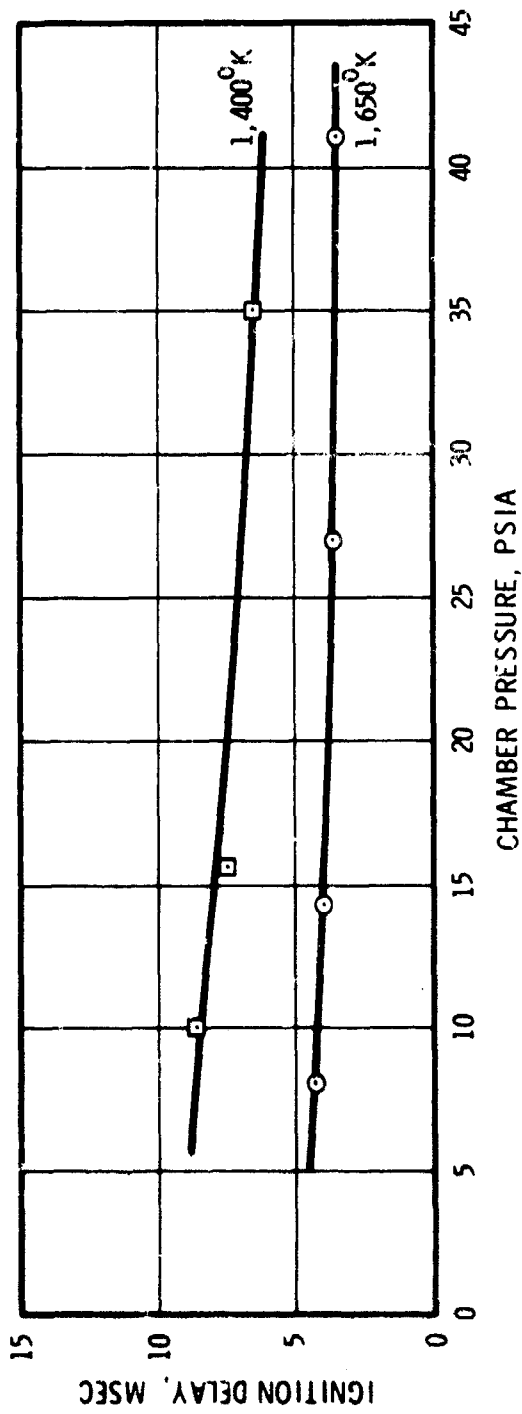
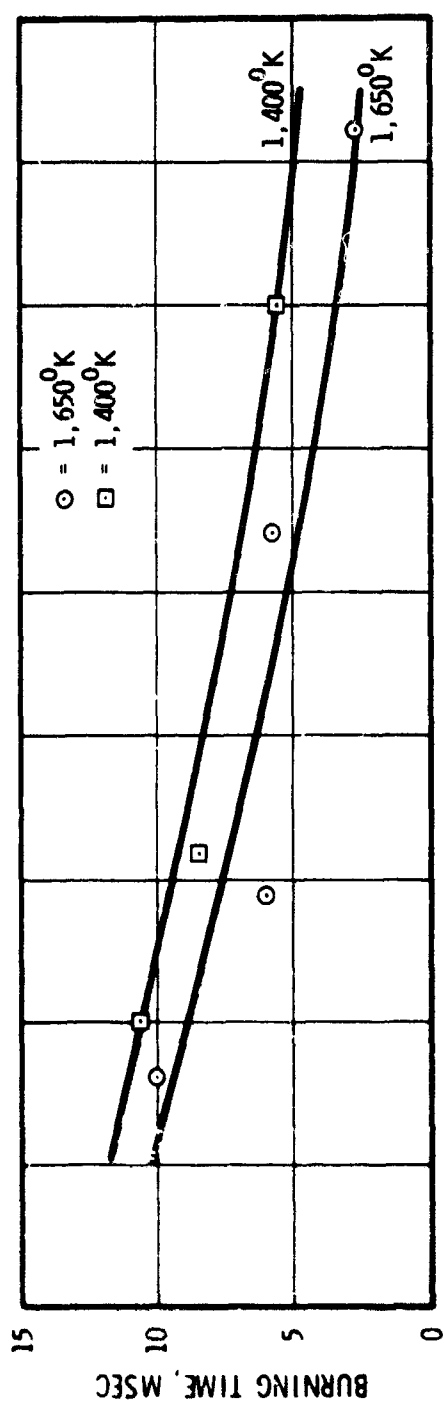


Figure 17. Ignition Delay and Burning Time for 44μ AlB<sub>2</sub>

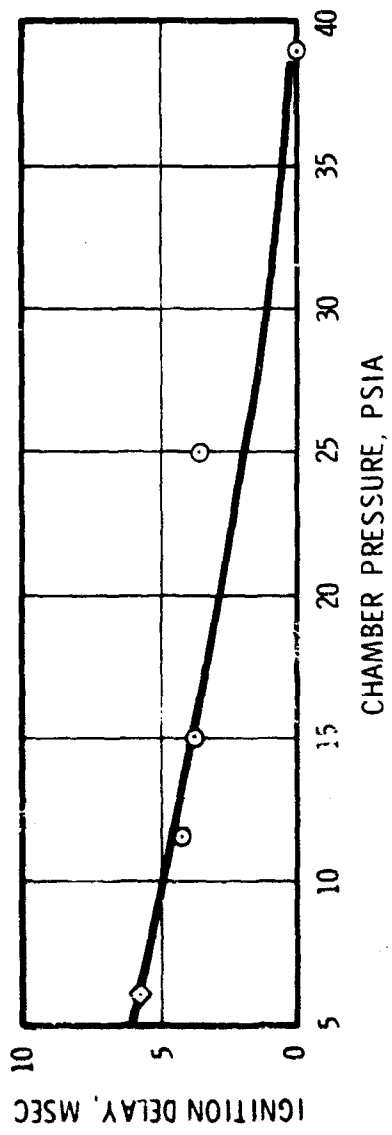
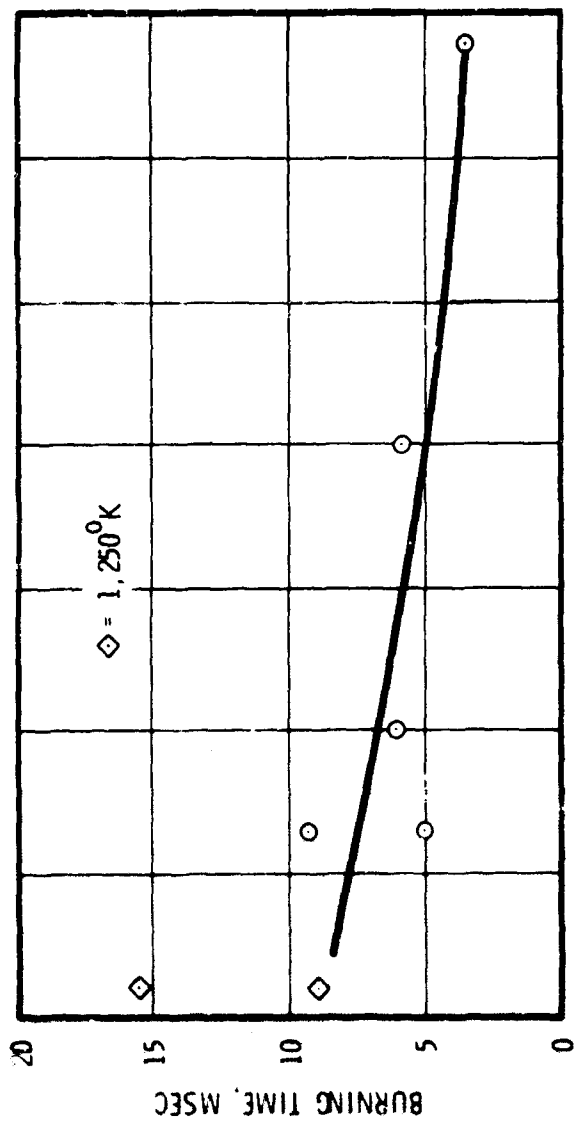


Figure 18. Ignition Delay and Burning Time for 37 to 44μ at 1,650°K

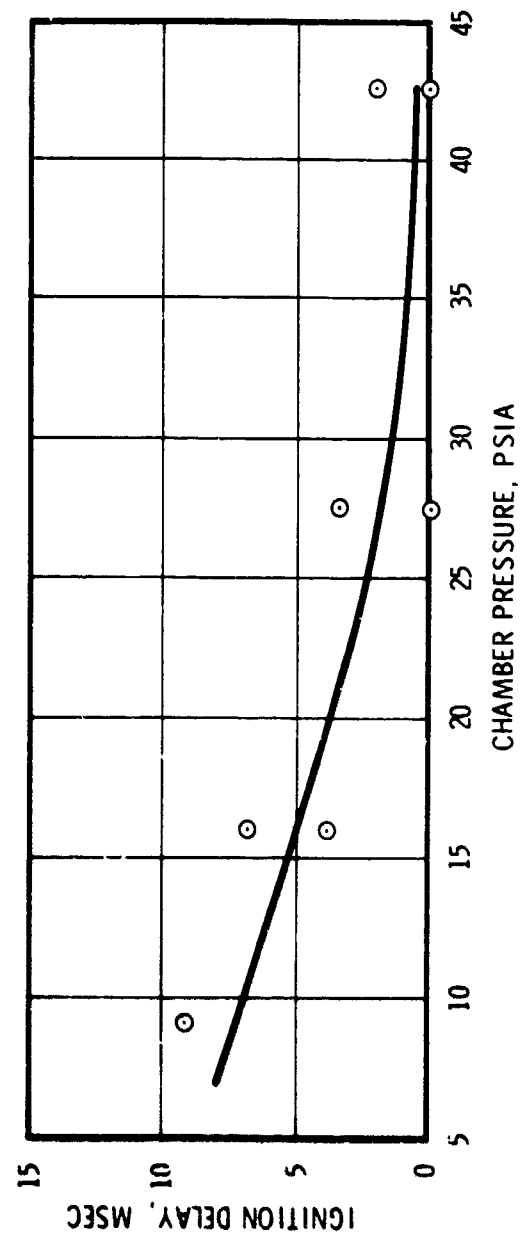
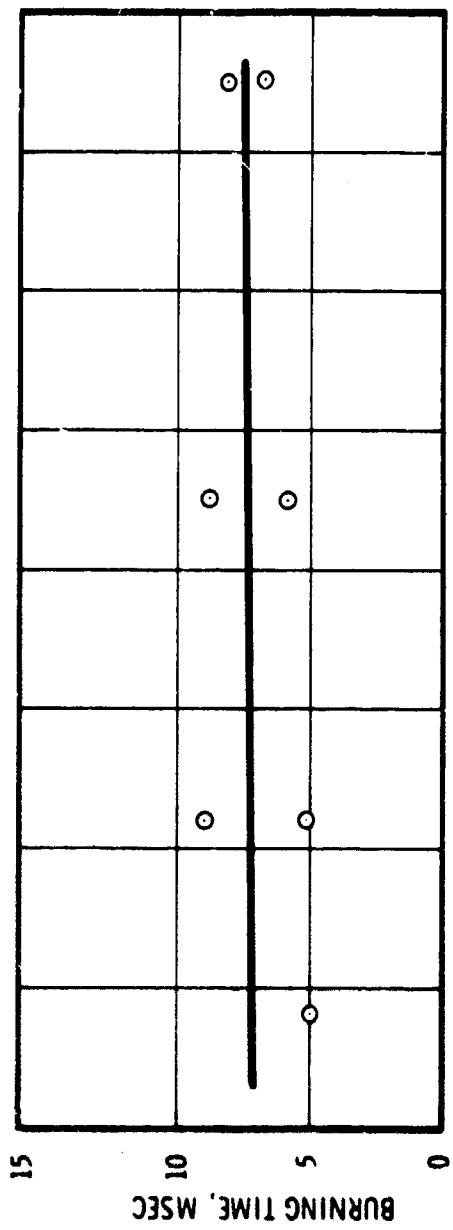


Figure 19. Ignition Delay and Burning Time for 37 to  $44\mu$   $\text{LiB}_{12}$  at  $1,650^\circ\text{K}$

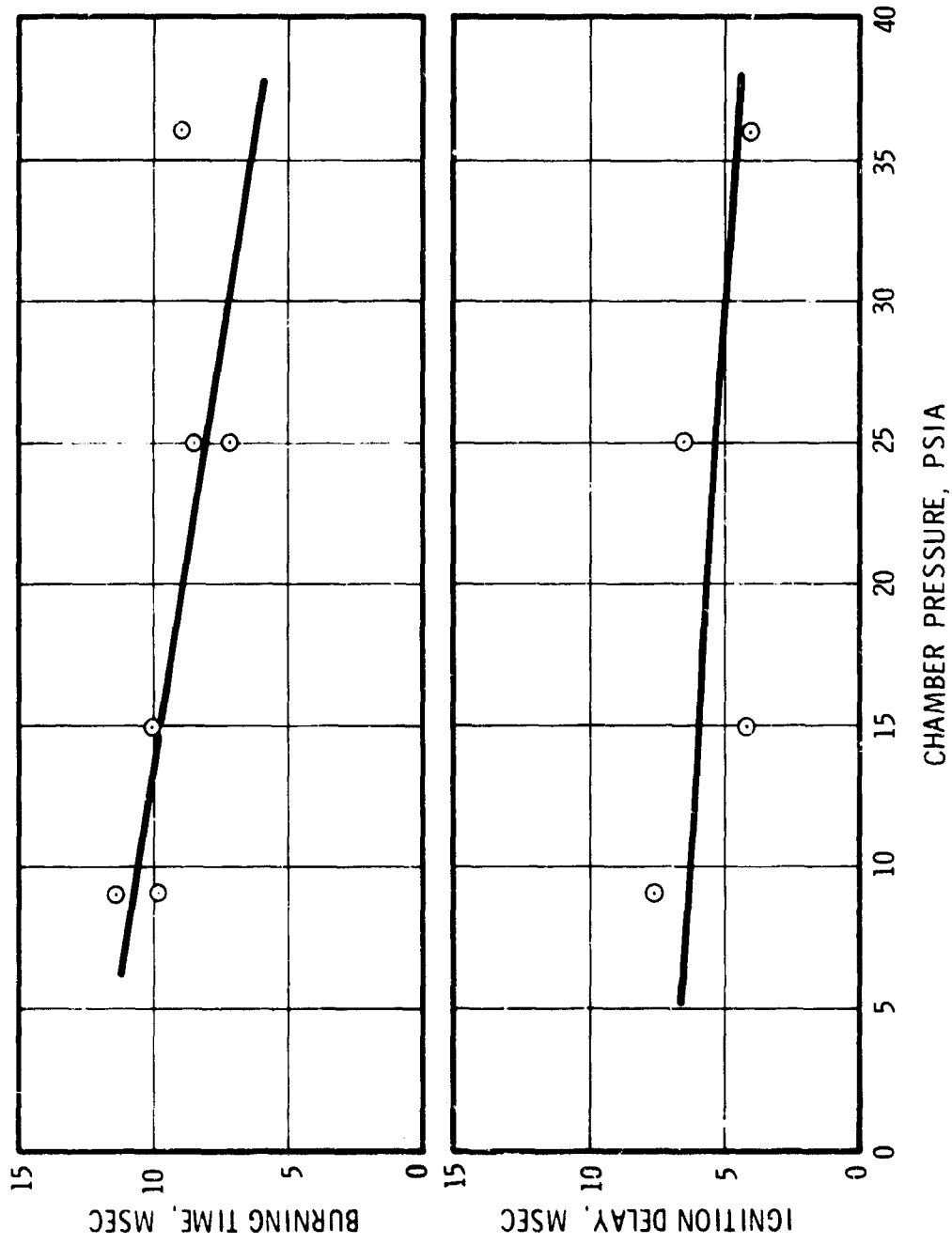


Figure 20. Ignition Delay and Burning Time for 37 to 44 $\mu$  AlB<sub>12</sub> at 1,650°C

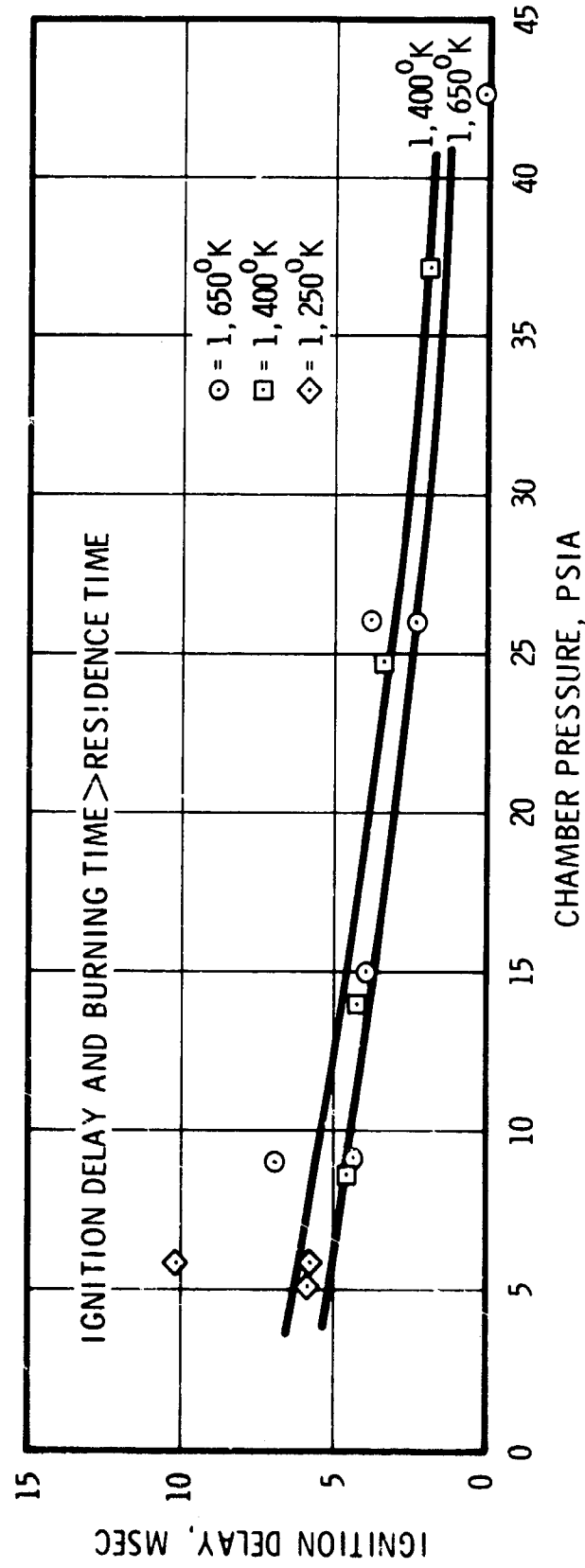


Figure 21. Ignition Delay for 37 to 4-μm Boron

MgB<sub>2</sub>, MgB<sub>12</sub>, AlB<sub>12</sub> and AlB<sub>2</sub>. Only MgB<sub>2</sub>, AlB<sub>2</sub> and boron were tested at 1400°K; their flame brightness and sharpness of the traces fell in the same order as observed in the 1650°K test runs.

The color cinematography used in the later tests showed a clear difference between burning and merely glowing particles. The glowing particles were only observed at the highest chamber pressures which does not favor vapor phase burning.

The effect of particle size on ignition delay and burning time is shown in Figures 22, 23 and 24, for AlB<sub>2</sub>, MgB<sub>2</sub> and B burning at 1650°K. In general, both times increase with particle size. Again, the burning time data for MgB<sub>2</sub> scatter so much that no definite trend can be identified. The scatter of the MgB<sub>2</sub> data may be due to a tendency to break-up of the particles into small pieces along their burning path.

To investigate the effect of dopants, small quantities of the seven materials were doped with 1.5% LiF. Ethanol was initially used as the solvent for LiF, but it reacts slowly with LiB<sub>2</sub> forming a layer of salt on top of the particles. White gasoline was therefore used as the solvent.

Two runs, at 40 psia and 1650°K, and at 5 psia and 1250°K, were made with each of the seven kinds of doped particles (Table VIII). Compared with the burning characteristics determined in the corresponding runs with undoped particles, the coating with LiF created an increase in luminosity, and shortened the ignition delay to where it was practically zero in most cases. The effect on burning time was irregular and no clear conclusion can be drawn.

#### b. Residue Collection and Analysis

A total of 81 runs were made for residue collection. In most of them test conditions duplicated those used in runs made for particle tracking. Tests with 44-53 $\mu$  size particles were omitted since not much difference in burning characteristics was observed with the particles of adjacent size lots. Only one lot of 37-44 $\mu$  size AlB<sub>2</sub> was used because the early X-ray diffraction analysis indicated some unburned aluminum. Additional test runs with MgB<sub>12</sub> were conducted at 1400°K in view of favorable results obtained at higher temperatures.

As described in Section II, a 1/8-in.-diameter tungsten rod was placed just downstream of the burner cell exhaust nozzle to collect the combustion residue. These were scraped off and submitted to analysis.

To insure that no leftover burned or unburned particles remained in the system, the apparatus was disassembled and thoroughly cleaned after each series of runs using a specific type of particle. Many runs had to be made, especially at the low pressure conditions when the flow rate was extremely low, before a sufficient amount of residue had been collected.

The residues collected from the combustion of magnesium borides were white

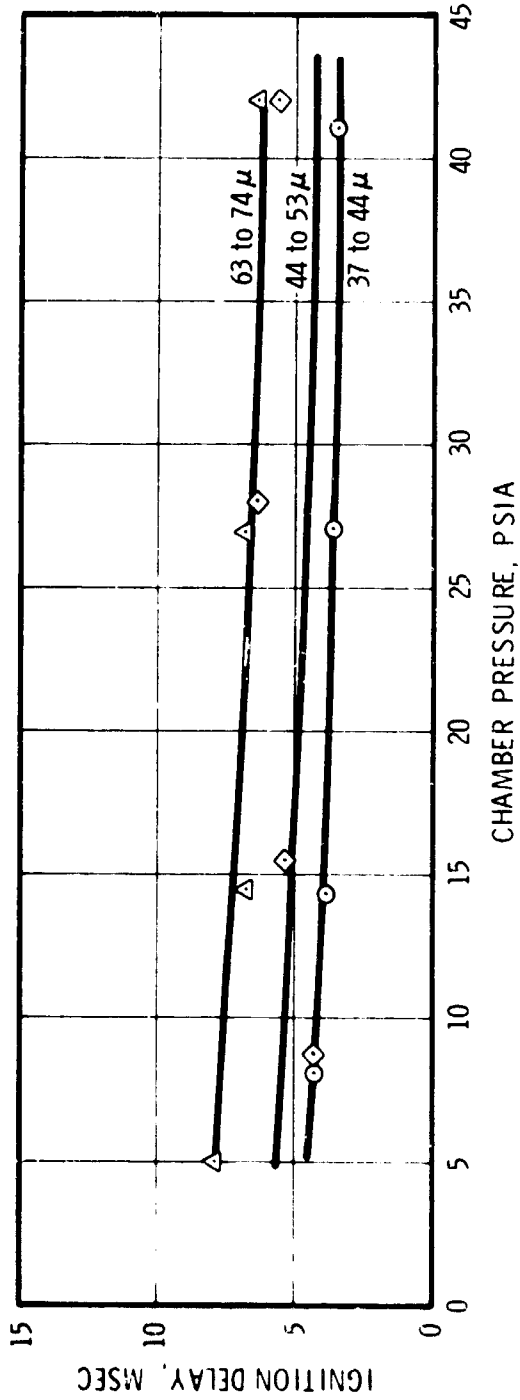
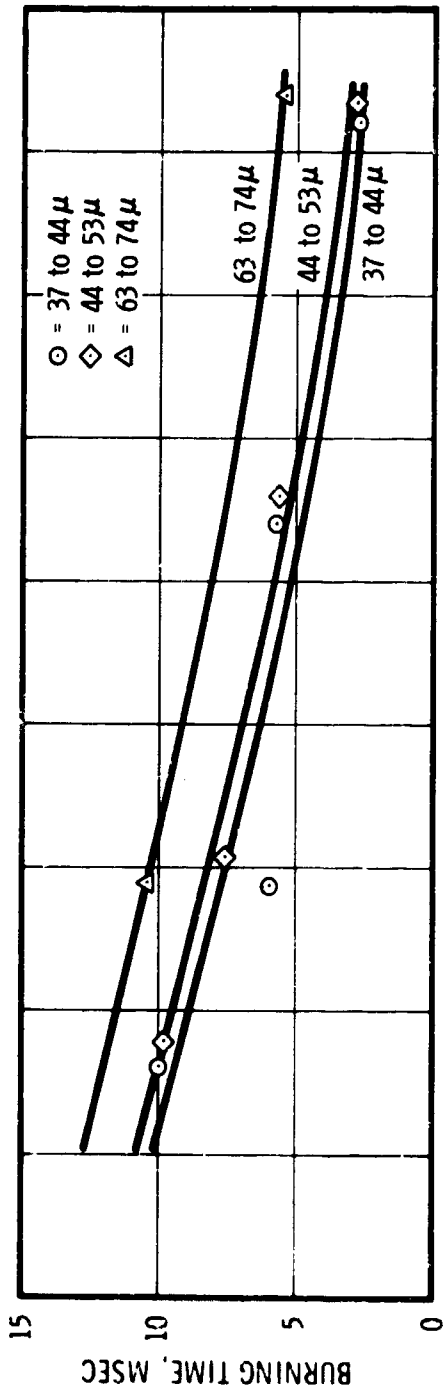


Figure 22. Ignition Delay and Burning Time for AlB<sub>2</sub> at 1,650°K

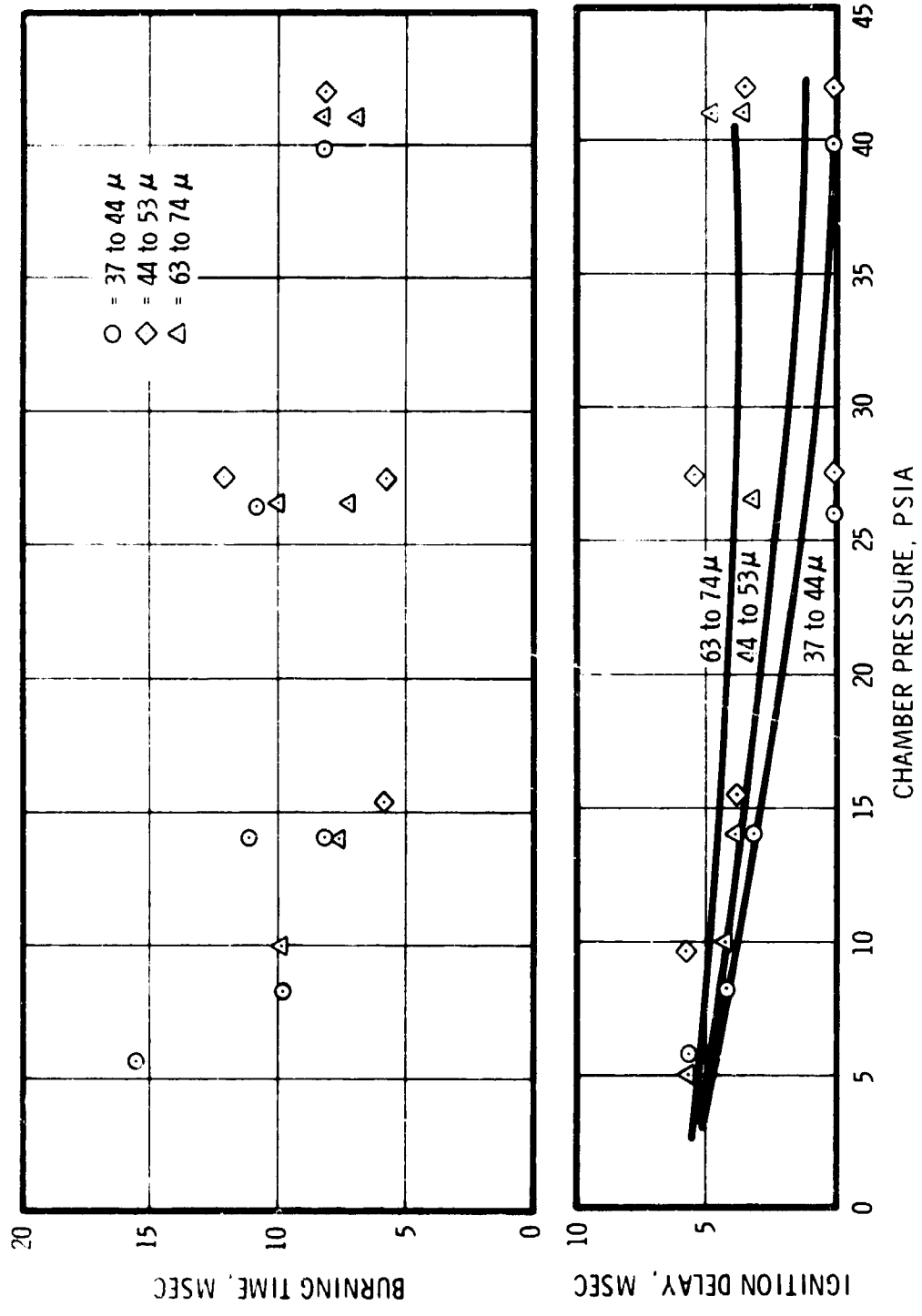


Figure 23. Ignition Delay and Burning Time for MgB<sub>2</sub> at 1,650°K

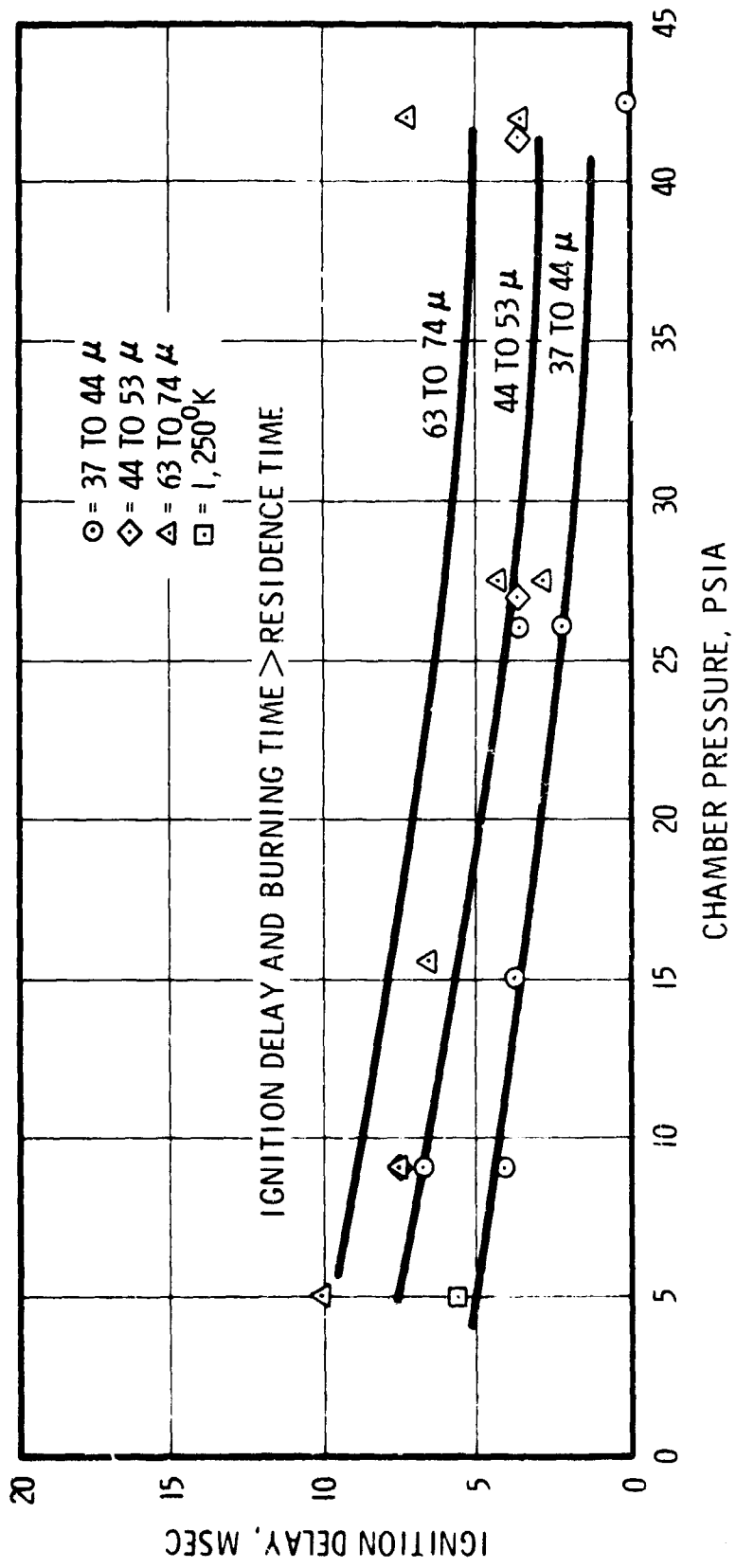


Figure 24. Ignition Delay for Boron at 1,650°K

and fluffy. The residues from lithium borides were dark, glassy and hard. There was not much difference between the appearance of the combustion residues of aluminum borides and boron; they were both dark in color, not as hard as the residues from lithium borides, and without glassy coating. Scanning electron micrographs of typical combustion residues of  $MgB_2$  and  $LiB_2$  are shown in Figure 25.

A summary of the X-ray analyses of the combustion residue is presented in Table VII. The X-ray diffraction data of the residues and original chemicals are attached as Appendix II. When  $MgB_2$  was burned at  $1400^\circ K$  or higher temperatures, the X-ray diffraction analysis indicated a strong pattern of  $Mg_2B_2O_5$ , a weak pattern of  $MgB_4$  and a trace of  $MgO$ . At the 5 psia and  $1250^\circ K$  condition the residue showed a strong pattern of  $MgO$ , a weak pattern of  $MgB_4$  and a trace of  $Mg_2B_2O_5$ . When  $MgB_{12}$  was burned at  $1400^\circ K$  or higher temperatures, the residues showed a strong pattern of  $Mg_3B_2O_5$  and in some cases  $B_2O_3$ , and a weak pattern or a trace of  $MgB_{12}$  or  $B_{25}$ . At 5 psia and  $1250^\circ K$ , the residue showed a strong pattern of unburned  $MgB_{12}$  and a weak pattern of  $B_2O_3$ . In the case of  $LiB_2$ , the exhaust residue showed lithium borates and boron oxides but no unburned particles or higher borides. The residue of  $LiB_{12}$  showed a strong pattern of unburned particles in every case. In tests with  $AlB_2$  and  $AlB_{12}$ , aluminum was identified alongside with aluminum borates and oxides. Unburned boron was found in almost all the tests burning boron.

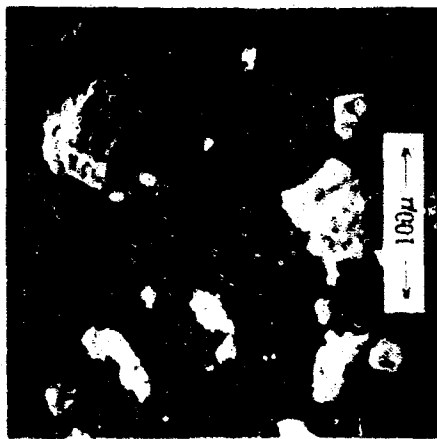
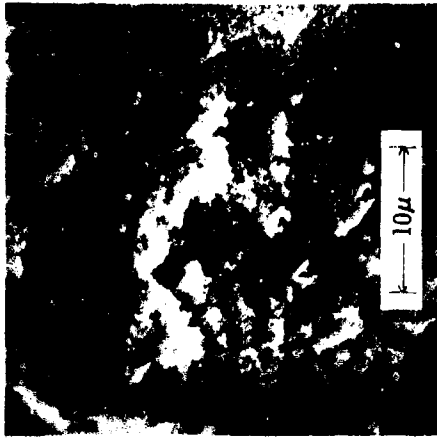
Based upon the indications from X-ray analysis, additional residue samples were taken with heavier loadings of  $MgB_{12}$  and  $MgB_2$  burning at 15 psia and  $1650^\circ K$ . These were subjected to wet chemical analysis, by dissolving in hot hydrogen peroxide and then boiling to remove excess peroxide. The percentages of B in  $MgB_2$  and  $MgB_{12}$  residues were determined by flame photometry to be 31.4 and 28% respectively. The magnesium contents were determined by E.D.T.A. titration as 36.3% for  $MgB_2$  and 5.6% for  $MgB_{12}$  residues. Referring these figures to the stoichiometric O/F ratio of these borides burning in oxygen, it is found that the combustion efficiencies were 62% for  $MgB_2$  and 100% for  $MgB_{12}$ , assuming no impurities were present in the original materials burned.

Not sufficient residue of  $LiB_2$  combustion was available for wet chemical analysis. Since the X-ray pattern showed promising results it would be worthwhile to collect more residue for such analysis in order to obtain a quantitative value for the combustion efficiency.

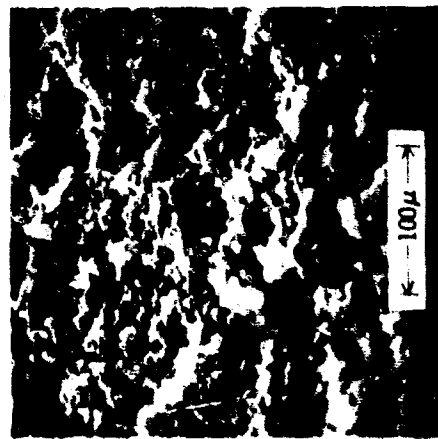
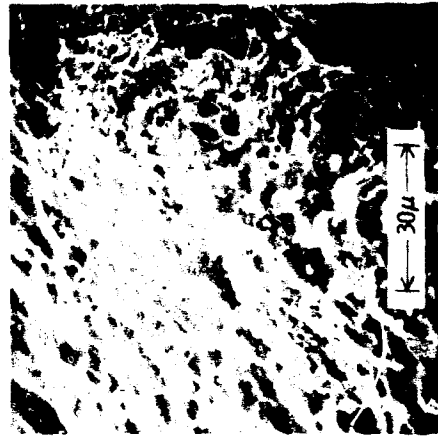
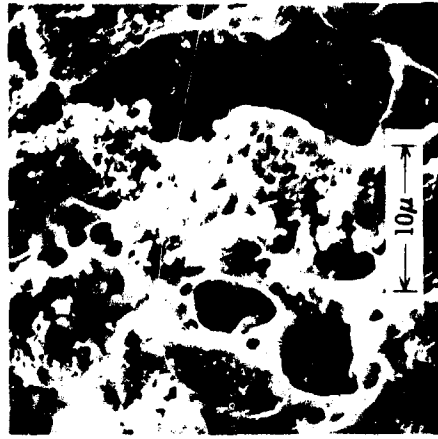
The results of X-ray diffraction analysis of the residues from the combustion of 1.5% LiF doped particles are summarized in Table VIII. Comparing these with the corresponding data in Table VII, doping appears to yield a small improvement in the degree of oxidation of  $MgB_{12}$ ,  $AlB_2$ ,  $AlB_{12}$ ,  $LiB_{12}$  and boron, but has no clear effect on  $MgB_2$ .

It is reported (21) that the efficacy of LiF is due in part to the low boiling point of lithium tetraborate, one of the products of combustion, compared to that of  $B_2O_3$  which is  $1000^\circ C$  higher, and in part to an exothermic reaction between lithium tetraborate and  $B_2O_3$  which provides

NOT REPRODUCIBLE



TEST NO. 4-27-71-2, 37-44 $\mu$  MgB<sub>2</sub> BURNED AT 28 PSIA, 1,675°K



TEST NO. 5-10-71-2, 37-44 $\mu$  LiB<sub>2</sub> BURNED AT 9 PSIA, 1,650°K

Figure 25. Typical Scanning Electron Micrographs of Combustion Residues

heat to enhance combustion. Since the combustion products of boron-metal compounds all consist of borates, it can be postulated that all borates may behave like lithium tetraborate and thus promote efficient burning.

### SECTION III

#### CONCLUSIONS AND RECOMMENDATIONS

The objectives planned for this program were successfully accomplished. It has proven feasible to modify and use an available optical burner for the study of the combustion characteristics of magnesium, lithium and aluminum borides in a CO-O<sub>2</sub>-air system at 5 to 40 psia chamber pressure and 1250 to 1650°K temperatures. Data taken by the high speed cinematography indicate that most of these borides were more readily burned than elemental boron. The ignition delay and burning times of these borides, determined from the motion pictures, were in the range of 0-8 and 2-15 msec respectively. These are considerably shorter than the corresponding measured times of boron, and also shorter than those published for boron elsewhere. (2,7)

X-ray diffraction analyses showed that the residues from the combustion of these borides contained mostly borates and oxides. The burning of LiB<sub>2</sub> and MgB<sub>12</sub> left no partially burned materials or unburned component metal in the residue, indicating essentially 100% combustion efficiency. This was confirmed by wet-chemical analysis of the residue of MgB<sub>12</sub> burned at 15 psia and 1650°K.

At the same condition, the combustion efficiency was 62% when MgB<sub>2</sub> was burned. X-ray diffraction analysis showed that the combustion residue of MgB<sub>2</sub> contained higher borides whose combustion was not complete.

Because of their high melting point (Table II), AlB<sub>2</sub> and AlB<sub>12</sub> would not achieve high combustion efficiency when burning at the test temperatures used. X-ray diffraction analysis of their combustion residues indicated the presence of unburned materials, either aluminum or aluminum borides. Previous investigation has shown that both magnesium and boron, and aluminum and boron, display a wide range of mutual solubility (11,13,14); the diborides are formed at low temperature and decompose into higher borides and elemental metal, Mg or Al, during the heating up process. Thus the diborides will be inferior to the dodecaborides as fuel since the decomposition process is endothermal.

However, this hypothesis may be contradicted by the experimental results obtained on lithium borides in this investigation. The X-ray analysis indicated a higher degree of oxidation of LiB<sub>2</sub> than of LiB<sub>12</sub> when these borides were burned in CO-O<sub>2</sub> flame. The X-ray method can only identify the components in the residue, not their relative proportions. Some uncertainty arose from the fact that there are no published X-ray pattern available for lithium borides. To draw firm conclusions regarding the relative merits of these two borides, it will be necessary to perform wet chemical analyses on the residues.

Wet chemical analysis should also be carried out on other residue samples, to extend the data on a few promising chemicals such as MgB<sub>12</sub> and LiB<sub>2</sub>, to cover the effects of pressure, temperature, particle size and doping. The necessary residues could be easily obtained on the present test apparatus. The combustion efficiency data obtained by wet chemical analysis will be invaluable in determining the full merits of these borides when burning under conditions under which

it is not possible to achieve satisfactory boron combustion.

The ratio of air and primary flow rates was low in the experiments conducted in the present program and no secondary combustion was involved. To investigate the effect of quenching when a large amount of secondary air is introduced downstream of the primary and to determine what the combustion performance would be in real air augmentation application, a parametric study is recommended, which would use the promising borides selected from this investigation and employing the small scale UTC connected pipe test facility.<sup>(20)</sup> A continuous particle feeding system capable of injecting particles evenly at high as well as low rates would be worked out. Alternatively a hybrid propellant system could be used as the fuel rich primary, with the boride particles cast in the fuel grain. The parameters of investigation would be the ratio of air and primary flow rates, the concentration of the boride particles in the primary system, the secondary chamber pressure, and the air temperature. Pressure would be the major measurement obtained and would be used to determine combustion efficiency, air-rocket specific impulse, and heat release in the secondary chamber. In the preparation of the fuel grain, consideration would be given to the stability, hygroscopicity, hypergolicity and other physical and chemical properties of the borides used.

The metal-boron compounds were prepared by fusing the elemental metal and boron in a furnace. This does not involve elaborate processes or complex equipment, and the compounds can be produced in a bulk scale. The cost in small quantity lots is high, but it will be greatly reduced on a mass production basis. For instance, the projected cost for  $MgB_{12}$  in 1000-lb. lots will drop to \$25.00 per pound which is comparable to the cost of boron. Estimates for the projected cost of  $MgB_2$ ,  $MgB_{12}$  and  $LiB_2$  are given in Appendix III.

It appears that the difficulty experienced with the combustion of boron under low temperatures and low pressure conditions can be resolved by substituting these boron-metal compounds for boron. The compounds are also reasonable in cost and thus can be considered as promising additives to solid, liquid, or a hybrid propellant for use in air-breathing rocket systems.

APPENDIX I  
THEORETICAL EQUILIBRIUM CALCULATION FOR  
CO-O<sub>2</sub>-AIR COMBUSTION

UTC1515		MCH = 4		DENSITY		MW		HF		UTC1515	
28 APR 1971										PAGE 1	
0189	11	0000	0.000	0.000	0.001	32.000	0.000	0	2.000	0.000	0.000
0496	11	0000	0.000	0.000	0.001	28.011	-26.417	C	1.0000	1.000	1.000
9997	12	0000	0.000	0.000	0.001	28.944	0.000	N	1.5620	0.419	0.419
9999	23	0000	0.000	0.000	0.000	0.000	0.000	0.000	0.000	0.000	0.000
C	G	5.0596	-0.1948	0.1076	-0.0103	-1.506	43.923	12.011	179.890	0.000	0.000
CO	G	6.8845	1.0442	0.0600	-0.0203	-2.207	56.202	26.018	104.000	0.000	0.000
CO	G	6.9591	1.3414	-0.2976	0.0228	-2.348	54.831	28.011	-26.417	0.000	0.000
CO2	G	11.0933	2.6353	-0.5921	0.0464	-4.230	61.995	44.010	-94.054	0.000	0.000
C2	G	7.5736	1.2438	-0.1422	0.0108	-1.922	57.351	24.022	200.224	0.000	0.000
C2H2	G	15.9000	3.2922	-0.7576	0.0578	-5.782	74.081	52.038	73.870	0.000	0.000
C3	G	8.7504	2.5534	-0.4940	0.0350	-3.060	65.865	36.033	196.000	0.000	0.000
C3H2	G	20.2371	4.4140	-1.0222	0.0783	-7.691	86.012	68.032	-22.380	0.000	0.000
C4	G	16.1854	3.1721	-0.7399	0.0570	-6.251	70.403	48.045	232.000	0.000	0.000
C5	G	20.5144	4.2770	-0.9975	0.0768	-8.061	77.544	60.056	234.000	0.000	0.000
N	G	5.1296	-0.1713	0.0333	0.0038	-1.567	42.780	14.008	113.000	0.000	0.000
NO	G	7.3014	1.1467	-0.2544	0.0194	-2.476	58.353	30.008	21.580	0.000	0.000
NO2	G	11.1841	1.8748	-0.4410	0.0341	-4.242	68.555	46.008	7.910	0.000	0.000
NO3	G	16.8670	2.1070	-0.5015	0.0391	-6.554	76.943	62.008	17.000	0.000	0.000
N2	G	6.7404	1.4678	-0.3268	0.0251	-2.238	53.197	28.013	0.000	0.000	0.000
N2O	G	11.5132	2.2790	-0.5268	0.0405	-4.327	64.112	44.016	19.610	0.000	0.000
N2O3	G	20.1617	3.1949	-0.7505	0.0581	-7.585	94.306	76.016	19.800	0.000	0.000
N2O4	G	25.5541	4.3006	-1.0130	0.0785	-9.920	97.772	92.016	2.170	0.000	0.000
O	G	5.1307	-0.1759	0.0551	-0.0033	-1.508	44.768	16.000	59.559	0.000	0.000
O2	G	7.5538	0.8949	-0.0788	0.0008	-2.546	57.338	31.999	0.000	0.000	0.000
AK	G	8.9680	0.0000	0.0000	0.0000	-1.481	43.007	39.944	0.000	0.000	0.000
C	S	4.3545	1.1983	-0.2773	0.0236	-2.035	4.781	12.011	0.000	9.999	9.999

UTC1515  
2A APR 1971

UTC151521-  
PAGE 1

INGREDIENTS	WT.PCT.	ELEMENTS	GM ATOMS
0498 CARBON MONOXIDE GAS	30.14	O	2.90708103E+00
0189 OXYGEN, GAS	17.07	C	1.07600585E+00
9999 AIR	52.79	N	2.84887991E+00
		AR	1.64148010E-02

PROPELLANT DENSITY, G/CC 1.0000000E+03

	THROAT	EXHAUST ( 1 )
AREA RATIO	1.0000000E+00	8.0262244E+00
OPTIMUM ISP, SEC	8.3932853E+01	1.9977592E+02
VACUUM ISP, SEC	1.56257157E+02	2.1612165E+02
C*, FT/SEC	4.06901895E+03	
VELOCITY, FT/SEC	2.70045561E+03	6.42759059E+03
DENSITY, GM/CC	4.19423756E+04	2.19548544E+05

	CHAMBER	THROAT	EXHAUST ( 1 )
PRESSURE, PSIA	6.21000000E+01	3.55133143E+01	1.00000000E+00
PRESSURE, ATM	4.22563963E+00	2.41652928E+00	6.80457267E-02
TEMPERATURE, DEG K	2.57640136E+03	2.40662548E+03	1.30496452E+03
HEAT CAP., CAL/DEG K/G	3.18927815E-01	3.17272898E-01	2.96035504E-01
ENTHALPY, KCAL/G	-2.84248467E-01	-3.65171608E-01	-7.42701721E-01
ENTROPY, CAL/DEG K/G	1.98611628E+00	1.98611628E+00	1.98611628E+00
MOLS OF GAS / 100 G	2.93605895E+00	2.91754024E+00	2.89439581E+00

COMBUSTION PRODUCTS

		CHAMBER	THROAT	EXHAUST ( 1 )
		MOLS/100 G	MOLS/100 G	MOLS/100 G
C	G	1.00000000E-10	1.00000000E-10	1.00000000E-10
C*	G	1.00000000E-10	1.00000000E-10	1.00000000E-10
Cn	G	7.26884782E-02	4.83211921E-02	1.90496078E-06
Cn2	G	1.00331707E+00	1.03568889E+00	1.07600451E+00
C2	G	1.00000000E-10	1.00000000E-10	1.00000000E-10
C2N2	G	1.00000000E-10	1.00000000E-10	1.00000000E-10
C3	G	1.00000000E-10	1.00000000E-10	1.00000000E-10
C3H2	G	1.00000000E-10	1.00000000E-10	1.00000000E-10
C4	G	1.00000000E-10	1.00000000E-10	1.00000000E-10
C5	G	1.00000000E-10	1.00000000E-10	1.00000000E-10
H	G	5.65405739E-07	1.53053906E-07	1.00000000E-10
Hn	G	4.94210031E-02	3.64466559E-02	4.06667966E-04
Hn2	G	5.94584731E-05	4.00406365E-05	1.70247993E-06
Hn3	G	2.67012549E-10	9.73425596E-11	1.00000000E-10
N2	G	1.39964528E+00	1.40619432E+00	1.42403578E+00
N2O	G	3.97104688E-06	2.22256297E-06	9.60409357E-09
N2O3	G	1.00000000E-10	1.00000000E-10	1.00000000E-10
N2H4	G	1.00000000E-10	1.00000000E-10	1.00000000E-10
N	G	1.07014045E-02	6.01080873E-03	7.68280100E-07
N3	G	3.8375815E-01	3.76425171E-01	3.77129658E-01
AR	G	1.64144010E-02	1.64148010E-02	1.64148010E-02
R	S	0.00000000E+00	0.00000000E+00	0.00000000E+00

UTC1515  
28 APR 1971

UTC151522-  
PAGE 1

INGREDIENTS	WT. PCT.	ELEMENTS	GM ATOMS
0078 CARBON MONOXIDE GAS	34.95	O	3.15131898E+00
0109 OXYGEN, GAS	20.03	O	1.24772411E+00
9099 AIR	45.02	N	2.42956191E+00
		AR	1.39987562E+02

PROPELLANT DENSITY, G/CC 1.0000000E+03

	THROAT	EXHAUST ( 1 )
AREA RATIO	1.0000000E+00	6.18306373E+00
ORIFICE ISP, SEC	8.47355023E+01	1.99616627E+02
VACUUM ISP, SEC	1.59766712E+02	2.20070847E+02
C*, FT/SEC	4.17225406E+03	
VELOCITY, FT/SEC	2.72628005E+03	6.42246516E+03
DENSITY, GM/CC	2.55760243E+04	1.75589284E+05

	CHAMBER	THROAT	EXHAUST ( 1 )
PRESSURE, PSIA	3.92000000E+01	2.26910066E+01	1.00000000E+00
PRESSURE, ATM	2.66739249E+00	1.54334559E+00	6.80457267E-02
TEMPERATURE, DEG K	2.69561172E+03	2.55804092E+03	1.68372855E+03
HEAT CAP., CAL/DEG K/G	3.21142210E-01	3.20244331E-01	3.07379241E-01
ENTHALPY, KCAL/G	-3.29611278E-01	-4.12089555E-01	-7.87333701E-01
ENTROPY, CAL/DEG K/G	2.02368618E+00	2.02368618E+00	2.02368618E+00
MOLS OF GAS / 100 G	2.90239018E+00	2.87480995E+00	2.80489819E+00

COMBUSTION PRODUCTS

		CHAMBER MOLS/100 G	THROAT MOLS/100 G	EXHAUST ( 1 ) MOLS/100 G
C	G	1.00000000E-10	1.00000000E-10	1.00000000E-10
CO	G	1.00000000E-10	1.00000000E-10	1.00000000E-10
CO2	G	1.73434762E+01	1.25171033E+01	7.64063710E-04
C2	G	1.07424453E+00	1.12255327E+00	1.24694043E+00
C2H2	G	1.00000000E-10	1.00000000E-10	1.00000000E-10
C2H4	G	1.00000000E-10	1.00000000E-10	1.00000000E-10
C2H6	G	1.00000000E-10	1.00000000E-10	1.00000000E-10
C4H2	G	1.00000000E-10	1.00000000E-10	1.00000000E-10
C4H6	G	1.00000000E-10	1.00000000E-10	1.00000000E-10
C6H6	G	1.00000000E-10	1.00000000E-10	1.00000000E-10
N	G	1.76228840E-06	7.27401740E-07	1.00000000E-10
N2	G	5.42941175E-02	4.29531876E-02	4.52181325E-03
N2O	G	4.62481452E-05	3.14220338E-05	2.71272149E-06
N2O2	G	1.73704999E-10	5.82155059E-11	1.00000000E-10
N2O4	G	1.14760666E+00	1.19328635E+00	1.21251867E+00
N2O6	G	3.22024978E-06	1.94566528E-06	4.57495065E-06
N2O8	G	1.00000000E-10	1.00000000E-10	1.00000000E-10
N2O10	G	1.00000000E-10	1.00000000E-10	1.00000000E-10
O	G	2.25091522E-02	1.58010430E-02	1.36571536E-04
O2	G	3.76205250E-01	3.61211142E-01	3.25995122E-01
O4	G	1.39987562E-02	1.39987562E-02	1.39987562E-02
C	S	0.00000000E+00	0.00000000E+00	0.00000000E+00

UTC1515  
24 APR 1971

UTC151523-  
PAGE 1

INGREDIENTS	WT.PCT.	ELEMENTS	GM ATOMS
0498 CARBON MONOXIDE GAS	57.06	O	4.21175491E+00
0189 OXYGEN, GAS	32.34	O	2.03705687E+00
9999 AIR	10.60	N	5.72042565E-01
		AR	3.29601990E-03

PROPELLANT DENSITY, G/CC 1.00000000E-03

	THRUAT	EXHAUST[ 1 ]
AREA RATIO	1.00000000E+00	4.60894214E+00
OPTIMUM ISP, SEC	8.71369115E+01	1.98025478E+02
VACUUM ISP, SEC	1.60022359E+02	2.25582142E+02
C*, FT/SEC	4.34750560E+03	
VELOCITY, FT/SEC	2.80354299E+03	6.37127044E+03
DENSITY, GM/CC	1.37609764E-04	1.31379975E-05

	CHAMBER	THRUAT	EXHAUST[ 1 ]
PRESSURE, PSIA	2.26000000E+01	1.31938104E+01	1.00000000E+00
PRESSURE, ATM	1.53781342E+00	8.97782420E-01	6.80457267E-02
TEMPERATURE, DEG K	2.96313081E+03	2.85301677E+03	2.40687622E+03
HEAT CAP., CAL/DEG K/G	3.26419999E-01	3.26238706E-01	3.24793238E-01
ENTHALPY, KCAL/G	-5.38129313E-01	-6.25348712E-01	-9.88583603E-01
ENTROPY, CAL/DEG K/G	2.07286318E+00	2.07286318E+00	2.07286318E+00
MOLS OF GAS / 100 G	2.82557908E+00	2.78678748E+00	2.62243212E+00

COMBUSTION PRODUCTS

		CHAMBER	THRUAT	EXHAUST[ 1 ]
		MOLS/100 G	MOLS/100 G	MOLS/100 G
C	G	1.00000000E-10	1.00000000E-10	1.00000000E-10
C1	G	7.59704796E-10	2.94563745E-10	1.00000000E-10
C2	G	7.76362059E-01	7.12012319E-01	4.26161787E-01
C22	G	1.26062495E+00	1.32504470E+00	1.61089529E+00
C222	G	1.00000000E-10	1.00000000E-10	1.00000000E-10
C2222	G	1.00000000E-10	1.00000000E-10	1.00000000E-10
C3	G	1.00000000E-10	1.00000000E-10	1.00000000E-10
C32	G	1.00000000E-10	1.00000000E-10	1.00000000E-10
C4	G	1.00000000E-10	1.00000000E-10	1.00000000E-10
C42	G	1.00000000E-10	1.00000000E-10	1.00000000E-10
C422	G	7.57358559E-06	4.64839418E-06	3.86322048E-07
C4222	G	3.79462494E-02	3.21736466E-02	1.35301021E-02
C42222	G	2.02812223E-05	1.40440641E-05	2.18941887E-06
C422222	G	5.46970875E-11	1.00000000E-10	1.00000000E-10
C4222222	G	2.67031383E-01	2.68924580E-01	2.79254891E-01
C42222222	G	8.29174750E-07	5.41417306E-07	6.50782232E-06
C422222222	G	1.00000000E-10	1.00000000E-10	1.00000000E-10
C4222222222	G	1.00000000E-10	1.00000000E-10	1.00000000E-10
C42222222222	G	8.43200917E-02	7.11430251E-02	2.83147370E-02
C422222222222	G	3.95847588E-01	3.73133951E-01	2.60976652E-01
C4222222222222	G	3.29601990E-03	3.29601990E-03	3.29601990E-03
C	S	0.00000000E+00	0.00000000E+00	0.00000000E+00

UTC1515  
24 APR 1971

UTC151524-  
PAGE 1

INGREDIENTS	WT.PCT.	ELEMENTS	GM ATOMS
0298 CARBON MONOXIDE GAS	58.78	O	4.31309233E+00
0139 OXYGEN, GAS	33.69	C	2.09846132E+00
9059 AIR	7.53	N	4.06366086E+01
		AR	2.34141791E+03

PROPELLANT DENSITY, G/CC 1.00000000E-03

	THROAT	EXHAUST[ 1 ]
AREA RATIO	1.00000000E+00	3.14216814E+00
OPTIMUM ISP, SEC	8.66851964E+01	1.82497061E+02
VACUUM ISP, SFC	1.65311418E+02	2.13583162E+02
C* FT/SFC	4.32893226E+03	
VELOCITY, FT/SEC	2.74900951E+03	5.87166044E+03
DENSITY, GM/CC	8.35980802E-05	1.26373480E-05

	CHAMBER	THROAT	EXHAUST[ 1 ]
PRESSURE, PSIA	1.36000000E+01	7.94750081E+00	1.00000000E+00
PRESSURE, ATM	9.25421884E-01	5.40793468E-01	6.80457267E-02
TEMPERATURE, DEG K	2.92649729E+03	2.82125398E+03	2.47020213E+03
HEAT CAP., CAL/DFG K/G	3.26037902E-01	3.25872963E-01	3.24891447E-01
ENTHALPY, KCAL/G	-5.5435527E-01	-6.40667984E-01	-9.36928984E-01
ENTROPY, CAL/DEG K/G	2.09987614E+00	2.09987614E+00	2.09987614E+00
MOLS OF GAS / 100 G	2.83382241E+00	2.79434019E+00	2.65643228E+00

COMBUSTION PRODUCTS

		CHAMBER	THROAT	EXHAUST[ 1 ]
		MOLS/100 G	MOLS/100 G	MOLS/100 G
O	G	1.00000000E-10	1.00000000E-10	1.00000000E-10
C	G	5.06840494E-10	1.95993151E-10	1.00000000E-10
CO	G	8.45530879E-01	7.81036805E-01	5.46101141E-01
CO2	G	1.25291059E+00	1.31742467E+00	1.55236037E+00
CO	G	1.00000000E-10	1.00000000E-10	1.00000000E-10
CO2	G	1.00000000E-10	1.00000000E-10	1.00000000E-10
CO	G	1.00000000E-10	1.00000000E-10	1.00000000E-10
CO2	G	1.00000000E-10	1.00000000E-10	1.00000000E-10
CO	G	1.00000000E-10	1.00000000E-10	1.00000000E-10
CS	G	1.00000000E-10	1.00000000E-10	1.00000000E-10
N	G	6.41327232E-06	4.00129992E-06	6.03920150E-07
NO	G	3.11589806E-02	2.65561977E-02	1.37215110E-02
NO2	G	1.36170248E-05	4.48031447E-06	2.20921096E-06
NO3	G	1.00000000E-10	1.00000000E-10	1.00000000E-10
NO	G	1.87591104E-01	1.89897922E-01	1.96320838E-01
NO2	G	4.41368192E-07	2.90186108E-07	5.50038443E-08
NO3	G	1.00000000E-10	1.00000000E-10	1.00000000E-10
NO2	G	1.00000000E-10	1.00000000E-10	1.00000000E-10
O	G	9.79802919E-02	8.35080398E-02	4.26237602E-02
NO	G	4.16264676E-01	3.93561362E-01	3.02960368E-01
AR	G	2.34141791E-03	2.34141791E-03	2.34141791E-03
C	S	0.00000000E+00	0.00000000E+00	0.00000000E+00

UTC1515  
24 APR 1971

UTC151525-  
PAGE 1

INGREDIENTS	WT,PCT.	ELEMENTS	GM ATOMS
0498 CARBON MONOXIDE GAS	18.47	O	2.35204447E+00
0189 OXYGEN GAS	10.67	C	6.59383814E+01
9999 AIR	70.86	N	3.82405058E+00
		AR	2.20335821E+02
PROPELLANT DENSITY, G/CC	1.00000000E+03		

	THROAT	EXHAUST [ 1 ]
AREA RATIO	1.00000000E+00	7.62908547E+00
OPTIMUM ISP, SEC	7.53006670E+01	1.69184286E+02
VACUUM ISP, SEC	1.35418773E+02	1.81514047E+02
C*, FT/SEC	3.48908181E+03	
VELOCITY, FT/SEC	2.42272366E+03	5.44333522E+03
DENSITY, GM/CC	5.89109014E+04	3.43686097E+05

	CHAMBER	THROAT	EXHAUST [ 1 ]
PRESSURE, PSIA	6.71000000E+01	3.71981819E+01	1.00000000E+00
PRESSURE, ATM	4.56584826E+00	2.53117732E+00	6.80457267E-02
TEMPERATURE, DEG K	1.89275817E+03	1.88359518E+03	7.75806683E+02
HEAT CAP., CAL/DEG K/G	3.04421402E-01	3.00271456E-01	2.74999926E-01
ENTHALPY, KCAL/G	-1.74184422E-01	-2.39323221E-01	-5.02987150E-01
ENTROPY, CAL/DEG K/G	1.93145490E+00	1.93145490E+00	1.93145490E+00
MOLS OF GAS / 100 G	3.11032809E+00	3.11010862E+00	3.11008103E+00

COMBUSTION PRODUCTS

	CHAMBER	THROAT	EXHAUST [ 1 ]
	MOLS/100 G	MOLS/100 G	MOLS/100 G
C	1.00000000E-10	1.00000000E-10	1.00000000E-10
CH	1.00000000E-10	1.00000000E-10	1.00000000E-10
CO	3.84972473E-04	5.69649492E-05	1.00000000E-10
CO2	6.58999188E-01	6.59327260E-01	6.59384911E-01
C2	1.00000000E-10	1.00000000E-10	1.00000000E-10
C2H2	1.00000000E-10	1.00000000E-10	1.00000000E-10
C3	1.00000000E-10	1.00000000E-10	1.00000000E-10
C3H2	1.00000000E-10	1.00000000E-10	1.00000000E-10
C4	1.00000000E-10	1.00000000E-10	1.00000000E-10
C4H2	1.00000000E-10	1.00000000E-10	1.00000000E-10
CR	1.00000000E-10	1.00000000E-10	1.00000000E-10
N	1.81774779E-10	1.00000000E-10	1.00000000E-10
NO	1.44697207E-02	7.11322882E-03	3.71434939E-02
NO2	5.35431944E-05	3.10179409E-05	3.48365337E-07
NO3	1.07154445E-10	1.00000000E-10	1.00000000E-10
N2	1.90474226E+00	1.90835266E+00	1.91202331E+00
N2O	1.39222682E-06	5.22972378E-07	5.98138450E-11
N2O3	1.00000000E-10	1.00000000E-10	1.00000000E-10
N2O4	1.00000000E-10	1.00000000E-10	1.00000000E-10
O	1.63904777E-04	2.85381256E-05	1.00000000E-10
O2	5.09459480E-01	5.13063845E-01	5.16835144E-01
AO	2.20335821E-02	2.20335821E-02	2.20335821E-02
C	0.00000000E+00	0.00000000E+00	0.00000000E+00

THE TEMPERATURE HAS BECOME LESS THAN 1000 DEG K, THE CURVE FIT MINIMUM

UTC1515  
24 APR 1971

UTC151526-  
PAGE 1

INGREDIENTS	WT.PCT.	ELEMENTS	GM ATOMS
0498 CARBON MONOXIDE GAS	31.93	O	3.00366105E+00
0185 OXYGEN, GAS	18.29	C	1.13990932E+00
9999 AIR	49.78	N	2.68644140E+00
		AR	1.54788557E-02

PROPELLANT DENSITY, G/CC 1.00000000E-03

	THROAT	EXHAUST [ 1 ]
AREA RATIO	1.00000000E+00	5.72062090E+00
OPTIMUM ISP, SEC	8.40133915E+01	1.93903119E+02
VACUUM ISP, SEC	1.57525030E+02	2.13464273E+02
C*, FT/SEC	4.10779731E+03	
VELOCITY, FT/SEC	2.70304686E+03	6.23863896E+03
DENSITY, GM/CC	2.49306977E-04	1.88823040E-05

	CHAMBER	THROAT	EXHAUST [ 1 ]
PRESSURE, PSIA	3.73000000E+01	2.14763753E+01	1.00000000E+00
PRESSURE, ATM	2.53810561E+00	1.46137556E+00	6.80457267E-02
TEMPERATURE, DEG K	2.61174312E+03	2.46159575E+03	1.53524048E+03
HEAT CAP., CAL/DEG K/G	3.19611912E-01	3.18361991E-01	3.02676294E-01
ENTHALPY, KCAL/G	-3.01129845E-01	-3.82208362E-01	-7.33025021E-01
ENTROPY, CAL/DEG K/G	2.02018322E+00	2.02018322E+00	2.02018317E+00
MOLS OF GAS / 100 G	2.92547550E+00	2.90199730E+00	2.86059113E+00

COMBUSTION PRODUCTS

	CHAMBER MOLS/100 G	THROAT MOLS/100 G	EXHAUST [ 1 ] MOLS/100 G
C	1.00000000E-10	1.00000000E-10	1.00000000E-10
CH	1.00000000E-10	1.00000000E-10	1.00000000E-10
CO	1.13703758E-01	7.27461793E-02	9.95195061E-05
CO2	1.02620575E+00	1.06716335E+00	1.13931075E+00
C2	1.00000000E-10	1.00000000E-10	1.00000000E-10
C2H2	1.00000000E-10	1.00000000E-10	1.00000000E-10
C3	1.00000000E-10	1.00000000E-10	1.00000000E-10
C3H2	1.00000000E-10	1.00000000E-10	1.00000000E-10
C4	1.00000000E-10	1.00000000E-10	1.00000000E-10
C5	1.00000000E-10	1.00000000E-10	1.00000000E-10
N	9.57670067E-07	3.25857651E-07	1.00000000E-10
NO	5.08576911E-02	3.89467230E-02	2.67664200E-03
NO2	4.62181477E-05	3.11949067E-05	2.49292675E-06
NO3	1.56135654E-10	4.58840004E-11	1.00000000E-10
N2	1.31774520E+00	1.32371979E+00	1.34166113E+00
N2O	3.02079878E-06	1.79824245E-06	2.90156104E-06
N2O3	1.00000000E-10	1.00000000E-10	1.00000000E-10
N2O4	1.00000000E-10	1.00000000E-10	1.00000000E-10
O	1.62351679E-02	1.02208774E-02	2.50043091E-05
O2	3.89134613E-01	3.73468197E-01	3.60617210E-01
OH	1.54788557E-02	1.54788557E-02	1.54788557E-02
Ar	1.00000000E+00	0.00000000E+00	0.00000000E+00

UTC1515  
24 APR 1971

UTC151527-  
PAGE 1

INGREDIENTS	WT.PCT.	ELEMENTS	GM ATOMS
0098 CARBON MONOXIDE GAS	37.28	O	3.26728140E+00
0109 OXYGEN GAS	21.31	C	1.33090572E+00
9099 AIR	41.41	N	2.23978364E+00
		AR	1.28762438E+02

PROPELLANT DENSITY, G/CC 1.00000000E-03

	THROAT	EXHAUST (1)
AREA RATIO	1.00000000E+00	0.38212871E+00
OPTIMUM ISP, SEC	8.46765000E+01	1.89725333E+02
VACUUM ISP, SFC	1.60326475E+02	2.14543526E+02
C*, FT/SEC	4.19100250E+03	
VELOCITY, FT/SEC	2.72438192E+03	6.10422288E+03
DENSITY, G/CC	1.49496164E+04	1.52258864E+05

	CHAMBER	THROAT	EXHAUST (1)
PRESSURE, PSIA	2.30000000E+01	1.33575259E+01	1.00000000E+00
PRESSURE, ATM	1.56505171E+00	9.08922556E-01	6.80457267E-02
TEMPERATURE, DEG K	2.70871724E+03	2.58417475E+03	1.96636564E+03
HEAT CAP., CAL/DEG K/G	3.21512733E+01	3.20839144E+01	3.13936149E+01
ENTHALPY, KCAL/G	-3.51585363E-01	-4.33948831E-01	-7.65070032E-01
ENTHALPY, CAL/DEG K/G	2.05853787E+00	2.05853787E+00	2.05853787E+00
MOLS OF GAS / 100 G	2.89807878E+00	2.86721915E+00	2.76974814E+00

COMBUSTION PRODUCTS

		CHAMBER MOLS/100 G	THROAT MOLS/100 G	EXHAUST (1) MOLS/100 G
C	G	1.00000000E-10	1.00000000E-10	1.00000000E-10
CM	G	1.00000000E-10	1.00000000E-10	1.00000000E-10
CM	G	2.42300799E-01	1.88778683E-01	1.49736131E-02
CN2	G	1.08860509E+00	1.14212722E+00	1.31593240E+00
C2	G	1.00000000E-10	1.00000000E-10	1.00000000E-10
C2H2	G	1.00000000E-10	1.00000000E-10	1.00000000E-10
C2	G	1.00000000E-10	1.00000000E-10	1.00000000E-10
C2H2	G	1.00000000E-10	1.00000000E-10	1.00000000E-10
C2H2	G	1.00000000E-10	1.00000000E-10	1.00000000E-10
C4	G	1.00000000E-10	1.00000000E-10	1.00000000E-10
C4	G	1.00000000E-10	1.00000000E-10	1.00000000E-10
N	G	2.44435461E+06	1.14059482E+06	3.65013458E+04
NH	G	5.32580514E+02	4.29400798E+02	1.05467792E+02
NH2	G	3.44436351E+05	2.35324361E+05	3.39091697E+04
NH3	G	6.7763175E+11	1.00000000E+10	1.00000000E+10
N2	G	1.09072202E+00	1.04586302E+00	1.11204565E+00
N2O	G	2.32139994E+08	1.43470557E+06	9.97577891E+04
N2H2	G	1.00000000E+10	1.00000000E+10	1.00000000E+10
N2H4	G	1.00000000E+10	1.00000000E+10	1.00000000E+10
O	G	3.11535522E+02	2.79458669E+02	1.74854316E+03
O2	G	3.78123773E+01	3.41411923E+01	3.01579409E+01
AR	G	1.28762438E+02	1.28762438E+02	1.28762438E+02
C	S	0.00000000E+00	0.00000000E+00	0.00000000E+00

UTC1515  
24 APR 1971

UTC151528-  
PAGE 1

INGREDIENTS	WT.PCT.	ELEMENTS	GM ATOMS
0498 CARBON MONOXIDE GAS	46.56	O	1.67098523E+00
0189 OXYGEN GAS	25.72	C	1.66220413E+00
9099 AIR	27.72	N	1.49594527E+00
		AR	8.61940299E-03

PROPELLANT DENSITY, G/CC 1.00000000E+03

	THROAT	EXHAUST( 1)
AREA RATIO	1.00000000E+00	3.13232331E+00
OPTIMUM ISP, SEC	8.54695141E+01	1.79588651E+02
VACUUM ISP, SEC	1.62732989E+02	2.09859455E+02
C*, FT/SEC	4.25973900E+03	
VELOCITY, FT/SEC	2.74989615E+03	5.77808527E+03
DENSITY, GM/CC	8.67979495E-05	1.31878873E-05

	CHAMBER	THROAT	EXHAUST( 1)
PRESSURE, PSTA	1.37000000E+01	7.99497058E+00	1.00000000E+00
PRESSURE, ATM	9.32224456E-01	5.84023584E-01	6.80857267E-02
TEMPERATURE, DEG K	2.80151496E+03	2.69294011E+03	2.31750575E+03
HEAT CAP., CAL/DEG K/G	3.23594560E-01	3.23279819E-01	3.21377439E-01
ENTHALPY, KCAL/G	-4.39104466E+01	-5.23017849E-01	-4.09585978E-01
ENTROPY, CAL/DEG K/G	2.09949009E+00	2.09949009E+00	2.09949011E+00
MOLS OF GAS / 100 G	2.87264616E+00	2.83640273E+00	2.71325599E+00

COMBUSTION PRODUCTS

		CHAMBER	THROAT	EXHAUST( 1)
		MOLS/100 G	MOLS/100 G	MOLS/100 G
C	G	1.00000000E-10	1.00000000E-10	1.00000000E-10
C*	G	2.17374633E-10	5.78792921E-11	1.00000000E-10
CO	G	5.03164434E-01	4.41651126E-01	2.24550458E-01
CO2	G	1.15901986E+00	1.22055315E+00	1.43765390E+00
CO*	G	1.00000000E-10	1.00000000E-10	1.00000000E-10
CO*2	G	1.00000000E-10	1.00000000E-10	1.00000000E-10
CO*	G	1.00000000E-10	1.00000000E-10	1.00000000E-10
CO*2	G	1.00000000E-10	1.00000000E-10	1.00000000E-10
CO*	G	1.00000000E-10	1.00000000E-10	1.00000000E-10
CO*	G	1.00000000E-10	1.00000000E-10	1.00000000E-10
CO*	G	1.00000000E-10	1.00000000E-10	1.00000000E-10
N	G	5.21400788E-06	2.95514091E-06	2.52898045E-07
N*	G	4.90064606E-07	4.08352677E-07	1.87120672E-07
N*2	G	2.23857514E-05	1.53701363E-05	3.36361937E-06
N*3	G	1.00000000E-10	1.00000000E-10	1.00000000E-10
N*	G	7.23454260E-01	7.27544983E-01	7.38614644E-01
N*2	G	1.35251655E-06	8.65955124E-07	1.43911893E-07
N*3	G	1.00000000E-10	1.00000000E-10	1.00000000E-10
N*4	G	1.00000000E-10	1.00000000E-10	1.00000000E-10
O	G	5.79470416E-02	4.67982694E-02	1.77999946E-02
O*	G	3.71349725E-01	3.50181111E-01	2.47304041E-01
AR	G	8.61940299E-03	8.61940299E-03	8.61940299E-03
C	S	0.00000000E+00	0.00000000E+00	0.00000000E+00

01C1514  
20 APR 1971

01C151529-  
PAGE 1

INGREDIENTS	WT. PCT.	ELEMENTS	GR. ATOMS
0128 CARBON DIOXIDE GAS	33.62	O	3.96567153E+00
0139 OXYGEN GAS	29.62	O	1.84264765E+00
9999 AIR	18.76	N	1.01240761E+00
		AN	5.83333333E-03

PROPELLANT DENSITY, G/CC 1.00000000E+03

	THROAT	EXHAUST [ 1 ]
AREA RATIO	1.00000000E+00	1.95355690E+01
DURATION ISP, SEC	4.52696670E+01	1.54088204E+02
VACUUM ISP, SEC	1.62680631E+02	1.94425506E+02
C* FT/SEC	4.26062811E+03	
VELOCITY, FT/SEC	2.74346627E+03	5.08632987E+03
DENSITY, G/CC	4.53963536E-05	1.23444405E-05

	CHAMBER	THROAT	EXHAUST [ 1 ]
PRESSURE, PSIA	7.15000000E+00	4.17965030E+00	1.00000000E+00
PRESSURE, ATM	4.86524946E-01	2.84407342E-01	6.80457267E-02
TEMPERATURE, DEG K	2.79823896E+03	2.69741469E+03	2.45483574E+03
HEAT CAP., CAL/DEG K/G	3.23414358E-01	3.23579242E-01	3.22735451E-01
ENTHALPY, KCAL/G	-4.86825012E-01	-5.70346437E-01	-7.73908155E-01
ENTROPY, CAL/DEG K/G	2.13807495E+00	2.13807495E+00	2.13607495E+00
MOLS OF GAS / 100 G	2.86869192E+00	2.83046928E+00	2.73648668E+00

COMBUSTION PRODUCTS

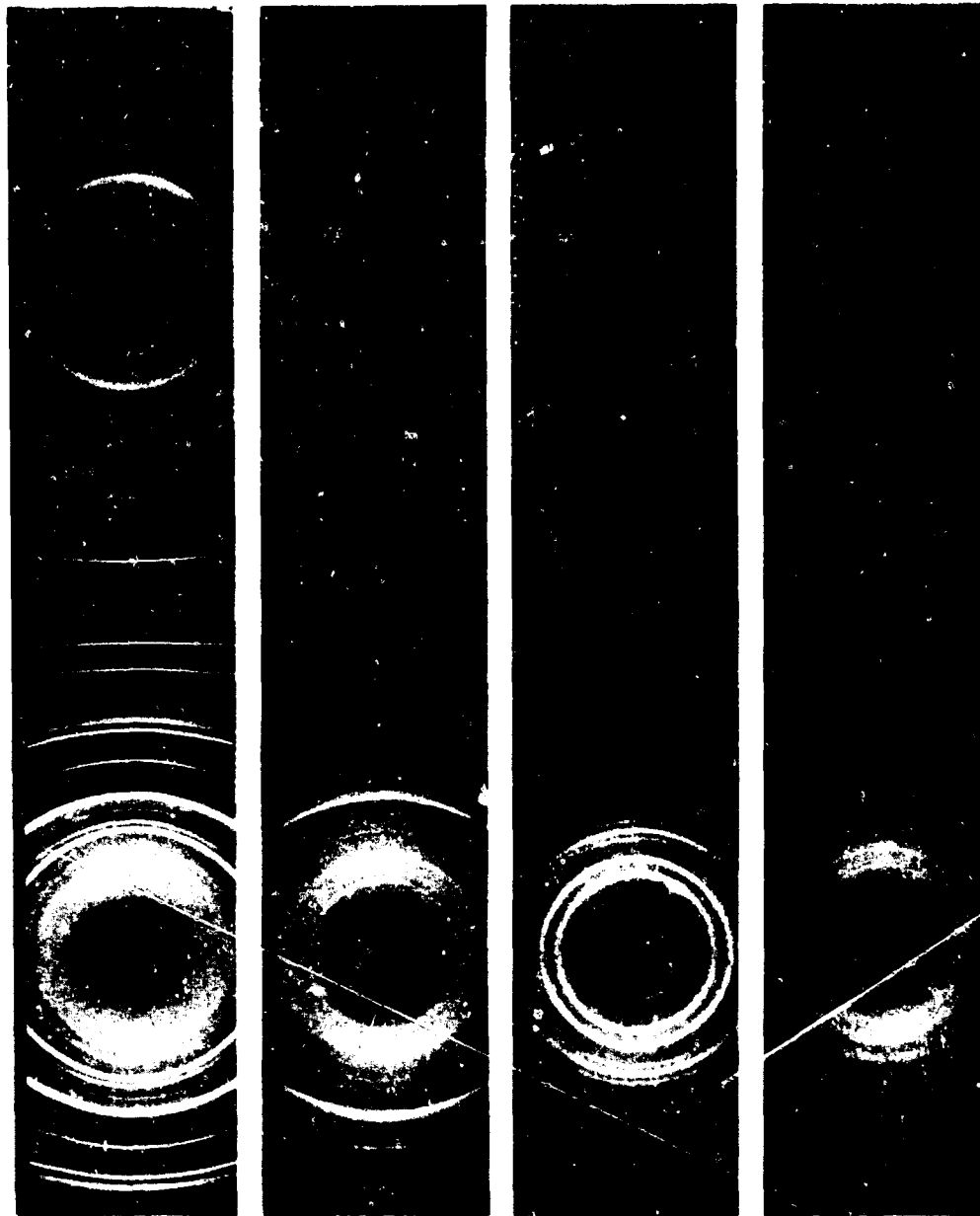
	CHAMBER MOLS/100 G	THROAT MOLS/100 G	EXHAUST [ 1 ] MOLS/100 G
C	1.00000000E-10	1.00000000E-10	1.00000000E-10
C*	2.17741846E-10	6.61340103E-11	1.00000000E-10
C#	6.64456675E-01	6.01524582E-01	6.41581792E-01
C#2	1.17832094E+00	1.24132304E+00	1.40130546E+00
C#3	1.00000000E-10	1.00000000E-10	1.00000000E-10
C#4	1.00000000E-10	1.00000000E-10	1.00000000E-10
C#5	1.00000000E-10	1.00000000E-10	1.00000000E-10
C#6	1.00000000E-10	1.00000000E-10	1.00000000E-10
C#7	1.00000000E-10	1.00000000E-10	1.00000000E-10
C#8	1.00000000E-10	1.00000000E-10	1.00000000E-10
C#9	1.00000000E-10	1.00000000E-10	1.00000000E-10
N	5.76834272E-06	3.46699942E-06	8.40811195E-07
N*	4.19605058E-02	3.54638437E-02	2.20811718E-02
N#1	1.45954816E-05	1.01291766E-05	3.71471774E-06
N#2	1.00000000E-10	1.00000000E-10	1.00000000E-10
N#3	4.85212599E-01	4.88468547E-01	4.95157214E-01
N#4	4.85557475E-07	4.46069687E-07	1.38527078E-07
N#5	1.00000000E-10	1.00000000E-10	1.00000000E-10
N#6	1.00000000E-10	1.00000000E-10	1.00000000E-10
D	4.31701900E-02	6.96754291E-02	4.16889129E-02
D*	4.09834402E-01	3.88170456E-01	3.28466694E-01
AN	5.83333333E-03	5.83333333E-03	5.83333333E-03
C	0.00000000E+00	0.00000000E+00	0.00000000E+00

## APPENDIX II

### X-RAY DIFFRACTION DATA

The diffraction patterns for the original particles are shown on pages II-1 and II-2; the diffraction patterns for the residues from combustion of particles at various pressures ( $P_c$ ) and temperatures ( $T_c$ ) are shown on pages II-3 through II-23.

NOT REPRODUCIBLE



All original particles at 37-44 $\mu$  size

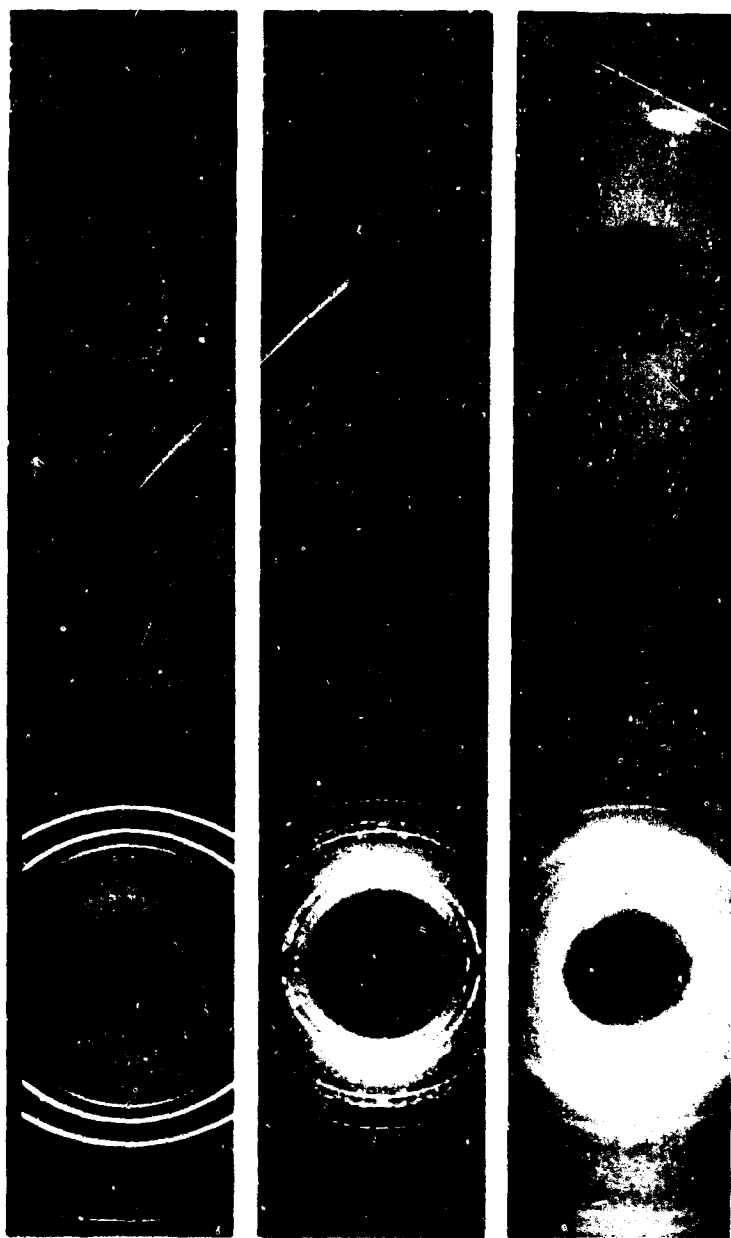
Particles

MgB<sub>2</sub>

MgH<sub>12</sub>

LiB<sub>2</sub>

LiB<sub>1</sub>



All original particles at 37-44  $\mu$  size

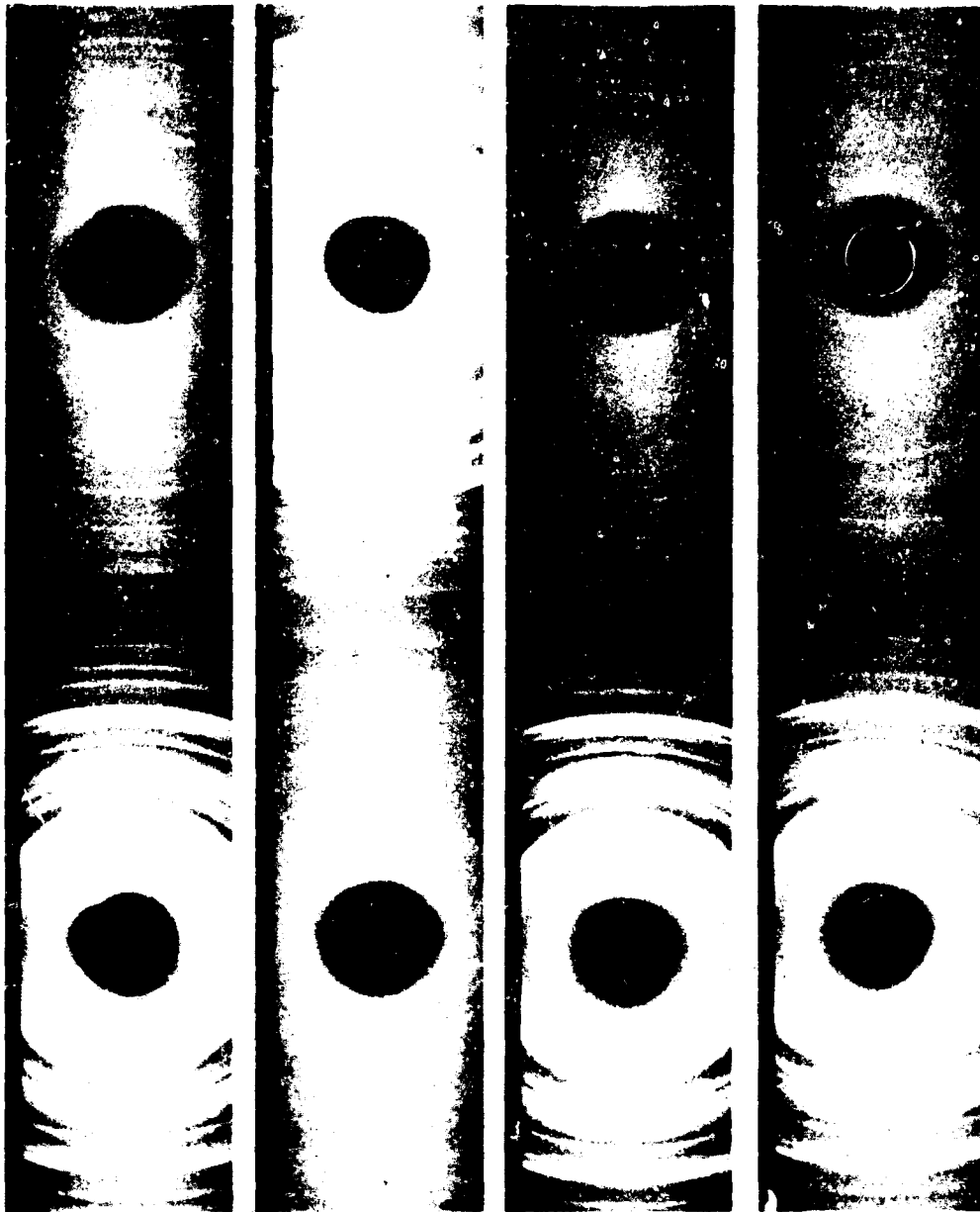
Particles

AIB<sub>2</sub>

AIB<sub>12</sub>

B

NOT REPRODUCIBLE

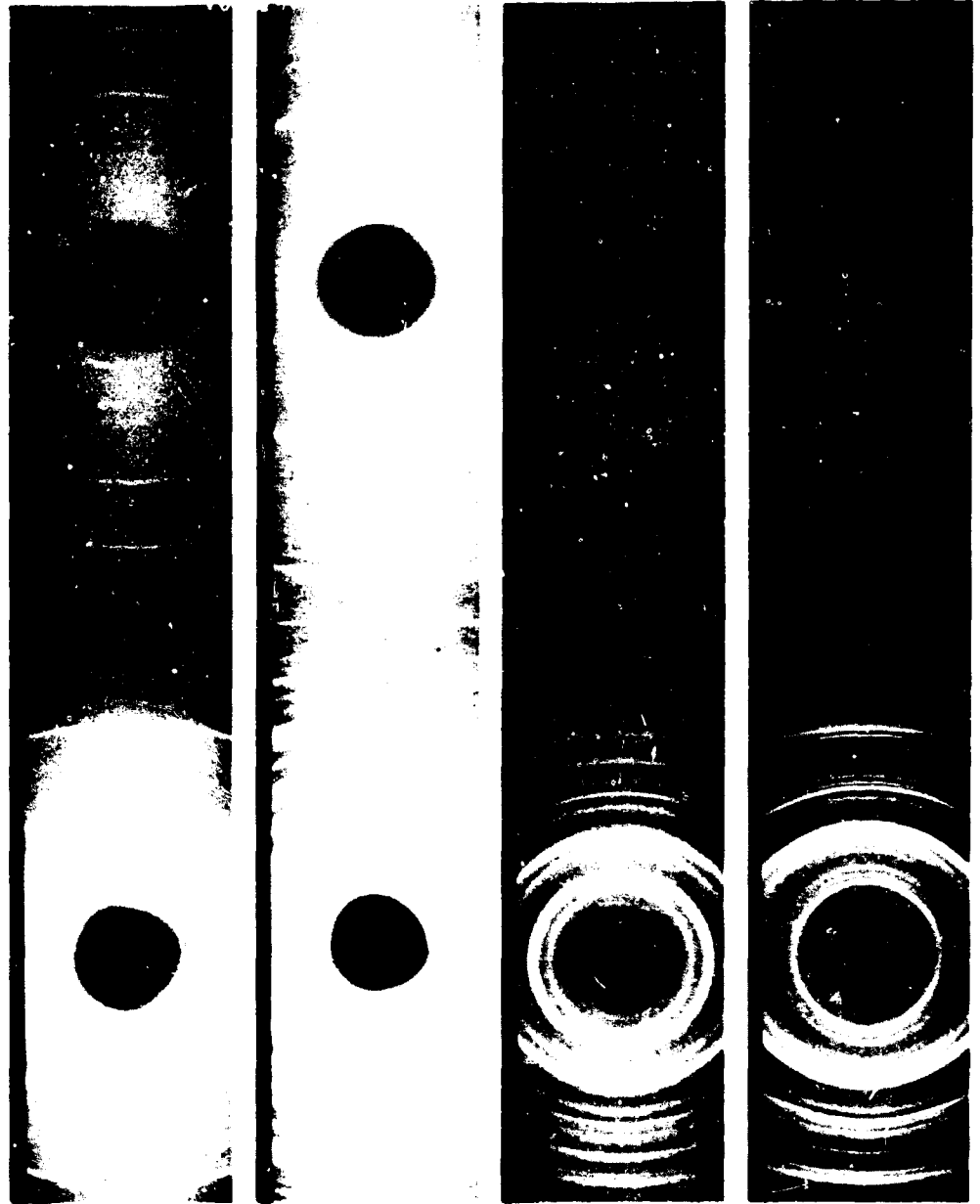


Particles

37-44 $\mu$   $\text{MgH}_2$

Test Run No.	4-28-71-3	4-28-71-4	4-28-71-5	4-28-71-6
$P_c$ , psia	37.0	25.5	15.5	9.0
$T_c$ , $^{\circ}\text{K}$	1430	1400	1400	1410

NOT REPRODUCIBLE

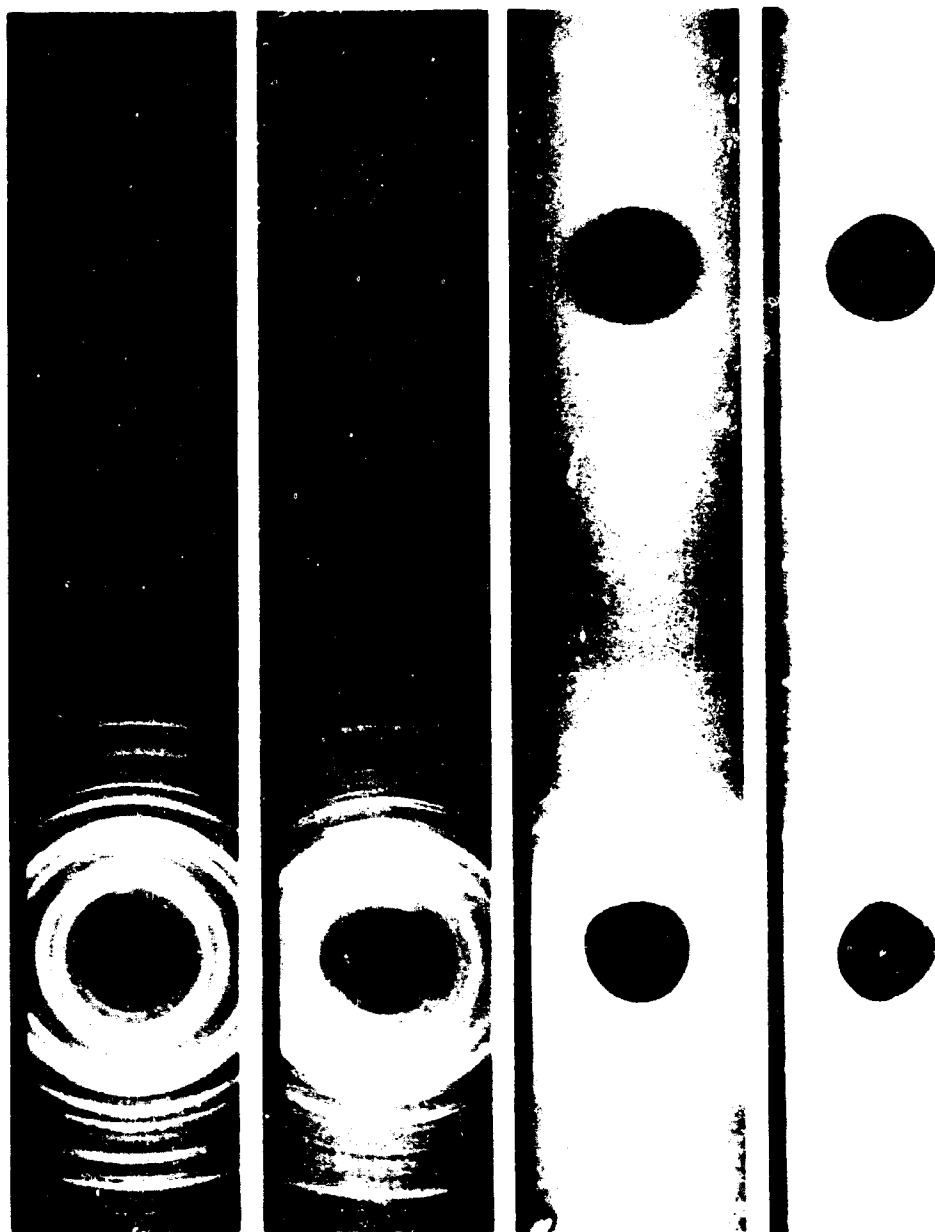


Particles

37-44 $\mu$  MgSi<sub>2</sub>

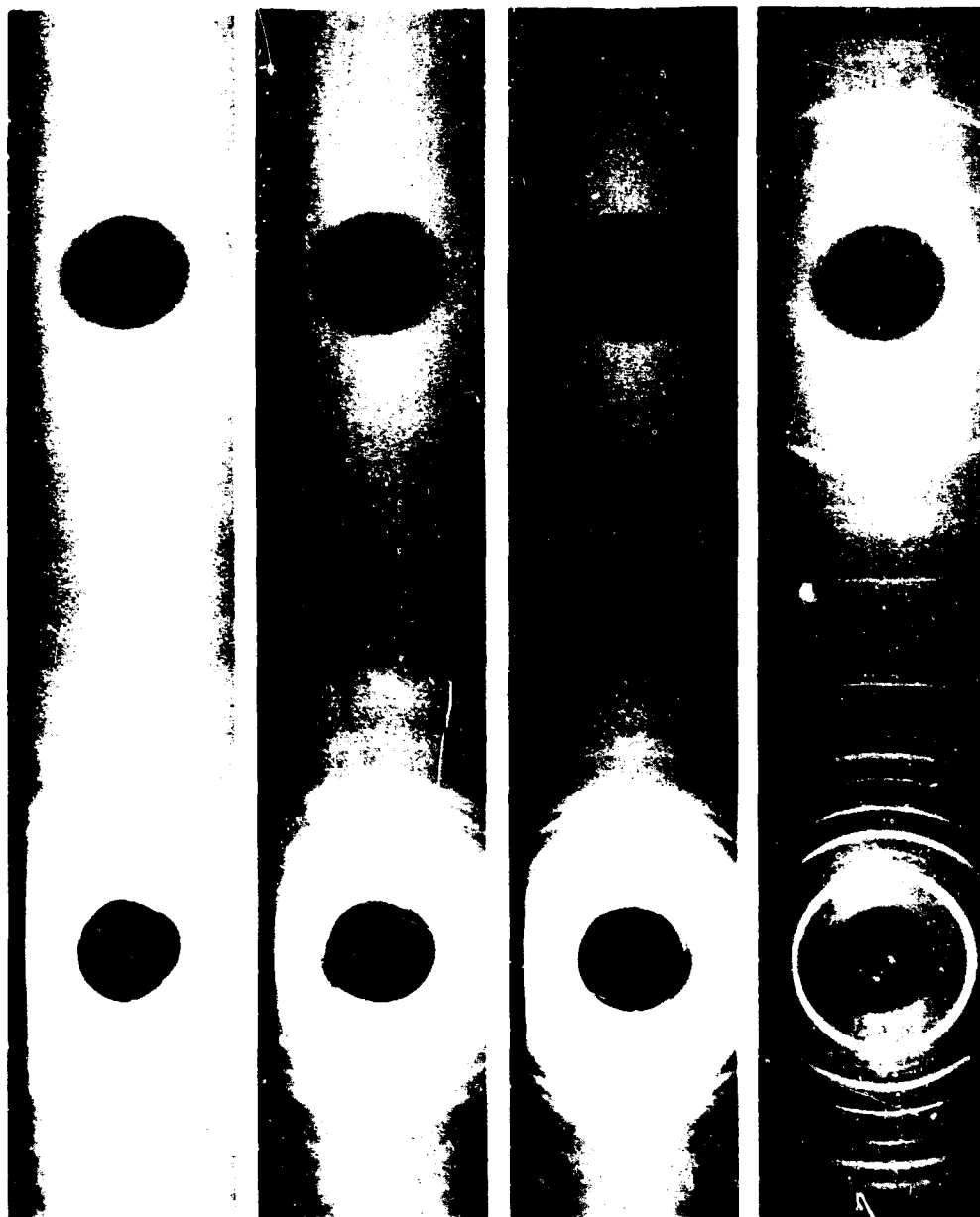
Test Run No.	4-28-71-1	4-28-71-7	4-28-71-11	4-28-71-2
P <sub>c</sub> , psia	5.0	43.0	42.5	28.0
T <sub>c</sub> , °K	1250	1935	1675	1675

NOT REPRODUCIBLE



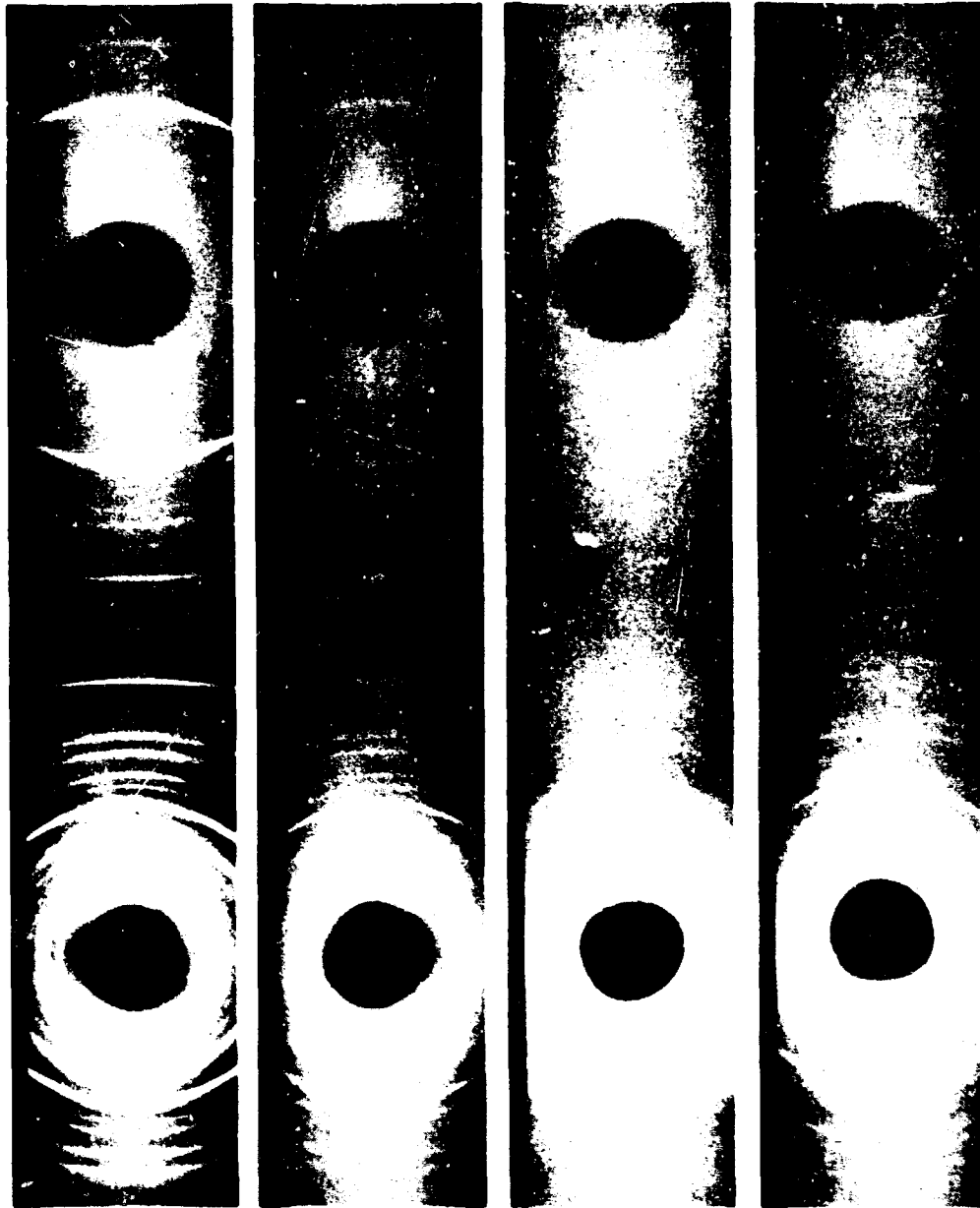
Particles	37-44 $\mu$ MgH <sub>2</sub>		37-44 $\mu$ B	
Test Run No.	4-27-71-3	4-28-71-2	5-3-71-5	5-3-71-6
P <sub>c</sub> , psia	15.5	10.0	42.0	1430
T <sub>c</sub> , °K	1650	1625	26.5	1400

NOT REPRODUCIBLE



Particles	37-44 $\mu$ B			
Test Run No.	5-3-71-7	5-3-71-8	5-3-71-9	5-3-71-10
P, psia	16.0	10.0	6.8	41.0
$\delta$ x	1400	1410	1250	1935

NOT REPRODUCIBLE

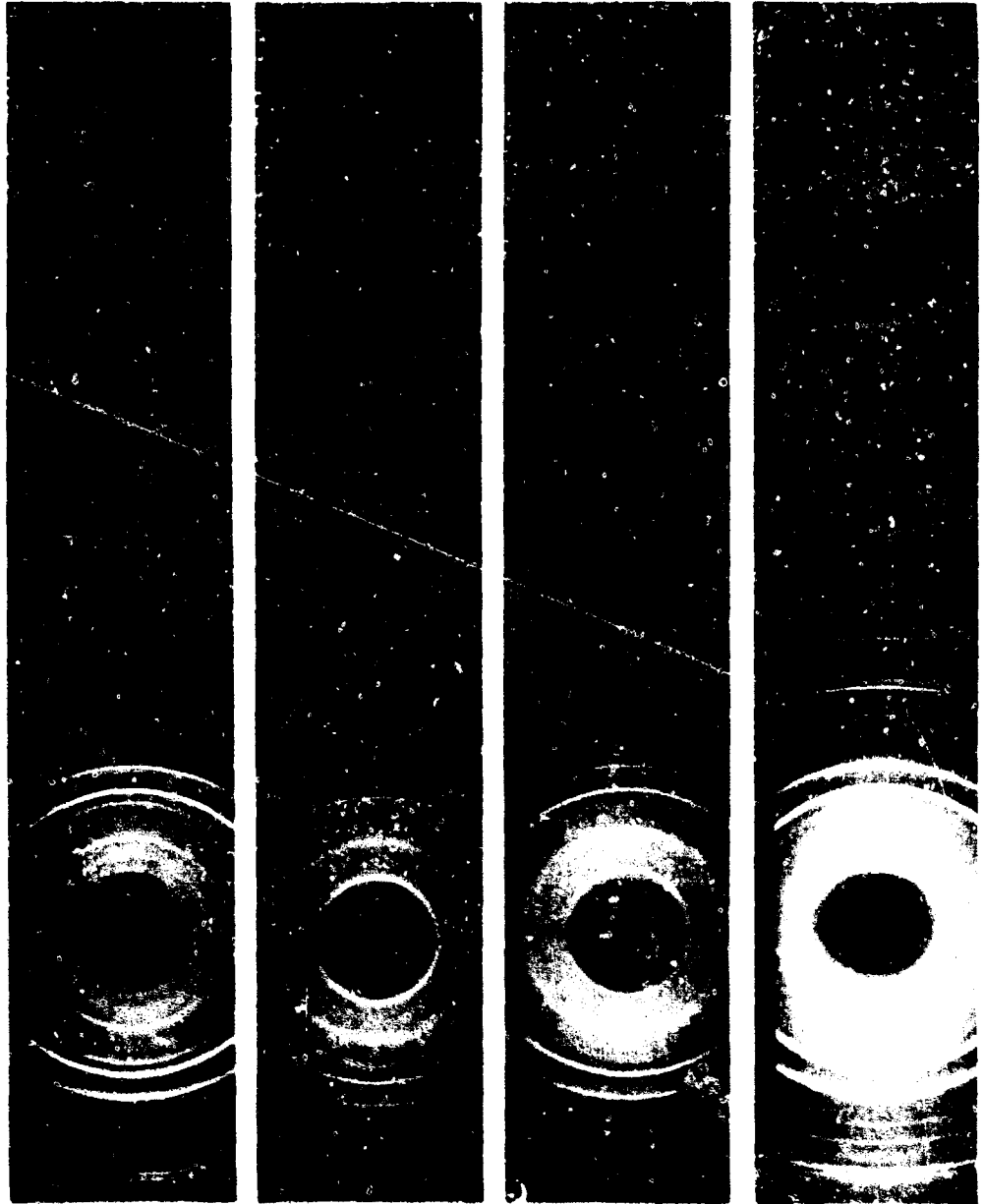


Particles

37-44 $\mu$  B

Test Run No.	5-3-71-1	5-3-71-2	5-3-71-3	5-3-21-4
$P_c$ , psia	39.0	27.5	15.2	11.5
$T_c$ , °K	1650	1675	1650	1625

NOT REPRODUCIBLE

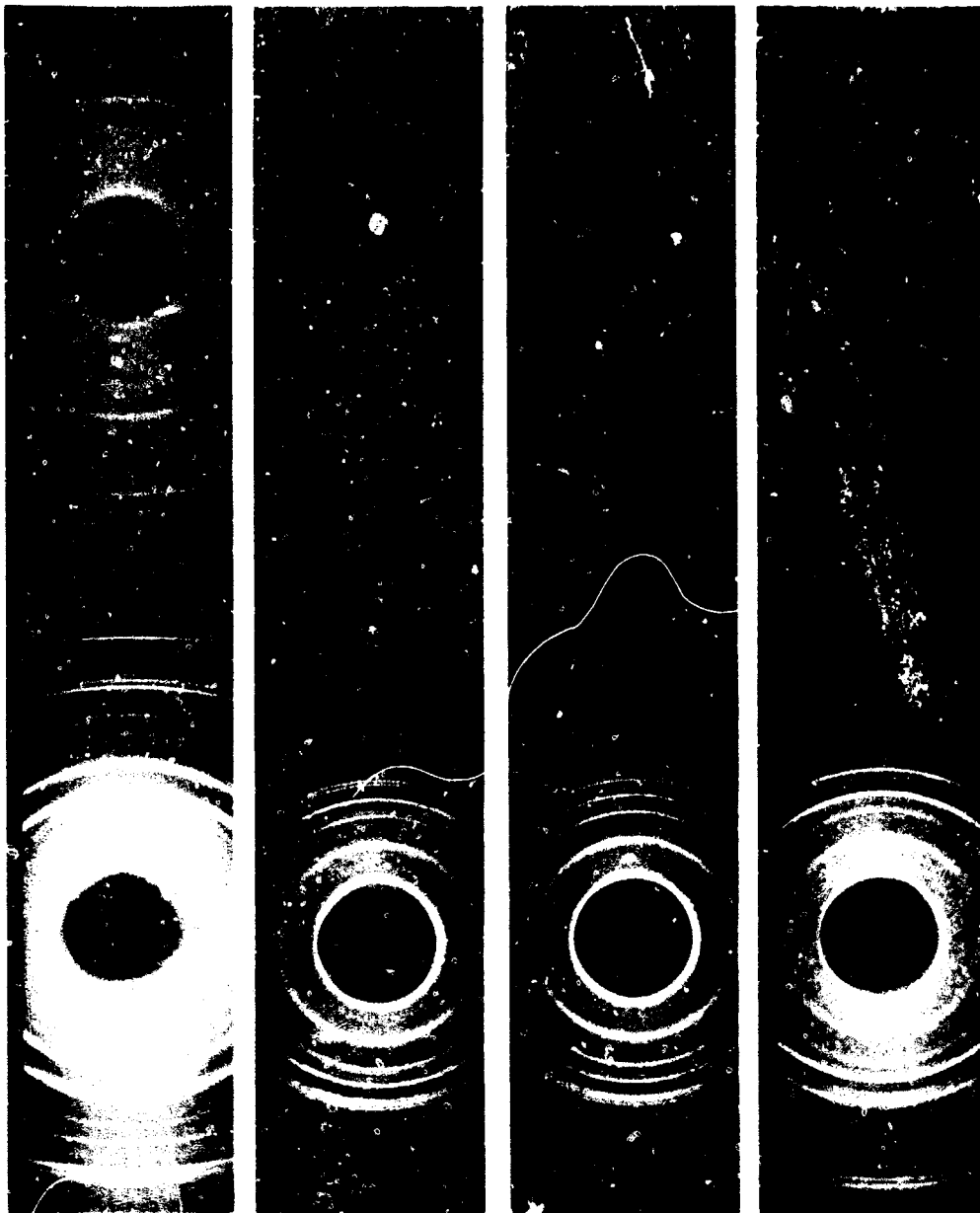


Particles

$17.44 \mu$  A.H.

Test Run No.	5-4-71-1	5-4-71-4	5-4-71-3	5-4-71-2
$P_c$ psm	19.0	25.0	15.8	10.5
$T_c$ °K	1430	1430	1400	1400

NOT REPRODUCIBLE

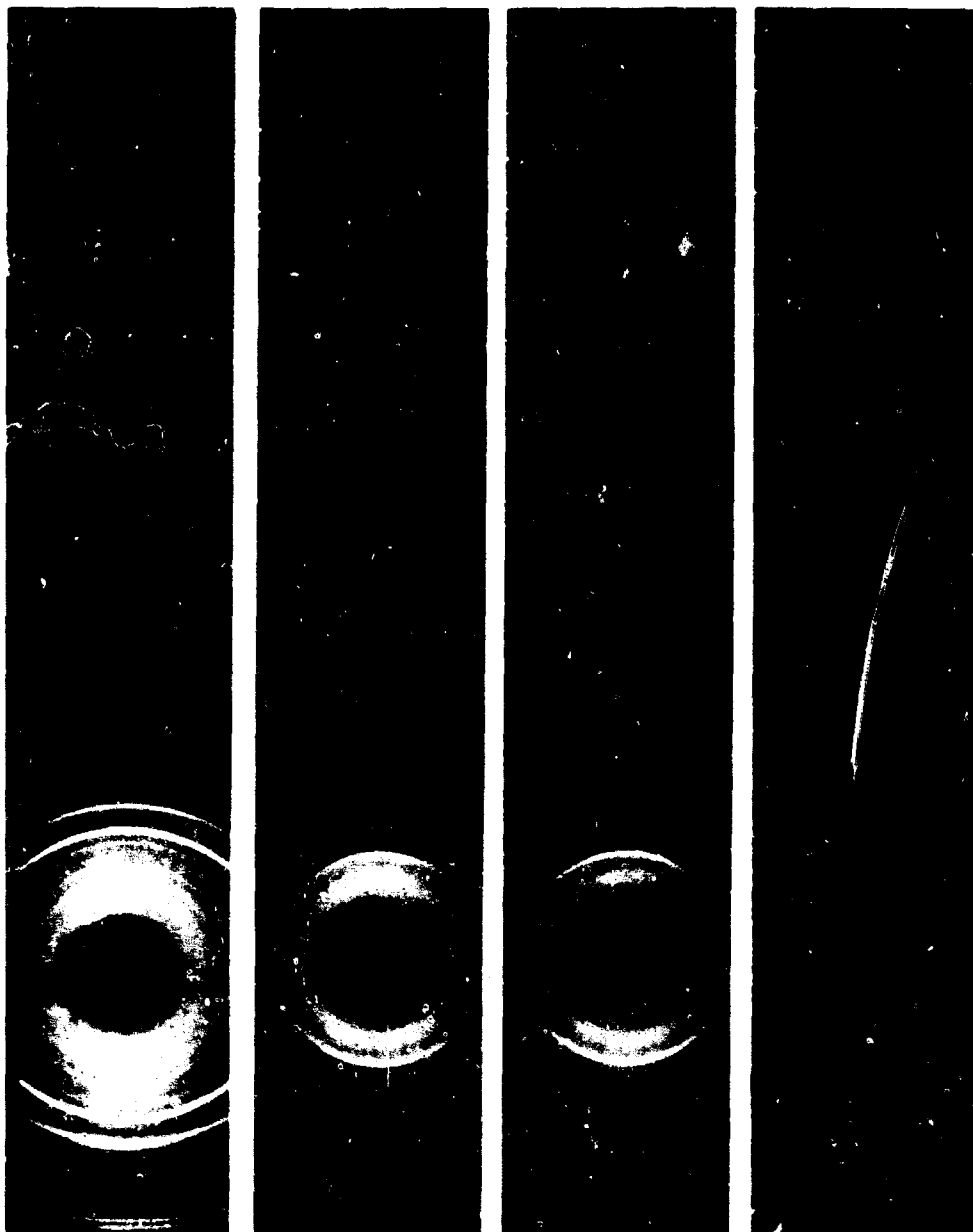


Particles

37-44 $\mu$  Al<sub>2</sub>O<sub>3</sub>

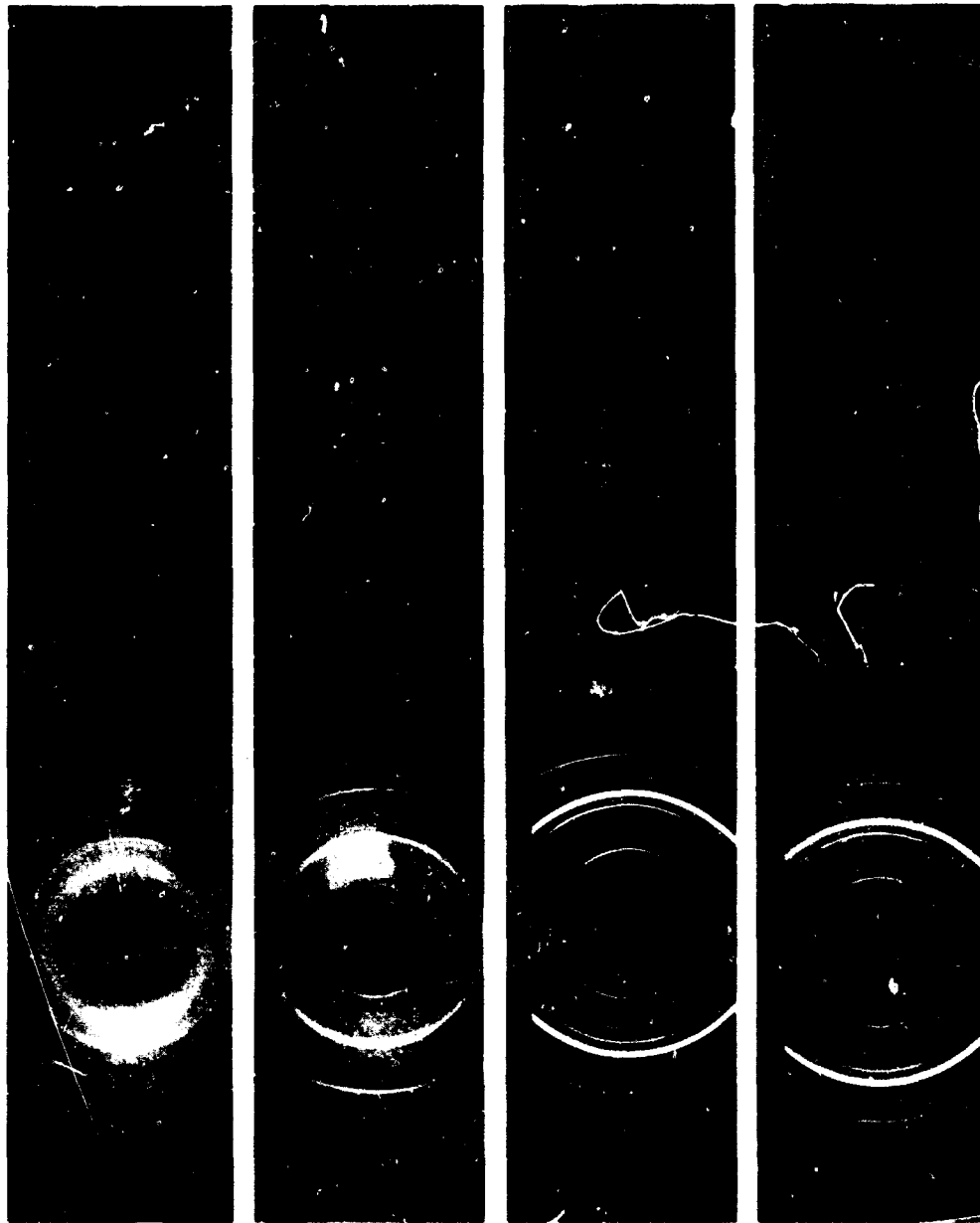
Test Run No.	5-4-71-1	5-4-71-9	5-4-71-8	5-4-71-7
P <sub>c</sub> , psia	6.0	42.0	26.0	14.5
T <sub>c</sub> , °K	1250	1650	1675	1650

NOT REPRODUCIBLE



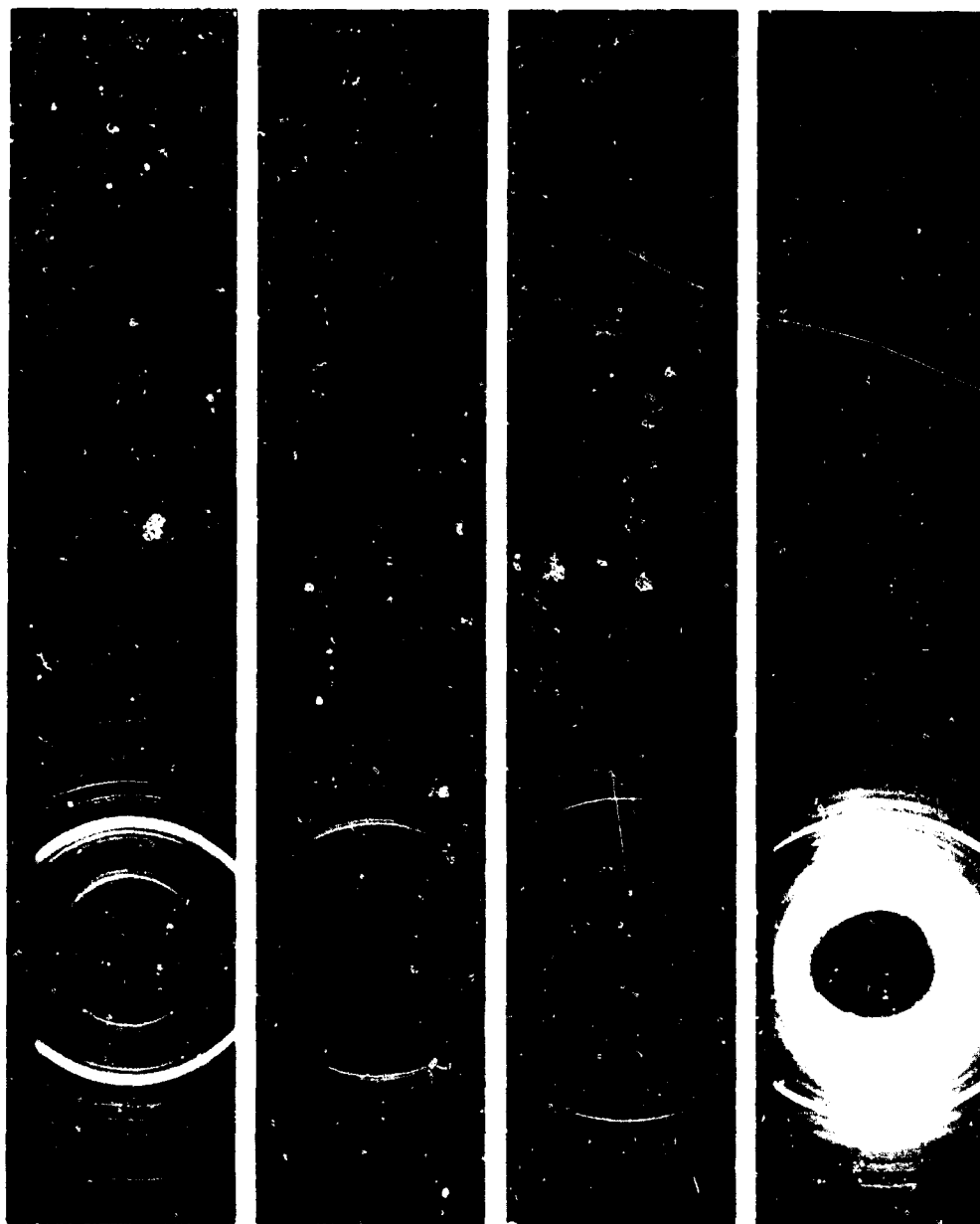
Particles	37-44 $\mu$ AlB <sub>2</sub>	63-74 $\mu$ B		
Test Run No.	S-4-71-6	S-19-71-5	S-19-71-4	S-19-71-3
P <sub>c</sub> psin	10.0	47.0	29.0	16.0
T <sub>c</sub> °K	1625	1650	1675	1650

NOT REPRODUCIBLE



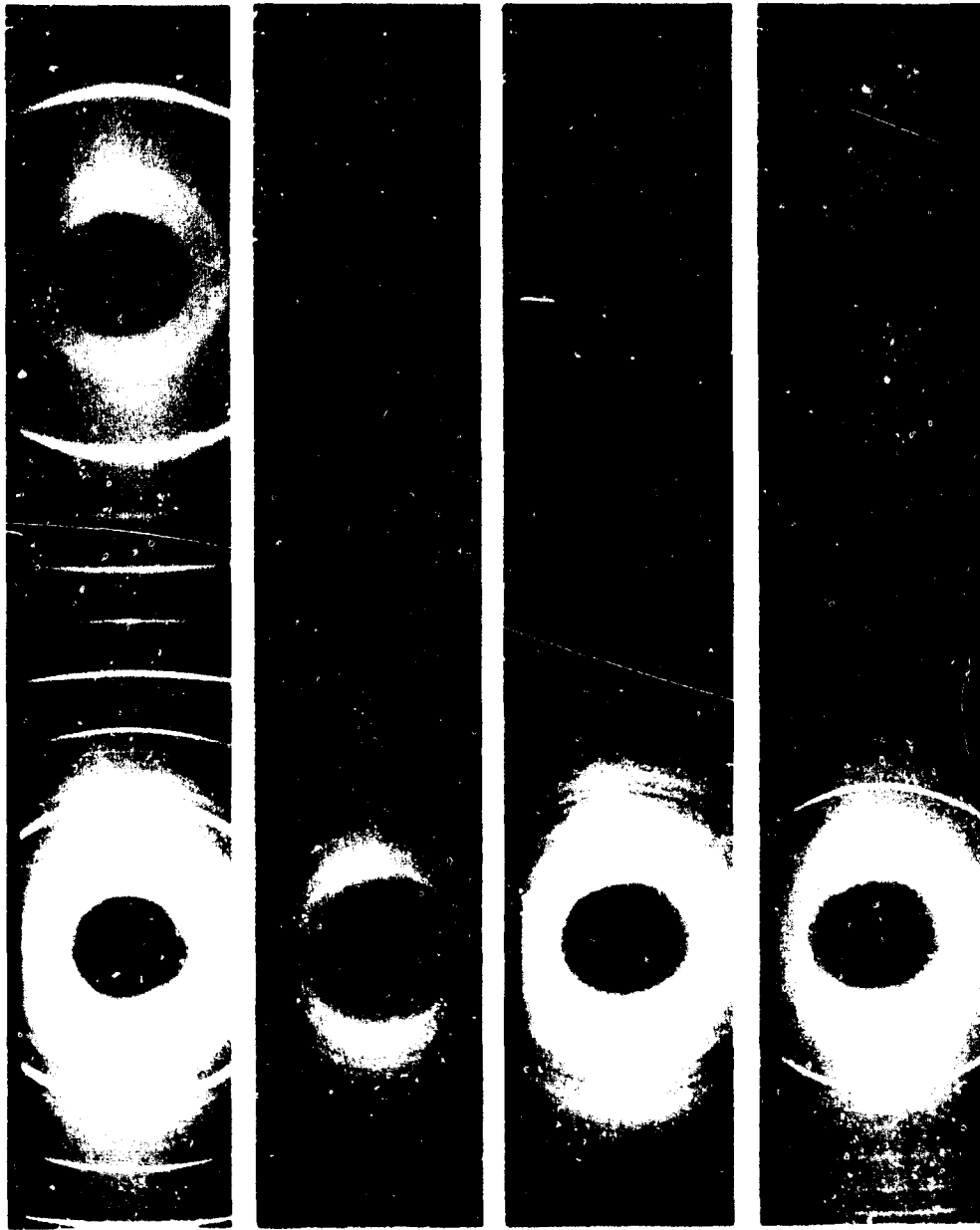
Particles	63-74 $\mu$ H		63-74 $\mu$ MgH <sub>2</sub>	
Test Run No.	S-19-71-2	S-19-71-1	S-20-71-5	S-20-71-4
P <sub>c</sub> , psia	10.5	5.0	44.0	30.0
T <sub>c</sub> , °K	1625	1250	1650	1675

NOT REPRODUCIBLE



Particles	63-74 $\mu$ MgH <sub>2</sub>			37-44 $\mu$ LiH <sub>2</sub>
Test Run No.	5-20-71-3	5-20-71-2	5-20-71-1	5-10-71-5
P <sub>c</sub> , psia	15.0	10.0	4.0	43.5
T <sub>c</sub> , °K	1650	1625	1250	1430

NOT REPRODUCIBLE



Particles

$37-44\mu \text{LiH}_2$

Test Run No.	5-10-71-4	5-10-71-3	5-10-71-2	5-10-71-1
$P_c$ , psia	26.0	15.0	9.0	4.0
$T_c$ , °K	1400	1400	1410	1250

NOT REPRODUCIBLE

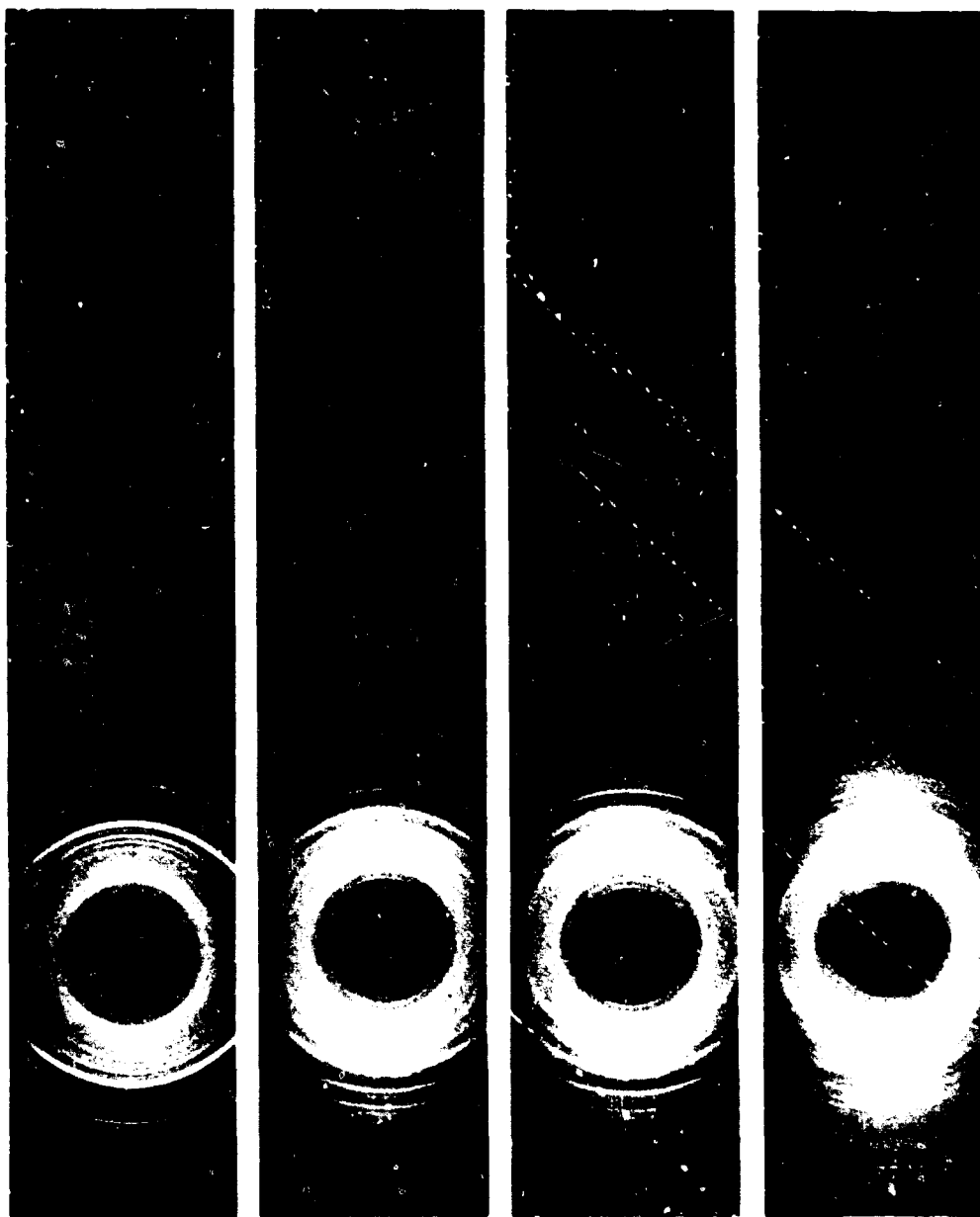


Particles

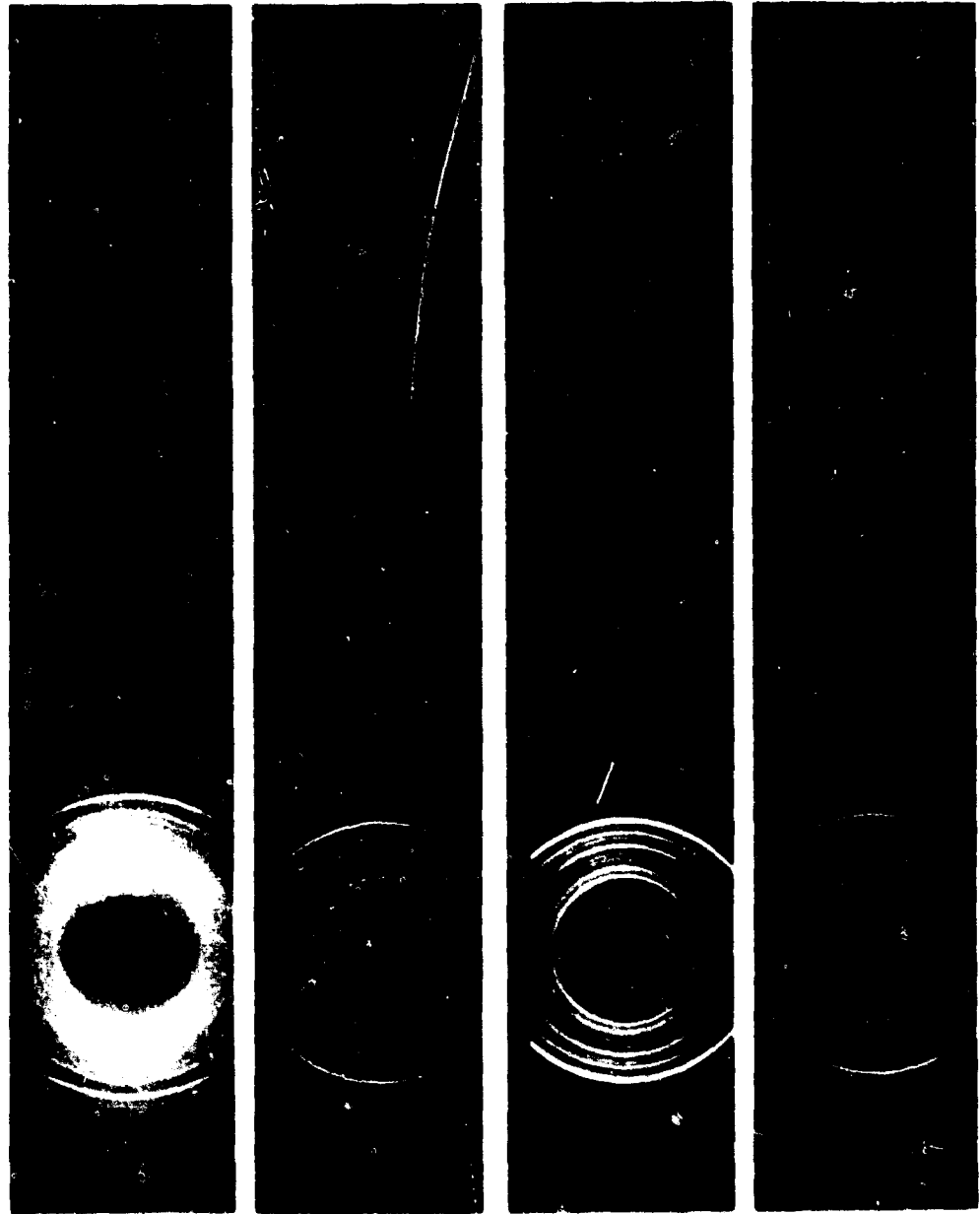
37-44  $\mu$  L.B<sub>2</sub>

Test Run No.	5-10-71-9	5-10-71-8	5-10-71-7	5-10-71-6
P <sub>c</sub> , psia	43.0	28.0	15.0	10.0
T <sub>c</sub> , °K	1650	1675	1650	1625

NOT REPRODUCIBLE



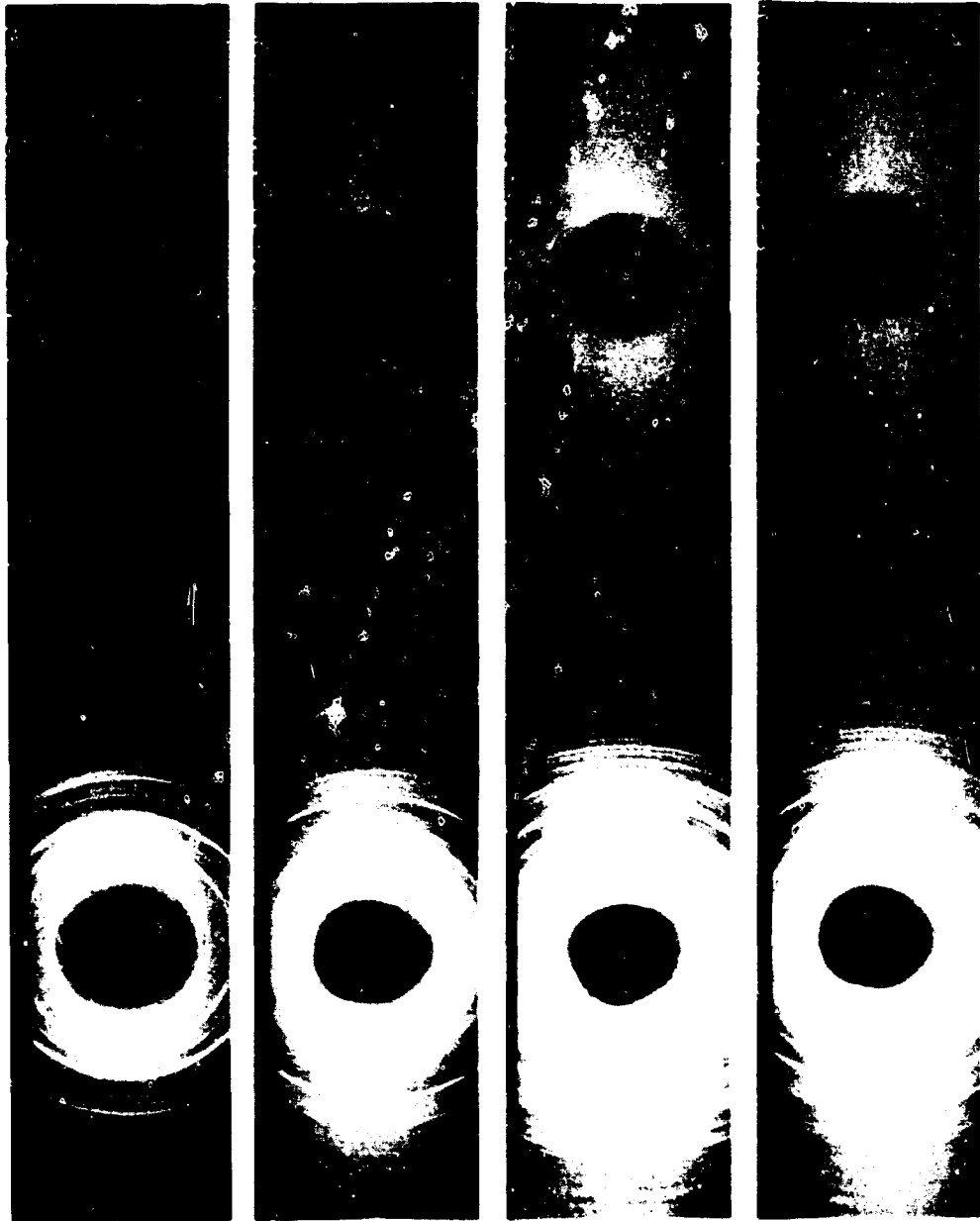
Particles	37-44 $\mu$ MgB <sub>12</sub>			
Test Run No.	5-13-71-5	5-13-71-4	5-13-71-3	5-13-71-2
P <sub>c</sub> , psia	39.0	25.0	15.0	11.5
T <sub>c</sub> , °K	1650	1675	1650	1625



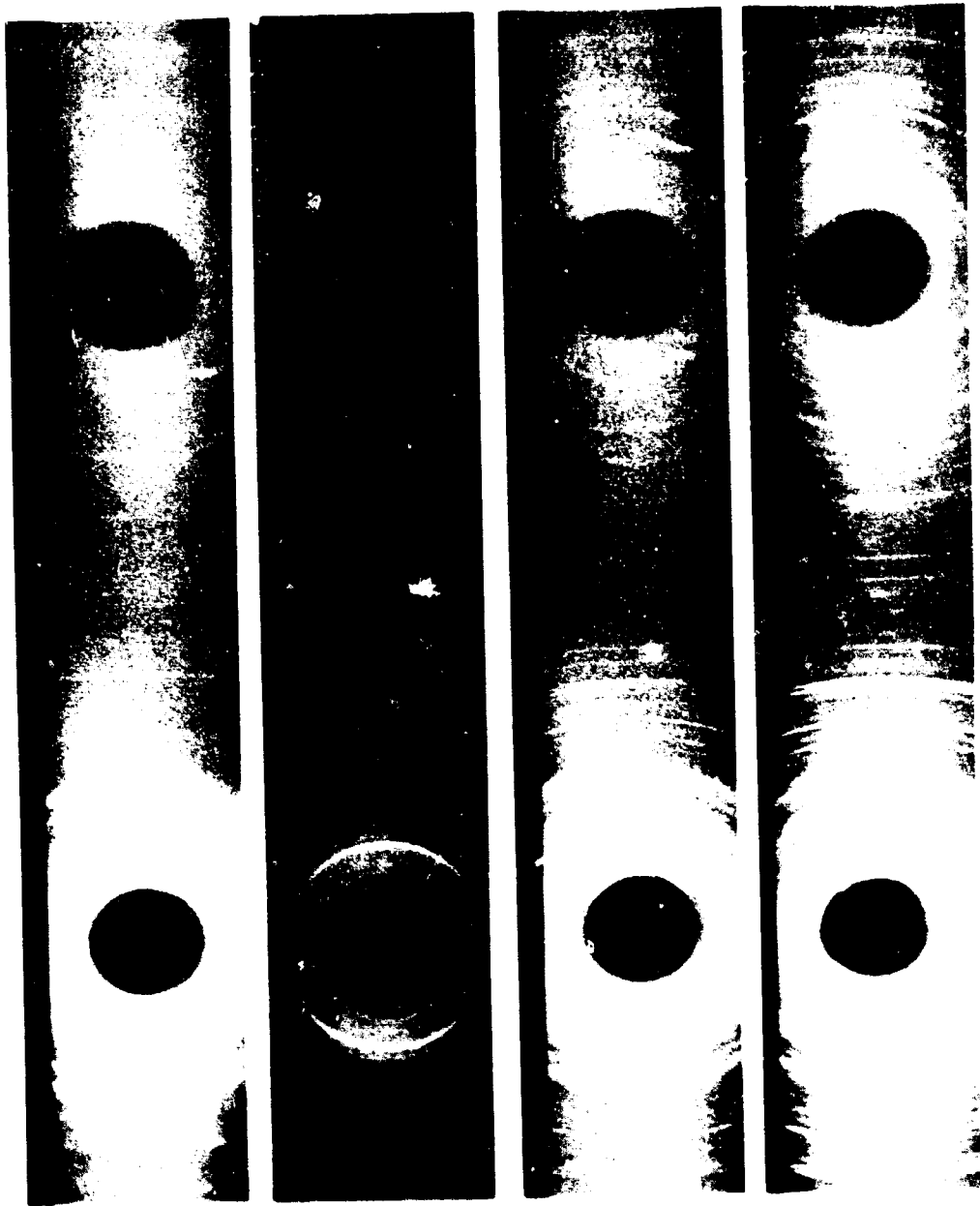
Particles

37-44 $\mu$  MgB<sub>12</sub>

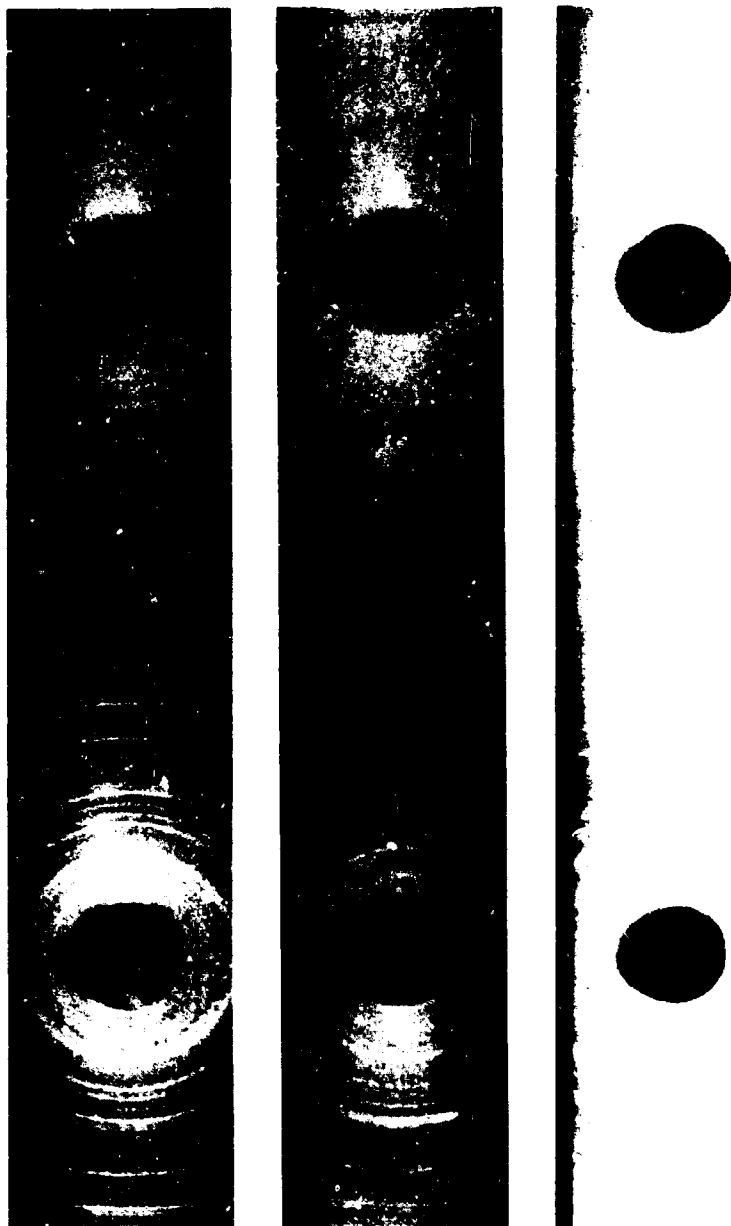
Test Run No.	5-13-71-1	5-21-71-4	5-21-71-3	5-21-71-2
P <sub>c</sub> , psm	5.0	45.0	26.0	16.0
T <sub>c</sub> , °K	1250	1430	1400	1400



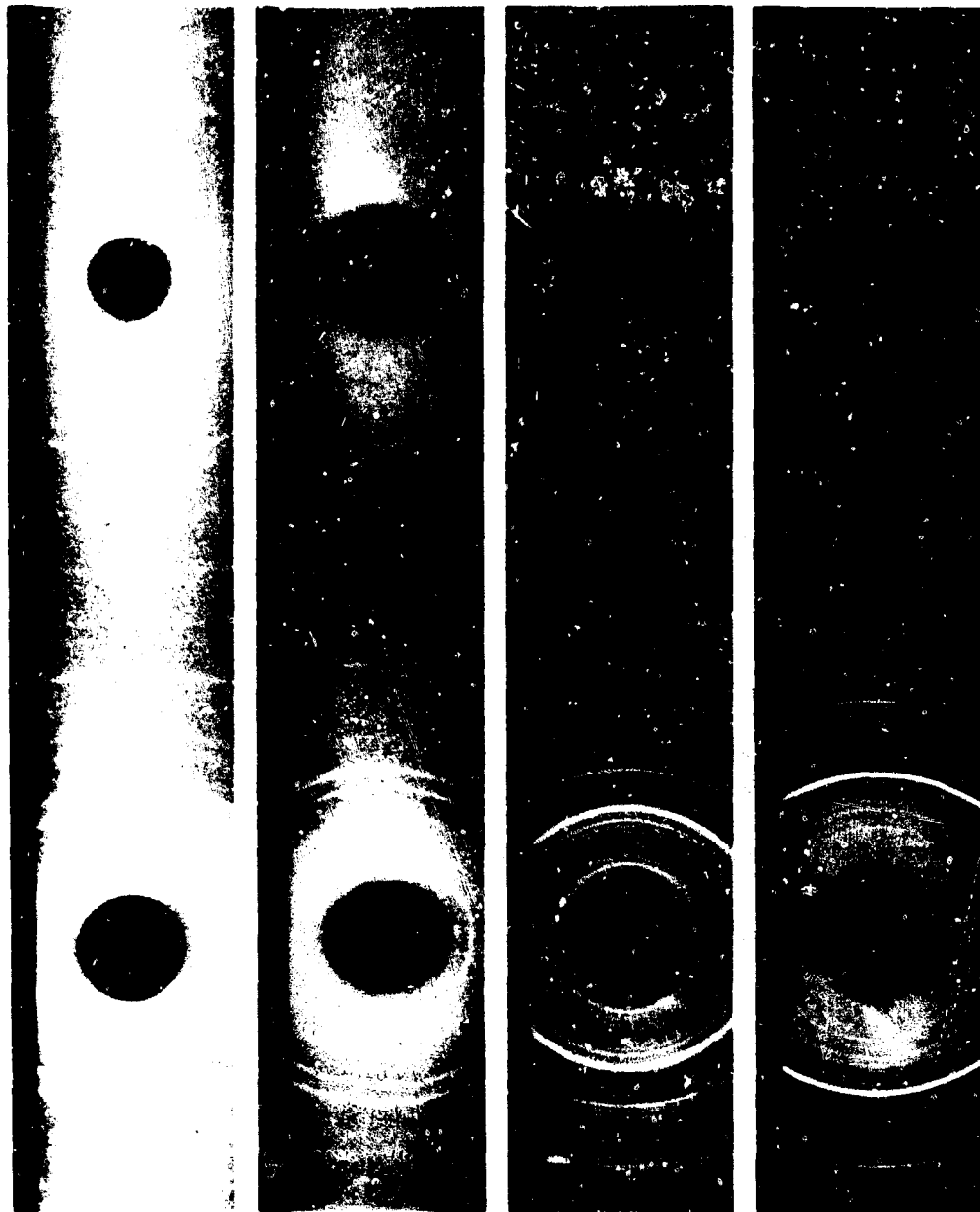
Particles	37-44 $\mu$ MgB <sub>12</sub>		37-44 $\mu$ LiB <sub>12</sub>	
Test Run No.	5-21-71-1	5-17-71-5	5-17-71-4	5-17-71-3
P <sub>c</sub> , psia	9.0	44.5	29.5	15.0
T <sub>c</sub> , °K	1410	1650	1675	1650



Particles	37-44 $\mu$ Lib <sub>12</sub>		37-44 $\mu$ AIB <sub>12</sub>	
Test Run No	S-17-71-2	S-17-71-1	S-14-71-5	S-14-71-4
P <sub>c</sub> , psia	10.0	4.9	4.6	27.5
T <sub>c</sub> , °K	1625	1250	1650	1675



Particles	37-44 $\mu$ AIB <sub>12</sub>		
Test Run No.	5-14-71-3	5-14-71-2	5-14-71-1
P <sub>c</sub> , psia	15.0	10.5	5.0
T <sub>c</sub> , °K	1650	1625	1250

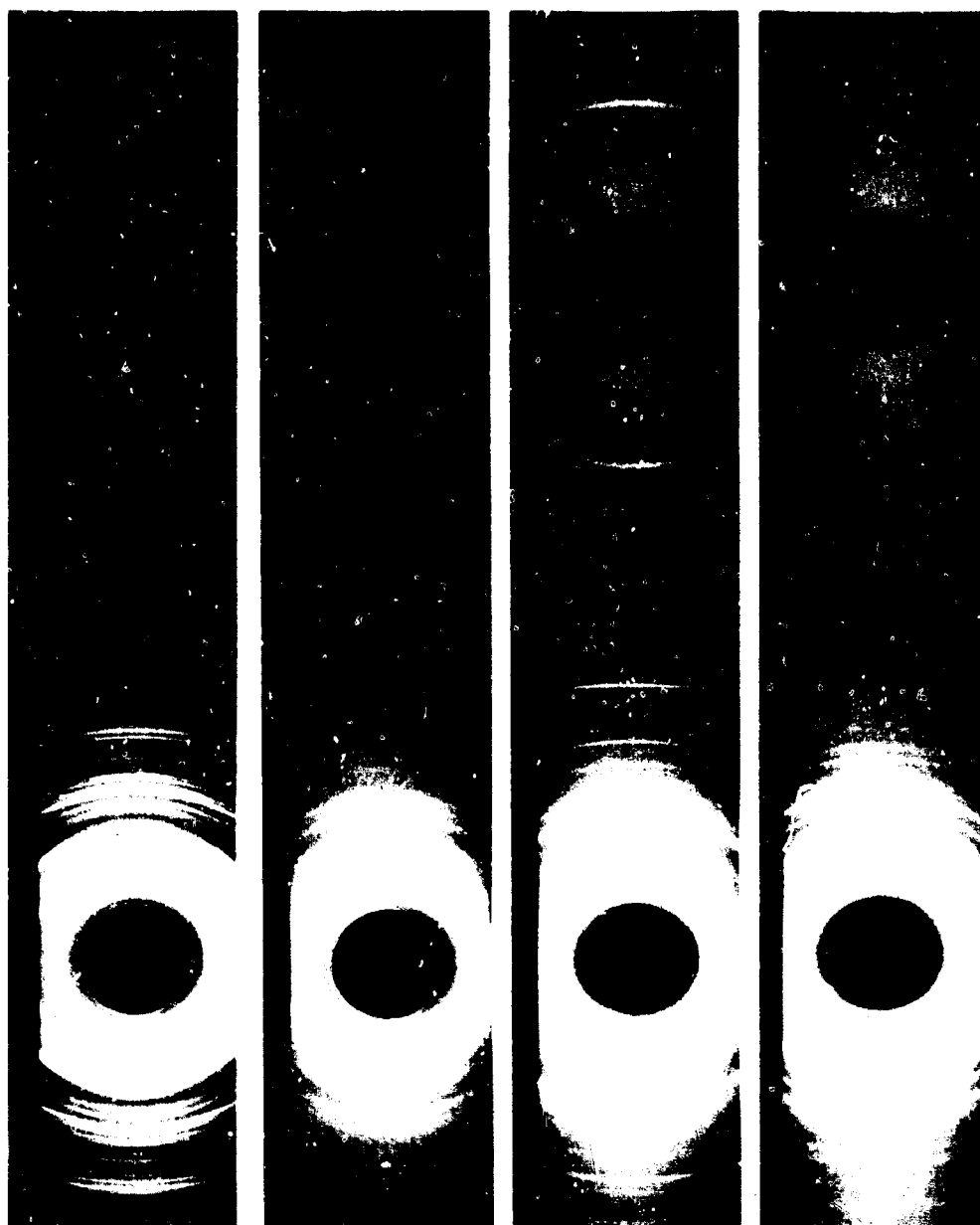


Particles

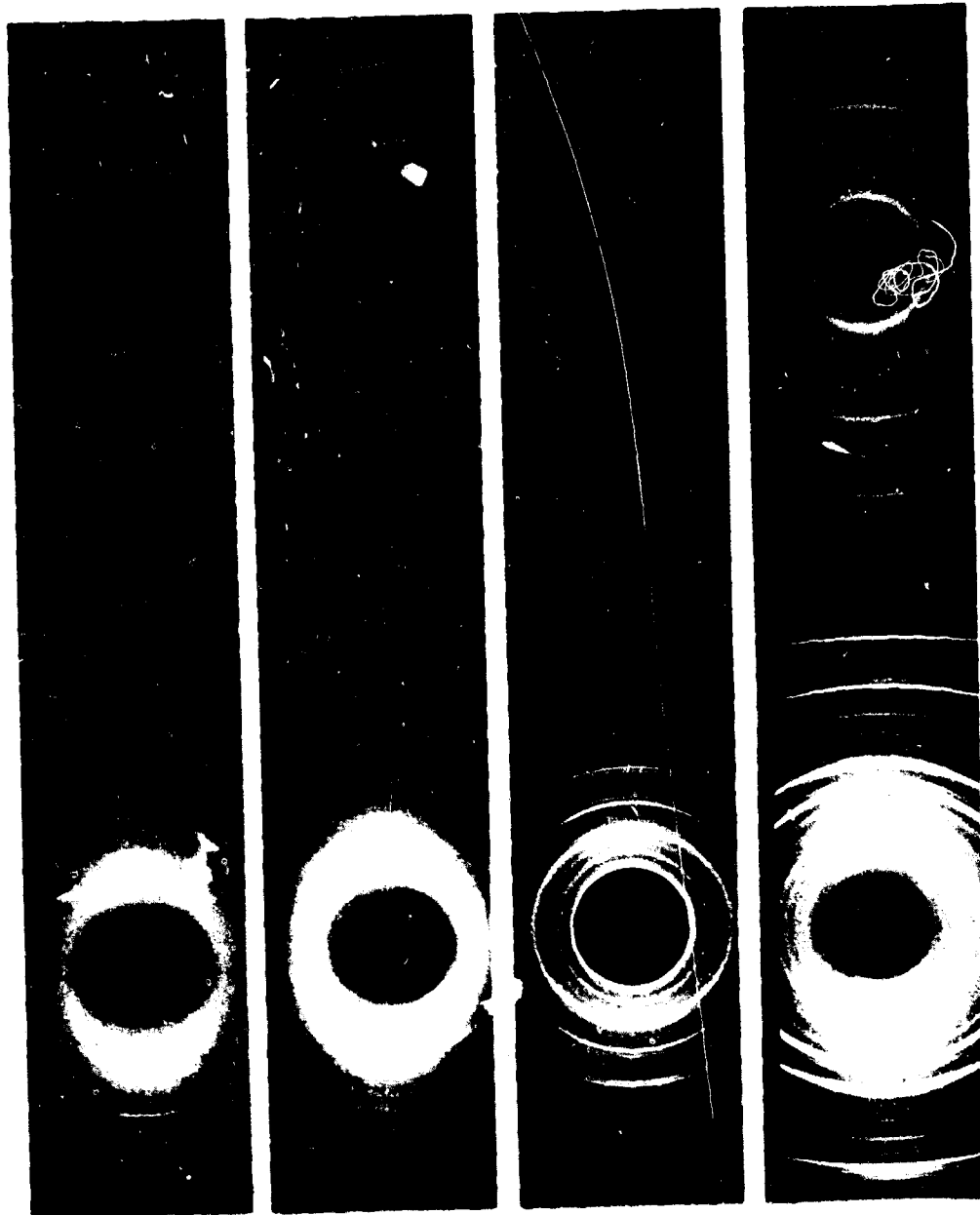
1 1/2% LiF doped 37-44 $\mu$  B

1 1/2% LiF doped 37-44 $\mu$  MgB<sub>2</sub>

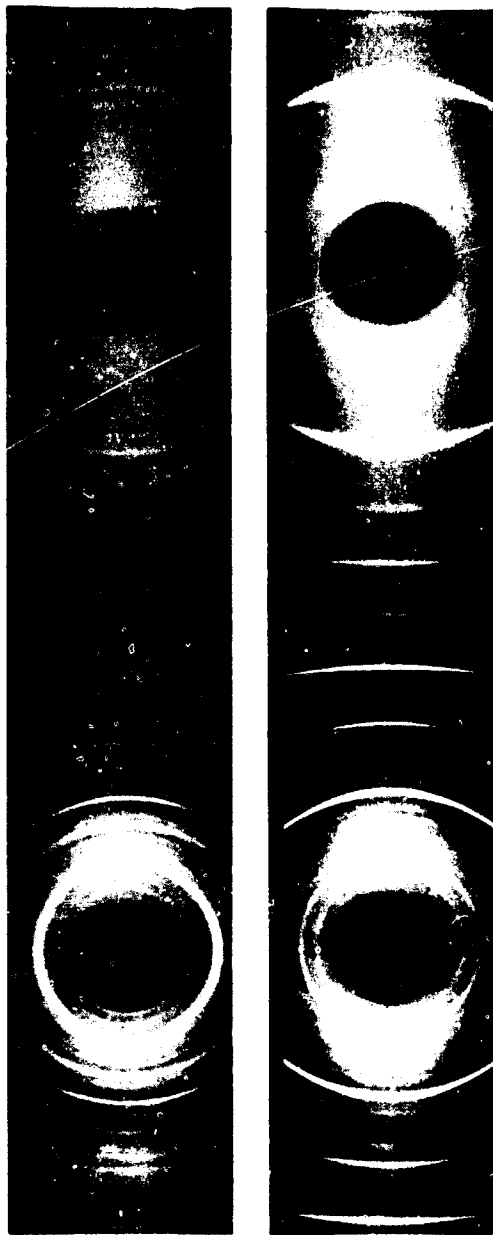
Test Run No.	S-24-71-D1	S-24-71-D2	S-24-71-D4	S-24-71-D3
P <sub>c</sub> , psia	44.0	5.0	42.0	5.0
T <sub>c</sub> , °K	1650	1250	1650	1250



Particles	1 1/2% LiF doped 37-44 $\mu$ MgH <sub>12</sub>		1 1/2% LiF doped 37-44 $\mu$ LiH <sub>2</sub>	
Test Run No.	5-24-71-D6	5-24-71-D5	5-24-71-D14	5-24-71-D13
P <sub>c</sub> , psia	42.3	4.8	42.0	4.8
T <sub>c</sub> , °K	1650	1250	1650	1250



Particles	1 1/2% LiF doped 37-44 $\mu$ LiB <sub>12</sub>		1 1/2% LiF doped 37-44 $\mu$ AlB <sub>2</sub>	
Test Run No.	5-24-71-D12	4-24-71-D11	5-24-71-D8	5-24-71-D7
P <sub>c</sub> psin	425	5.0	42.0	6.0
T <sub>c</sub> °K	1650	1250	1650	1250



Particles	1 1/2% dopod 37-44 $\mu$ AIB <sub>12</sub>	
Test Run No.	S-24-71-D 10	S-24-71-D9
P <sub>c</sub> , psia	42.0	5.0
T <sub>c</sub> , °K	1650	1250

## APPENDIX III

### PREPARATION METHODS AND COST OF BORON-METAL COMPOUNDS

According to Reference II, with a very few exceptions, boron-metal compounds are prepared only by high-temperature reactions. There are seven general methods:

- A. Synthesis from the elements or from boron and a metal or a hydride of the metal
- B. Reduction of the metal oxide with boron
- C. Simultaneous decomposition of a volatile boron compounds and of a volatile compound of the metal, usually on a hot filament and in the presence of hydrogen
- D. Fused-salt electrolysis of the metal oxide with a source of boric oxide
- E. Co-reduction of a source of the metal oxide and of boric oxide with carbon at high temperature
- F. Reduction of the metal oxide with carbon in the presence of boron carbide or the boride of another metal, e.g.  $\text{CaB}_6$
- F. Thermit-type reduction of a metal oxide and boric oxide by a metal such as aluminum or magnesium.

The first three methods are generally used only on a laboratory scale. Fusion electrolysis has been used for the preparation of kilogram quantities of boride powders. Methods E and F are of commercial significance, as is method G if residual aluminum, magnesium, or their oxides can be tolerated in the product or can be removed by acid leaching. Whichever method is used, it is important to maintain an inert atmosphere at high temperatures because metal borides react with oxygen, nitrogen, carbon monoxide, or carbon dioxide at most of the temperatures involved; hydrogen or an inert gas may be employed.

As can be seen, the preparation does not involve elaborate processes or complex equipment, and the compounds can be produced on a bulk scale. The cost in small quantities is high, but would be reduced on a mass production basis. The price of boron-metal compounds is more or less tied to the price of boron. The vendor's projected prices\* for some of the promising boron-metal compounds, all as -200 or -325 mesh particles, are as follows:

\*Quotation from CERAC, Inc., dated June 8, 1971

<u>Quantity</u> <u>lbs</u>	<u>MgB<sub>2</sub></u> <u>\$/lb</u>	<u>MgB<sub>12</sub></u> <u>\$/lb</u>	<u>LiB<sub>2</sub></u> <u>\$/lb</u>
5	100	100	195
10	75	85	175
50	50	60	135
100	37	45	95
1,000	20	25	35

It should be noted that the prices of these compounds in large quantities are lower than that of elemental boron.

## REFERENCES

1. Glassman, I., "Combustion of Metals, Physical Considerations." Solid Propellant Rocket Research, New York: Academic Press, 1960.
2. Macek, A., and J. M. Semple, "Combustion of Boron Particle at Atmospheric Pressure." AIAA Preprint 69-562, June 1969.
3. Talley, Claude P., "Combustion of Elemental Boron." Aero/Space Engr., 18:37, 1959.
4. Hottel, H. C., and I. M. Stewart, Ind. Engr. Chem. 32:719, 1940.
5. Spalding, D. B., Fourth Symposium (International) on Combustion, 1952, p. 847.
6. Belyaev, A. F., "Combustion, Detonation and Explosion Work in Condensed Systems." Moscow: Nanka Publishers, 1968. pp. 63-68.
7. Uda, R. T., "A Shock Tube Study of the Ignition Limit of Boron Particles," M. S. Thesis, Air Force Institute of Technology Report GA/ME/68-2. June 1968.
8. Sims, J. R., B. Y. S. Lee, and J. Gonzales, "Solid Boron Propellants for Air-Augmented Propulsion," Naval Weapons Center TP 4438. April 1968.
9. Freeman, E. S., W. Rudloff, and A. J. Becker, "Feasibility Study to Increase Activity of Oxides with Oxygen and to Lower the Ignition Temperature of Slurry Fuel Metals," Technical Report AFAPL-TR-66-68. Air Force Aero Propulsion Laboratory, August 1968.
10. Rosenberg, S. D., R. E. Yates, and R. C. Adrian, "Air-Augmented Combustion Studies," Technical Report AFRPL-TR-70-70 Air Force Rocket Propulsion Laboratory, September 1970.
11. Thompson, R., "Borides: Their Chemistry and Applications," Lecture Series No. 5. The Royal Institute of Chemistry, London, 1965.
12. Kohn, J. A., "Crystallography of the Aluminum Borides," Proceedings of the Conference on Boron, New York, 1960.
13. Serebryanskii, V. T., and V. A. Epel'baum, "The Phase Diagram of the Al-B System," Zh.Strukt, Khim. 2:748-50, 1961.
14. Ateda, T., I. Higashi, and M. Kobayashi, "Formation and Decomposition of Aluminum Borides." Scientific Paper for the Inst. Phys. Chem. Res. 61(3):92-9, Tokyo, 1967.
15. Domalski, E. S., and G. T. Armstrong, "Heats of Formation of Aluminum Diboride and  $\alpha$ -Aluminum Dodecaboride," J. Res. Nat. Bur. Standards, A 71(4):307-15, 1967.

16. Duhart, P., "The Borides of Magnesium and Aluminum." Ann. Chim. 7:339-65, 1962.
17. Germaidze, M. S., P. V. Gel'd, and S. M. LeFun, "Heat Capacity, Enthalpy, Entropy, and Dissociation Pressure of Magnesium Dodecaboride." Zh. Prikl. Khim. 39(9):1941-7, 1966.
18. Markovskii, L. Ya and Yu. D. Kondrashev, "Composition and the Properties of the Borides of Group I and II of the Periodic System," Zhur. Neorg. Khim. 2:34-41, 1957.
19. Casaletto, G. J., and T. N. Scortia, "Combustion Study of Light Metal Based Fuels," Technical Report AFRPL-TR-67-308. Air Force Rocket Propulsion Laboratory, December 1967.
20. Hsia, H. T-S., and R. Dunlap, "A Parametric Study of Secondary Combustion," Astronautica Acta 16:127-36, 1971.
21. Flanigan, D. A., R. E. Askins, W. H. Rush, and J. W. Blanks, "Chemical Techniques for Successful Boron Combustion at High Altitudes Low Speed Conditions," 7th JANNAF Combustion Meeting Bulletin, February 1971.